



KTH Electrical Engineering

Stability of Power Systems with Large Amounts of Distributed Generation

VALERIJS KNAZKINS

Doctoral Thesis
Stockholm, Sweden 2004

TRITA-ETS-2004-09
ISSN-1650-674x
ISRN KTH/R-0409-SE
ISBN 91-7283-876-0

KTH Institution för Elektrotekniska System
SE-100 44 Stockholm
SWEDEN

Akademisk avhandling som med tillstånd av Kungl Tekniska högskolan framlägges till offentlig granskning för avläggande av teknologie doktorsexamen fredagen den 22 oktober 2004 i sal D3, Lindstedtsvägen 5, Kungl Tekniska Högskolan, Stockholm.

© Valerijs Knazkins, oktober 2004

Tryck: Universitetsservice US AB

Abstract

This four-part dissertation is essentially concerned with some theoretical aspects of the stability studies of power systems with large penetration levels of distributed generation. In particular, in Parts I and II the main emphasis is placed upon the transient rotor angle and voltage stability. The remaining two parts are devoted to some system-theoretic and practical aspects of identification and modeling of aggregate power system loads, design of auxiliary robust control, and a general qualitative discussion on the impact that distributed generation has on the power systems.

One of the central themes of this dissertation is the development of analytical tools for studying the dynamic properties of power systems with asynchronous generators. It appears that the use of traditional tools for nonlinear system analysis is problematic, which diverted the focus of this thesis to new analytical tools such as, for example, the Extended Invariance Principle. In the framework of the Extended Invariance Principle, new extended Lyapunov functions are developed for the investigation of transient stability of power systems with both synchronous and asynchronous generators.

In most voltage stability studies, one of the most common hypotheses is the deterministic nature of the power systems, which might be inadequate in power systems with large fractions of intrinsically intermittent generation, such as, for instance, wind farms. To explicitly account for the presence of intermittent (uncertain) generation and/or stochastic consumption, this thesis presents a new method for voltage stability analysis which makes an extensive use of interval arithmetics.

It is a commonly recognized fact that power system load modeling has a major impact on the dynamic behavior of the power system. To properly represent the loads in system analysis and simulations, adequate load models are needed. In many cases, one of the most reliable ways to obtain such models is to apply a system identification method. This dissertation presents new load identification methodologies which are based on the minimization of a certain prediction error.

In some cases, DG can provide ancillary services by operating in a load following mode. In such a case, it is important to ensure that the distributed generator is able to accurately follow the load variations in the presence of disturbances. To enhance the load following capabilities of a solid oxide fuel plant, this thesis suggests the use of robust control.

This dissertation is concluded by a general discussion on the possible impacts that large amounts of DG might have on the operation, control, and stability of electric power systems.

Acknowledgments

This doctoral dissertation finalizes the work which I have carried out in the Department of Electrical Engineering, Royal Institute of Technology (KTH) since February 1999.

First, I would like to express my sincere gratitude to my supervisor Prof. Lennart Söder for his skilled guidance, valuable comments, and encouragement that he give me over the years of work on the project.

Special thanks go to Mehrdad Ghandhari and Thomas Ackermann, whose valuable comments, constructive suggestions, and collaboration have been indispensable.

A word of gratitude goes to Prof. Claudio Cañizares of the University of Waterloo, Canada for productive and educative collaboration, sharing his knowledge in power system dynamics and stability, and hosting me in the Department of Electrical and Computer Engineering, University of Waterloo from November 2002 to April 2003.

The financial support of the project from the Competence Centre in Electric Power Engineering at the Royal Institute of Technology and Nordisk Energiforskning is gratefully acknowledged.

Many thanks go to Mr. Per Ivermark, the manager for Electrical Maintenance of “Billerud” in Grums, Sweden for very productive collaboration and diverse help in obtaining and interpreting the data for one of the case studies presented in the thesis.

The invaluable help of the secretaries of the department, Mrs. Margaretha Surjadi and Lillemor Hyllengren is also highly appreciated. My colleagues, former and

present, at the Division of Electric Power Systems are acknowledged for creating the stimulating ambient for research. In particular, I would like to express a word of gratitude to Viktoria Neimane for bringing genetic algorithms to my attention and helping me with practical issues at early stages of my work in the Department. I am indebted to: Anders Wikström and Magnus Lommerdal for inviting me to lunch; my former roommate Jonas Persson for teaching me some Swedish and for the heroic road trip on the Western Coast of the US; Nathaniel Taylor for introducing me to the GNU world and helping with various computer-related issues; Lawrence Jones for numerous discussions on power systems dynamics and getting me interested in system identification; Julija Matevosyan, Dmitry Svechkarenko, Gavita Mugala, Ruslan Papazyan, and Timofei Privalov for great friendship and support.

I am also greatly indebted to my friend and colleague Waqas M. Arshad, who has had a major impact on the course of many events for his practical help.

Finally, I wish to express my utmost gratitude to my dear wife, Olga for her care and support, love and friendship, and giving birth to our son Victor. You have harmonized and enriched my life in the way I could never dream of; yet, I will always be grateful to you for standing by my side throughout all the sorrow and happiness.

V. KNAZKINS

October 2004
Stockholm, Sweden

Contents

Contents	vii
List of Figures	x
List of Tables	xii
1 Introduction	1
1.1 Background and Motivation of the Project	1
1.2 Outline of the Thesis	3
1.3 Main Contributions	4
1.4 List of Publications	5
I Transient Stability of Electric Power Systems	7
2 Background	9
2.1 Definition Of Distributed Generation	9
2.2 Dynamic Phenomena in Power Systems	10
2.3 Formal Definition of Power System Stability	11
2.4 Rotor Angle Stability	15
2.5 Voltage Stability	17
2.6 Frequency Stability	17
2.7 Summary	18
3 Power System Modeling	19
3.1 Main Components of Power Systems	19
3.2 Modeling of Solid Oxide Fuel Cells	28
3.3 Algebraic Constraints in Power Systems	33

4	Energy Function Analysis	35
4.1	Mathematical Preliminaries	36
4.2	Extended Invariance Principle	38
4.3	Single Asynchronous Machine-Infinite Bus System	39
4.4	Transient Stability Analysis of the SAMIB System	40
4.5	Alternative Formulation of the System Model	45
4.6	Use of Interval Arithmetics for Set Inversion	53
4.7	Numerical Examples	53
4.8	Summary	62
II	Voltage Stability	63
5	Assessment of Voltage Stability of Uncertain Power Systems	65
5.1	Introduction	65
5.2	Voltage Stability Formulation	66
5.3	Application of Interval Arithmetics to Voltage Collapse Analysis	69
5.4	Summary	73
III	Power System Load Modeling and Identification	75
6	Identification of Aggregate Power System Loads	77
6.1	Introduction	77
6.2	Aggregate Models of Power System Loads	79
6.3	System Identification	83
6.4	Application Examples	94
6.5	Summary	101
IV	Qualitative Analysis of Operation, Control, and Stability of Distributed Generation	103
7	Design of Robust Control for SOFC Power Plant	105
7.1	Robust Control	105
7.2	Application of Robust Control to the SOFC Plant	114
7.3	Discussion	121
7.4	Summary	122

8	Interaction Between DG and the Power System	123
8.1	Introduction	123
8.2	Historical Background	124
8.3	Distributed Generation Technology	125
8.4	General Impact of DG on Power System Operation and Control . .	127
8.5	Network Control and Stability Issues	138
9	Closure	149
9.1	Conclusions	149
9.2	Suggestions for Future Work	152
A	Interval Arithmetics	155
B	Some Mathematical Facts	157
B.1	Linear Algebra	157
B.2	Calculus	158
C	Linearized Model of SOFC	159
	Bibliography	161

List of Figures

2.1	Simplified chart of dynamic phenomena in power systems	11
2.2	Stable system. Phase portrait	15
2.3	Stable system. Time domain	15
2.4	Asymptotically stable system. Phase portrait	16
2.5	Asymptotically stable system. Time domain	16
3.1	Domain of attraction of system (3.2)	22
3.2	IEEE Type DC1 exciter system with saturation neglected	25
3.3	Simplified schematic diagram of a fuel cell	28
3.4	One-line diagram of a fuel cell-driven power plant.	30
3.5	SOFC system block diagram	32
4.1	Graphical illustration of the Extended Invariance Principle. All trajectories $x(t)$ with $x(0) \in \Omega_L$ converge to the largest invariant set contained in E	39
4.2	Single Asynchronous Machine Infinite Bus system	40
4.3	Impedance diagram of the SAMIB system	40
4.4	Equivalent circuit of the model (4.20)–(4.22)	46
4.5	Simple three-machine power system.	49
4.6	Set C found by the SIVIA algorithm. Only two components of C are shown.	55
4.7	Level curves of V and $\mathcal{L}_f V$	56
4.8	Potential energy curve vs. time for the system (4.46)–(4.47). The potential energy was computed for a hypothetical fault on the transmission system, which resulted in a 60% voltage drop at the terminals of the asynchronous generator.	56
4.9	Three-machine power system	58

4.10	The deviation of state variable, ΔE_2 , i.e., the EMF of the asynchronous generator as a function of time	58
4.11	The total $V(t)$ and potential $V_p(t)$ energies of the 3-machine power system and the Lie derivative $\mathcal{L}_f V(t)$ of $V(t)$	59
4.12	Phase portrait of G_1	60
4.13	Phase portrait of G_2	60
4.14	Phase portrait of G_3	61
5.1	Three-bus power system	71
5.2	Variation of the loadability limit in $\delta_1 - \delta_2$ plane	71
5.3	Variation of the Saddle-node bifurcation point in $\delta_1 - \delta_2$ plane	72
6.1	Variance of the estimated parameter vector $\hat{\theta}$ versus number of samples and the corresponding Cramér-Rao Lower Bounds for the artificial data set. Nonlinear load model	96
6.2	Variance of the estimates of the linear and nonlinear model parameters	96
6.3	Electrical diagram of the studied part of Grums paper mill	98
6.4	Application of the proposed identification scheme to field measurements. Estimation of the parameters of active power load. Linearized model	99
6.5	Application of the proposed identification scheme to field measurements. Estimation of the parameters of active power load. Nonlinear Identification	100
7.1	Standard diagram of the plant and controller	107
7.2	Single-input single-output plant	107
7.3	Nyquist plot of the SISO system	109
7.4	Parametrization of all suboptimal \mathcal{H}_∞ controllers	113
7.5	Transfer function of a fuel cell plant	116
7.6	Preliminary control configuration of the fuel cell plant	117
7.7	Disturbance rejection by one degree-of-freedom controller.	118
7.8	Step response by one degree-of-freedom controller.	119
7.9	Final control configuration of the fuel cell plant	119
7.10	Disturbance rejection by the two degrees-of-freedom controller.	120
7.11	Step response of the plant with the two degrees-of-freedom controller.	121
8.1	Hypothetical Distribution Network	128
8.2	Simplified model of a power system with DG	129
8.3	P - V curve: Enlargement of voltage stability margin	145

List of Tables

2.1	Relative size of distributed generation	10
4.1	Parameters of the equivalent model of the wind farm. All values are given in per unit on the base of the generator	54
4.2	System parameters for 3-machine power system. All values are given in per unit, except δ_0 and T_2 . With minor modifications, the parameters values are similar the values in [60].	57
6.1	Comparison of the load parameters identified using linear and nonlinear models	100
8.1	Technologies for distributed generation [13].	125
8.2	Fault currents levels of some DG [21].	135
C.1	Parameters in SOFC plant model	160

To my family

“The idea is to try to give all the information to help others to judge the value of your contribution; not just the information that leads to judgment in one particular direction or another.”

— Richard P. Feynman

Chapter 1

Introduction

1.1 Background and Motivation of the Project

The rapid development of distributed generation (DG) technology is gradually reshaping the conventional power systems in a number of countries in the Western Europe and North America. Wind power, microturbines, and small hydropower plants are among the most actively developing distributed generation. For instance, only for the period from January to June 2003, in the EU countries approximately 1500 MW of wind power were installed to reach the landmark of 24626 MW installed capacity [1]. Moreover, it is projected that approximately 20% of all newly installed capacity will belong to DG [24]. It is important to observe that the overwhelming majority of the aforementioned DG technologies utilize asynchronous generators for electric power generation. As for the “inertialess” generators, fuel cells are apparently the most attractive long-term alternative. Very high efficiency and reliability, modularity, environmental friendliness, noiseless operation, and high controllability make fuel cell-driven power plants a sound competitor on the future power market.

Presently, the impact of DG on the electric utility is normally assessed in planning studies by running traditional power flow computations, which seemingly is a reasonable action, since the penetration ratios of the DG are still relatively small. However, as the installed capacity of DG increases, its impact on the power system behavior will become more expressed and will eventually require full-scale detailed dynamic analysis and simulations to ensure a proper and reliable operation of the power system with large amounts of DG. To address the need for dynamic

simulations, a number of models of the distributed generators were created in the recent years [14, 15, 98]. However, to the best knowledge of the author, no systematic analytic investigations of the dynamic properties of the power systems with large amounts of DG have been reported in the literature. That is, the immense amount of case studies that can be found in the literature on DG focus mainly on numerical experiments with either existing or artificial networks. While the numerical experiments are of paramount importance to a better understanding of the mechanisms which cause interaction between the DG and the utility, the development of appropriate analytical tools for stability studies will open new perspectives for dynamic security assessment of the power system and design of new control systems, e.g., \mathcal{L}_fV controllers.

One of the main objectives of this dissertation is to partially fill this gap by presenting a systematic method for analyzing the transient stability of a large-scale, asynchronous generator-driven distributed generation.

Another important theme of this thesis is the voltage collapse analysis of power systems with large fractions of intermittent power generators. It is known that the majority of available tools for voltage collapse analysis make use of the implicit assumption that the power system parameters are deterministic. While this is a valid engineering approximation for conventional power systems with negligibly small uncertainties, it might become an oversimplification in power systems with large penetration ratios of DG. To account for the uncertainty due to the fluctuating power output of the DG and possibly some other uncertainties in the system (such as load variations, transformer tap-changer position, certain impedances, etc.) this thesis proposes the use of interval arithmetics which is well suited for such operations. In simple terms, we suggested to restate the voltage collapse problem in terms of an interval-valued optimization problem and then to solve it by applying the Generalized Newton method. In this method, it is explicitly assumed that the variables are uncertain, but are bounded.

It is a well-known fact that power system loads have a significant impact on the dynamic behavior of the system. It appears that both power system damping and voltage stability are dependent on the load properties. Therefore, the reliable determination of load characteristics becomes an important engineering task. In some cases, it is more practical to aggregate several loads to an equivalent aggregate load model. Several aggregate load models parameterized by 3 parameters have been in use for a long time; however, no systematic effort has been made to develop an algorithm for determining those parameters. Such an algorithm is developed and presented in this thesis.

1.2 Outline of the Thesis

Conceptually, the thesis consists of 4 parts describing the results of the research in the fields of

1. Transient stability of power systems with large penetration ratios of DG
2. Voltage collapse of power systems with significant amounts intermittent distributed generation
3. Identification and modeling of aggregate power system loads
4. Design of robust controllers enhancing the performance of distributed generators and a general discussion on the impact that DG has on the operation, control, and stability of the electric utility.

Part I briefly presents the definition of power system stability and the system-theoretic foundations of the Lyapunov direct method as well as the concept of Extended Invariance Principle (EIP). The framework of EIP is used for the construction of new extended Lyapunov functions for a small-scale power system consisting of synchronous and asynchronous machines. It is also demonstrated in this part of the thesis that several well-known methods cannot yield a valid Lyapunov (energy) function for the power system consisting of a single asynchronous generator.

Part II addresses some issues related to the voltage collapse analysis of uncertain power systems. Here, the emphasis is placed upon finding the critical system loading in the presence of uncertain generation and/or consumption. The uncertain quantities are assumed to be bounded, which allows us to explicitly deal with them by using interval analysis.

Part III presents a new method for identifying the parameters of aggregate nonlinear dynamic power system loads modeled by the Wiener-Hammerstein structure. The properties of this new identification method [belonging to the family output error methods] are studied both analytically and by using artificial data as well as field measurements.

Part IV demonstrates the use of robust controllers for the enhancement of the performance of a solid oxide fuel cell-driven DG power plant, which substantially improves the load following capability of the power plant in the presence of system uncertainties and bounded (structured) disturbances. Part IV also contains a discussion on the impact that large amounts of DG have on the operation, protection system, and control of the power system.

1.3 Main Contributions

The main results of this research project contain contributions to several fields of electric power engineering, namely, the transient rotor angle and voltage stability of electric power systems, as well as the applied identification of aggregate load parameters. Other key contributions are related to the design of auxiliary robust controllers enhancing the performance of DG and the general assessment of the impact that large amounts of DG might have on the utility. More specifically, the key contributions can be briefly summarized as follows.

1. An overview of DG technologies relevant to this project was made.
2. The DG technologies were qualitatively analyzed and their impact on the power system was discussed. Here, such questions as the impact on the voltage control, inertia constants, power quality, fault current levels, protection system, reliability, and stability were studied.
3. Models of asynchronous generators applicable to transient stability analysis of the power system are discussed in detail.
4. The applicability of direct Lyapunov method to stability analysis of a power system consisting of both synchronous and asynchronous generators was studied theoretically.
5. It was shown that the Energy Metric Algorithm, First Integral of Motion, and the Krasovskii method are incapable of synthesizing a valid Lyapunov/energy function for a single asynchronous generator.
6. Extended Invariance Principle was reviewed and its application to the power system with asynchronous generators was discussed.
7. New Extended Lyapunov functions were developed for the second and third order models of the asynchronous generator.
8. To simplify the use of Extended Invariance Principle, the use of interval arithmetics for certain set operations was proposed.
9. It was shown analytically that there exists an Extended Lyapunov function for a mixed three-machine power system.
10. Several basic numerical experiments were conducted to further explore the properties of the new Extended Lyapunov functions.

11. The use of interval analysis is proposed for the voltage collapse analysis of power systems with large fractions of intermittent power generation and uncertain loading.
12. Two new methods were proposed for the identification of linear and nonlinear models of aggregate power system loads.
13. The properties of the proposed methods were studied analytically and by means of numerical experiments. The identification methods were successfully applied to identification of load models of a real-world paper mill.
14. The load following capabilities of a solid oxide fuel cell-driven power plant were explored by means of a numerical experiment.
15. To enhance these load following capabilities, a two-degree-of-freedom \mathcal{H}_∞ controller was designed and verified.

1.4 List of Publications

The work on this doctoral project resulted in a number of publications, some of which are listed below.

1. V. Knyazkin¹, M. Ghandhari, and C. Cañizares, “Application of Extended Invariance Principle to Transient Stability Analysis of Asynchronous Generators”, Proceedings of “Bulk Power System Dynamics and Control VI, August 22-27, 2004, Italy.
2. V. Knyazkin, M. Ghandhari, and C. Cañizares, “On the Transient Stability of Large Wind Farms”, Proceedings of “The 11th International Power Electronics and Motion Control Conference”, September 2–4, Latvia, 2004.
3. V. Knyazkin, L. Söder, and C. Cañizares, “Control Challenges of Fuel Cell-driven Distributed Generation”, Proceedings of IEEE Power Tech Conference Bologna, 2003, Volume: 2, June 23–26, 2003 Pages:564–569.
4. V. Knyazkin and T. Ackermann, “Interaction Between the Distributed Generation and the Distribution Network: Operation, Control, and Stability Aspects”. In CIREN 17th International Conference on Electricity Distribution, Barcelona, 12–15 May 2003.

¹This is an anglicized version of the name that according to the Latvian Regulations No. 295 “On Spelling and Identification of Surnames” must be spelled as Valerijs Knazkins.

5. V. Knyazkin, C. Cañizares, and L. Söder, “On the Parameter Estimation and Modeling of Aggregate Power System Loads”. *IEEE Transactions on Power Systems*, Volume: 19, Issue: 2, May 2004 Pages:1023–1031.
6. V. Knyazkin, L. Söder, and C. Cañizares, “On the Parameter Estimation of Linear Models of Aggregate Power System Loads”. *The Proceedings of IEEE PES General Meeting, 2003*, Volume: 4, 13–17 July 2003 Pages: 2392–2397 Vol. 4.
7. T. Ackermann and V. Knyazkin, “Interaction Between Distributed Generation And The Distribution Network: Operation Aspects”, *The Proceedings IEEE PES Transmission and Distribution Conference and Exhibition 2002: Asia Pacific*, 6–10 October 2002, Yokohama, Japan.
8. V. Knyazkin, “On the Use of Coordinated Control of Power System Components for Power Quality Improvement”, *Technical Licentiate. Royal Institute of Technology, Stockholm, TRITA-ETS-2001-06*, ISSN 1650-675X, Dec. 2001.
9. L. Jones, G. Andersson, and V. Knyazkin, “On Modal Resonance and Inter-area Oscillations in Power Systems”, *The Proceedings of The IREP Symposium “Bulk Power System Dynamics and Control V”* in August, 2001, Onomichi, Japan.
10. V. Knyazkin and L. Söder, “Mitigation of Voltage Sags Caused by Motor Starts by Using Coordinated Control and a Fast Switch”, *The Proceedings of PowerTech 2001*, held September 9–13 2001, Porto, Portugal.
11. V. Knyazkin and L. Söder, “The Use of Coordinated Control for Voltage Sag Mitigation Caused by Motor Start”, *The Proceedings of the 9th International Conference on Harmonics and Quality of Power*, vol. 3, pp. 804–809, 2000.
12. V. Knyazkin, “The Oxelösund Case Study”, A–EES–0010, Internal report, Electric Power Systems, Royal Institute of Technology, Sweden, August, 2000.
13. V. Knyazkin, “The Use of the Newton Optimization for Close Eigenvalues Identification”, A–EES–0012, Internal report, Electric Power Systems, Royal Institute of Technology, Sweden, September, 2000.

Part I

Transient Stability of Electric Power Systems

“ Analysis of stability, . . . , is greatly facilitated by classification of stability into appropriate categories. Classification, therefore, is essential for meaningful practical analysis and resolution of power system stability problems.”


— A quotation from [75]

Chapter 2

Background

This chapter briefly presents the key definitions and concepts used throughout the thesis.

2.1 Definition Of Distributed Generation

 In the literature, a large number of terms and definitions are used to designate generation that is not centralized. For instance, in Anglo-Saxon countries the term “embedded generation” is often used, in North American countries the term “dispersed generation”, and in Europe and parts of Asia, the term “decentralised generation” are used to denote the same type of generation. This thesis will follow the general definition proposed in [13]:

Definition 1 *Distributed generation is an electric power source connected directly to the distribution network or on the customer side of the meter.*

The distinction between distribution and transmission networks is based on the legal definition. In most competitive markets, the legal definition for transmission networks is usually part of the electricity market regulation. Anything that is not defined as transmission network in the legislation can be regarded as distribution network. It should be noted that Definition 1 does not specify the rating of the generation source, as the maximum rating depends on the local distribution network conditions, e.g. voltage level. Furthermore, Definition 1 does neither define the area of the power delivery, the penetration, the ownership nor the treatment within the network operation as some other definitions do.

Table 2.1: Relative size of distributed generation

Micro distributed generation	$\sim 1 \text{ Watt} < 5 \text{ kW}$
Small distributed generation	$5 \text{ kW} < 5 \text{ MW}$
Medium distributed generation	$5 \text{ MW} < 50 \text{ MW}$
Large distributed generation	$50 \text{ MW} < \sim 300 \text{ MW}$

To further clarify the concept of distributed generation, it is also necessary to define the relative size of the DG unit. The classification of distributed generators according to their relative sizes is briefly summarized in Table 2.1. The penetration level¹ (PL) can be defined in two ways as is shown below.

$$PL = \frac{P_{DG}}{P_{Load}} \cdot 100 [\%] \quad (2.1)$$

$$PL = \frac{P_{DG}}{P_{Load} + P_{DG}} \cdot 100 [\%], \quad (2.2)$$

where P_{DG} stands for the total active power of all distributed generators installed in a given area and P_{Load} is the total active power of the load in the same area. In this thesis the first definition is assumed.

2.2 Dynamic Phenomena in Power Systems

The importance of power system stability has been recognized at the early stage of the power system development [91, 121]. The dimension and complexity of power systems have been gradually increasing over the years, making the power system stability phenomenon a more important and challenging problem. For instance, modern interconnected power systems are large, integrated, and complex dynamic structures which are subject to constantly acting various (possibly overlapping) physical phenomena ranging from very fast ones such as transients due to lightning strokes to quite slow ones, such as, for instance, the dynamics of a boiler.

A first step towards a better understanding of the power system stability phenomenon is to adequately define and categorize the various phenomena occurring in the power system. Normally, all power system phenomena are studied in the framework of three general structures, i.e., administrative, physical, and time-scale

¹In this thesis ‘penetration level’ and ‘penetration ratio’ are used synonymously.

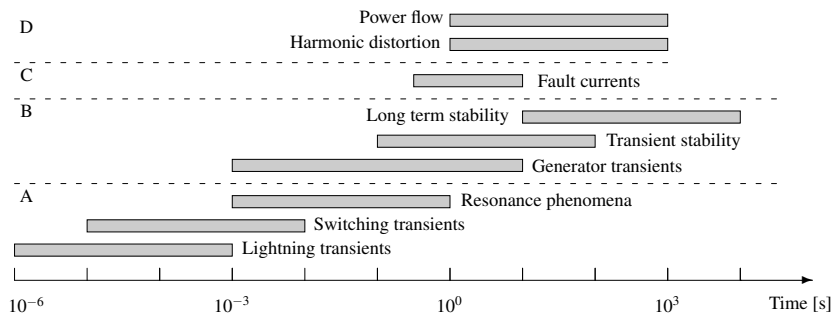


Figure 2.1: Simplified chart of dynamic phenomena in power systems [18]. Zones A, B, C, and D denote fast transients, generator dynamics, quasi steady state, and steady state, respectively.

structures [107]. The administrative structure regulates the political organization of the power grid, i.e., it establishes the hierarchical structure of various layers of the power grid. The physical structure describes the main components of the power system, relations between them, control equipment, as well as the energy conversion principles. Finally, the time-scale structure categorizes the dynamic phenomena that occur in the power system according to the time scale of the underlying physical processes. The latter structure is arguably the most appropriate for studying the dynamics of the power system and hereby is adopted in this thesis. Figure 2.1 shows an approximate time-scale structure of power system phenomena of interest, which will be used in this thesis. In general, all the phenomena can be divided in two large groups corresponding to fast and slow dynamics, depending on the time scale of the underlying physical processes triggering the mechanisms of power system instability. In the remainder of this chapter various definitions of power system stability are presented and discussed.

2.3 Formal Definition of Power System Stability

The concept of stability is one of the most fundamental concepts in most engineering disciplines. Due to the devastating impact that instabilities might cause in dynamical systems, numerous definitions of stability have been formulated, emphasizing its various aspects that reflect the manifestation of the system's stable state. It is known that over 28 definitions of stability were introduced for technical

and physical reasons in the systems theory. Some of the definitions might be quite useful in one situation, but inadequate in many others. To avoid possible ambiguities and establish rigorous foundations of the subsequent discussion, the main emphasis in this thesis is placed upon the so-called stability in the sense of A. M. Lyapunov [103].

Technical assumptions

A1: The power system can in general be satisfactorily described by a set of first-order ordinary differential-algebraic equations (DAE) of the form:

$$\begin{bmatrix} \dot{x} \\ 0 \end{bmatrix} = \begin{bmatrix} f(t, x, y, p) \\ g(t, x, y, p) \end{bmatrix} = F(t, x, y, p), \quad (2.3)$$

where variable $t \in \mathcal{I} \subseteq \mathbb{R}$ represents time, the derivative with respect to time is denoted as $\dot{x} = dx/dt$, $x \in U \subseteq \mathbb{R}^n$ designates the vector of state variables, $y \in \mathbb{R}^m$ is the vector of algebraic variables, $p \in \mathbb{R}^l$ is the vector of controllable parameters, $f: \mathcal{I} \times \mathbb{R}^n \times \mathbb{R}^m \times \mathbb{R}^l \rightarrow \mathbb{R}^n$ stands for a certain nonlinear function, and $g: \mathbb{R}^n \times \mathbb{R}^m \times \mathbb{R}^l \rightarrow \mathbb{R}^m$ denotes a nonlinear vector-valued function.

A2: We assume that the Jacobian matrix

$$D_y g(x, y, p) = \frac{\partial g}{\partial y} \quad (2.4)$$

is nonsingular along all the trajectories of (2.3), thus ensuring that the set of DAE can be reduced to a set of ODE's by virtue of the Implicit Function Theorem [54, 104].

A3: It is also assumed that the function F is sufficiently smooth to ensure existence, uniqueness, and continuous dependence of the solutions of (2.3) on the initial conditions over the domain of F .

A4: Without loss of generality, it will be assumed that the origin is a critical point of (2.3).

Finally, let \mathcal{B}_r denote an open ball of radius r , i.e., $\mathcal{B}_r = \{x \in U : \|x\| < r\}$, where $\|\cdot\|$ is any norm and σ stands for the right maximal interval where $x(\cdot, t_0, x_0, p)$ is defined.

Definition 2 *Let assumptions A1–A4 hold. Then, the solution $x = 0$ is called stable if $\forall \varepsilon > 0$ and $\forall t_0 \in \mathcal{I}$ there exists a positive number δ such that $\forall x_0 \in \mathcal{B}_\delta$ and $\forall t_0 \in \sigma$, the following inequality holds: $\|x(t, t_0, x_0, p)\| < \varepsilon$.*

This definition can be loosely restated in other terms: for every given positive ε and $t_0 \in \mathcal{I}$, there exists a positive δ , which in general is a function of ε , such that for all initial values of x that belong to an open ball of radius δ , the solution $x(t)$ remains in an open ball of radius ε for all time.

Definition 3 *The system is termed unstable if it is not stable.*

Definition 4 *The solution $x = 0$ of system (2.3) is referred to as uniformly stable if $\forall \varepsilon > 0$ there exists a $\delta(\varepsilon) > 0 : \forall x_0 \in B_\delta$ and $\forall t_0 \in \mathcal{I}$ such that $\|x(t, t_0, x_0, p)\| < \varepsilon$.*

Remark: Stated differently, uniform stability of (2.3) is obtained by relaxing the dependence of δ on t_0 .

Definition 5 *The solution $x = 0$ of system (2.3) is called attractive if for each $t_0 \in \mathcal{I}$ there is a positive number $\eta = \eta(t_0)$, and for each positive ε and $\|x(x_0, p)\| < \eta$ there is a positive $\omega = \omega(t_0, \varepsilon, x_0, p)$ such that $t_0 + \omega \in \sigma$ and $\|x(t, t_0, x_0, p)\| < \varepsilon$ for all $t \geq t_0 + \omega$.*

Definition 6 *The solution $x = 0$ is asymptotically stable if it is both stable and attractive.*

Note: In the definition above it is necessary to require that the system is both stable and attractive, since attractivity does not—in general—imply stability. In other words, it is possible to construct an example in which the origin is attractive, i.e., every solution tends to it as $t \rightarrow \infty$, but yet the origin is unstable [129].

Definition 7 *Let x^* be a hyperbolic equilibrium point. Its stable and unstable manifolds, $W^s(x^*)$ and $W^u(x^*)$, are defined as follows:*

$$W^s(x^*) = \{x \in \mathbb{R}^n : \Phi(t, x) \rightarrow x^* \text{ as } t \rightarrow \infty\}$$

$$W^u(x^*) = \{x \in \mathbb{R}^n : \Phi(t, x) \rightarrow x^* \text{ as } t \rightarrow -\infty\},$$

where $\Phi(t, x)$ is the solution of (2.3). Then the stability region (or region/domain of attraction) of a stable equilibrium x^* is defined as

$$A(x^*) = \{x \in \mathbb{R}^n : \lim_{t \rightarrow \infty} \Phi(t, x) = x^*\}.$$

Definition 8 *If there exists an energy function for system (2.3), then the stability boundary $\partial A(x^*)$ is contained in the union of the stable manifolds of the unstable equilibria on $\partial A(x^*)$. That is,*

$$\partial A(x^*) \subseteq \bigcup_{x_i \in \partial A(x^*)} W^s(x_i),$$

where x_i are the hyperbolic equilibria of (2.3).

Definition 9 *The system (2.3) falls into the category of linear systems if F is a linear function.*

Most of physical dynamic systems, including power systems, are essentially nonlinear; however, it has become a common practice to study the local behavior of the original nonlinear system by linearizing it around an equilibrium point of interest. Then some of the dynamic properties of the nonlinear system can be inferred by analyzing the corresponding linear model. These properties, however, hold true only in some sufficiently small neighborhood of the equilibrium point. To obtain results that are valid globally, the nonlinear model has to be analyzed.

Definition 10 *The system (2.3) is referred to as autonomous if F is not an explicit function of time; otherwise it is termed non-autonomous.*

Remark: Often studying the dynamic properties of power systems, it is assumed that the system at hand is autonomous. This assumption allows the use of much more simple analytical tools; however, in general, strictly speaking, power systems are non-autonomous [47].

Some of the presented concepts are further clarified by the following two examples.

Example: Consider the system of 2 nonlinear autonomous differential equations

$$\begin{bmatrix} \dot{x}_1 \\ \dot{x}_2 \end{bmatrix} = \begin{bmatrix} x_2 - x_1 x_2 \\ -0.9x_1 - (x_1^2 - 0.7)x_2 \end{bmatrix}. \quad (2.5)$$

Clearly, the origin is a critical point of (2.5), but no system trajectory converges to it. However, as the simulations indicate, all the trajectories are bounded for all sufficiently small $\|x_0\|$. Thus, the origin of the system is unstable. Figure 2.2 shows the phase portrait of (2.5) for some initial conditions. It can be seen in the figure that the system trajectory does not converge to a single point in the plane

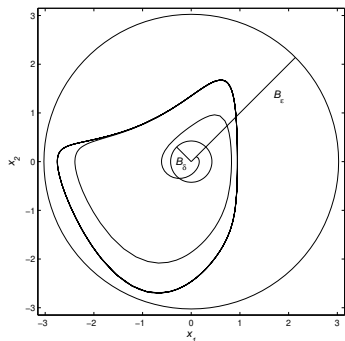


Figure 2.2: Stable system. Phase portrait

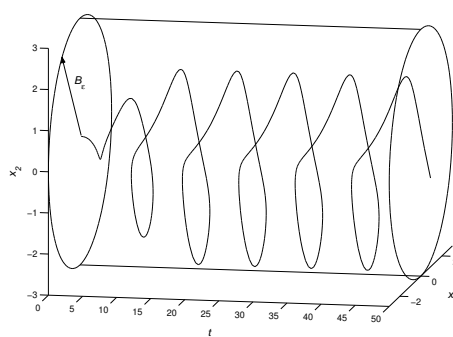


Figure 2.3: Stable system. Time domain

but approaches a limit cycle. The qualitative behavior of the system trajectory is clearer when the state variables are plotted versus time, see Fig. 2.3.

Example: Consider the following system of autonomous linear ODE

$$\begin{bmatrix} \dot{x}_1 \\ \dot{x}_2 \end{bmatrix} = \begin{bmatrix} -x_2 \\ x_1 - 0.5x_2 \end{bmatrix}. \quad (2.6)$$

Again, the origin is an equilibrium point of (2.6), but the behavior of this system differs drastically from that of (2.5), as numerical simulations confirm, see Fig. 2.4–2.5. Now, all the trajectories of (2.6) converge the unique asymptotically² stable equilibrium point—the origin—as time progresses. This is an intrinsic property of all autonomous linear systems: the stability property is invariant in the whole state space. That is, if a linear system is stable it is stable globally, and conversely: an unstable linear system is unstable for any initial condition.

2.4 Rotor Angle Stability

To better understand the mechanisms of the instability phenomenon in power systems and devise tools suitable for preventing system instabilities, the general concept of stability is categorized into three different but—in general—not disjoint concepts of rotor angle, voltage, and frequency stability. Historically, the power system researchers and practitioners investigating system's stability placed emphasis on the rotor angle stability; only in the relatively recent years the importance of

²In fact, in this case the origin is an exponentially stable equilibrium.

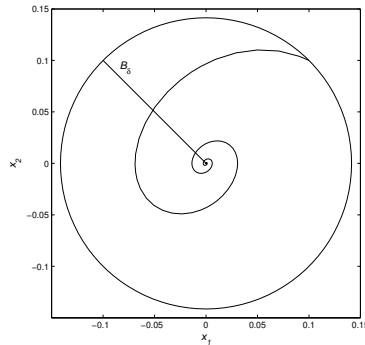


Figure 2.4: Asymptotically stable system. Phase portrait

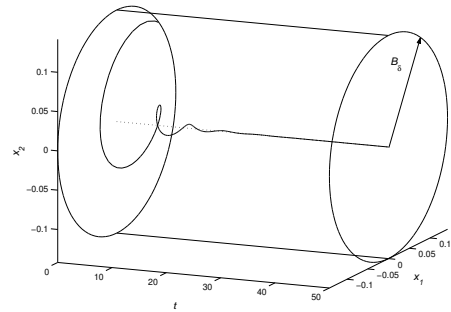


Figure 2.5: Asymptotically stable system. Time domain

voltage stability was recognized. We therefore commence by quoting the classical definition of power system stability due to E. Kimbark [69]:

Definition 11 *Power system stability is a term applied to alternating-current electric power systems, denoting a condition in which the various synchronous machines of the system remain in synchronism, or “in step,” with each other.*

While this definition is valid and satisfactorily conforms to the system-theoretic definitions presented above, a more elaborated definition of power system stability was proposed in [75]:

Definition 12 *Power system stability is the ability of an electric power system, for a given initial operating condition, to regain a state of operating equilibrium after being subjected to a physical disturbance, with most system variables bounded so that practically the entire system remains intact.*

This new definition allows a more subtle distinction between various instability scenarios based on the characteristics of the physical disturbance.

It is known that power systems are subject to continuously acting disturbances. The vast majority of them are relatively small, compared to the power system capacity; however, more severe disturbances also occur. Therefore, it is natural to subdivide the general concept of angle stability to the so-called small-disturbance and transient stability. Thus, a power system is termed stable in the sense of small-disturbance stability if the system’s generators are able to remain in step with each

other after being subjected to a small disturbance. Similarly, a power system is said to be transiently stable if it remains intact when subjected to a large disturbance. Normally, a disturbance is considered small if it does not cause significant deviations of the state variables from the pre-fault steady state equilibrium. Otherwise, the disturbance is said to be large. Switching of a capacitor or a load are typical examples of small disturbances; while a short circuit on a major power line is an example of a large disturbance. Unlike the transient stability, the small-disturbance stability is usually studied by analyzing the linearized equations of a given power system.

2.5 Voltage Stability

In large-scale integrated power systems, the mechanisms that might lead to voltage instability are to a certain extent interlinked with the rotor angle stability properties of the system, making the analysis of the instability phenomenon quite complicated [122]. Nevertheless, in the literature it is customary to distinguish between voltage and rotor angle stability phenomena. To facilitate the understanding of the various aspects of voltage instability mechanisms, the general and broad concept of ‘voltage stability’ is subdivided into two subcategories, namely Small and Large Disturbance Voltage Stability. These two concepts are defined as follows [75, 122].

Definition 13 *A power system is said to be small-disturbance voltage stable if it is able to maintain voltages identical or close to the steady values when subjected to small perturbations.*

Definition 14 *A power system is said to be large-disturbance voltage stable if it is able to maintain voltages identical or close to the steady values when subjected to large perturbations.*

Thus, a voltage stable power system is capable of maintaining the post-fault voltages near the pre-fault values. If a power system is unable to maintain the voltage within acceptable limits, the system undergoes voltage collapse.

2.6 Frequency Stability

Loosely defined, the term ‘frequency stability’ refers to the ability of the power system to maintain steady acceptable frequency following a severe system event

resulting in a large generation-load imbalance. Technically, the frequency stability is a system-wide phenomenon which primarily depends on the overall system response to the event and the availability of substantial power reserves.

It is not very likely that distributed generation will have significant impact on the frequency stability phenomenon in the near future; due to this fact, the frequency stability phenomenon is not studied in this thesis.

2.7 Summary

It can be noted that the definitions of voltage stability follow closely those of the rotor angle. Analogously, the analytical tools for studying the voltage stability phenomena are the same. That is, the small-disturbance stability can be effectively studied with the help of linearized models of the power system. Inspection of the eigenvalues of the state matrix provides sufficient information regarding the small-disturbance voltage stability of the power system in some neighborhood of a given operating point. On the other hand, the investigation of the large-disturbance voltage stability properties of the power grid, requires the use of nonlinear system analysis. This observation concludes the presentation of the various stability definitions relevant to the work presented in this thesis. The next section will briefly present modeling issues of such power system components as the synchronous and asynchronous generators, and solid oxide fuels cells.

*“All these constructions and the laws connecting them
can be arrived at by the principle of looking
for the mathematically simplest concepts
and the link between them.”*
— A. Einstein.

Chapter 3

Power System Modeling

“Obtaining maximum benefits from installed assets on an interconnected power system is becoming increasingly dependent on the coordinated use of automatic control systems. The ability to optimize the configuration of such control devices and their settings is dependent on having an accurate power system model, as well as controllers themselves” [5].

This compendious but neat quotation from a CIGRE report is cited here to signify the importance of having an accurate model of the system studied. Indeed, the development of an adequate model of the process is an essential part of engineering work. This chapter is therefore devoted to describing the basic models of some relevant power system components.

3.1 Main Components of Power Systems

The modern power systems are characterized by growing complexity and size. For example, the energy consumption in India doubles every 10 years, which also applies to some other countries [87]. As the dimensions of the power systems increase, the dynamical processes are becoming more complicated for analysis and understanding the underlying physical phenomena. In addition to the complexity and size, power systems do exhibit nonlinear and time-varying behavior.

In an electrical system the power cannot be stored¹, at each time instant there should be a balance between the total produced and consumed power. Mathe-

¹There are some exceptions e.g., a pump storage; however in those *energy* rather than *power* is stored.

matically this balance is expressed by differential and algebraic equations. The presence of algebraic equations significantly complicates both analytical and computational aspects of work when tackling with power systems.

To obtain a meaningful model of the power system, each component of the power system should be described by appropriate equations be it algebraic equations, differential equations, or both. For example, there are different models of an electrical generator; depending on the application a model of suitable exactness and complexity should be chosen to represent the generator in the study. On the one hand, very simple models of a generator are rarely used in power system studies when accuracy of the results is a great concern. On the other hand, if a system consists of 300 generators, each modeled by a set of three differential equations, the system analyst would have to process at least 900 differential equations describing the system as well as quite a few algebraic equations, the number of which depends on the topology of the network. The presence of other equipment, e.g., high voltage direct current (HVDC) systems, further contributes to the aforementioned number of equations. Clearly, it is barely possible to carry out any analytical study on such systems.

To overcome the problem of high dimension, the order of the system has to be reduced. This can be done in several ways:

- Based on the physical insights, several generators are aggregated in a group of coherent generators [88].
- Having set up the system equations, one applies a model reduction technique and eliminates the states that have little effect on the system dynamics [88].
- Using field measurements, one applies a system identification technique to obtain an equivalent model of the system [79].

Depending on the case study, any of the methods or a combination of them can be used to obtain ‘best’ dynamical models.

Linear and Nonlinear Systems

As was already mentioned, the nature of power systems is essentially nonlinear. Mathematically speaking, nonlinear systems are known to be very hard to manage. To work around this problem, when studying the behavior of a power system in a neighborhood of an equilibrium point, it is a common assumption that the power system is a linear, time-invariant system [101]. That is, the initial nonlinear system is approximated by a linear one. In many cases of practical importance, this

assumption works quite well yielding numerous advantages. However, when transient stability of the system is investigated, the use of a linear model may not be justified. There are several reasons for questioning the validity of the linear model; the main reason is the dependence of the qualitative behavior of a nonlinear model on the level of disturbance. This statement is further illustrated by the following

Example: Consider the following two systems described by second order homogeneous differential equations (DE)

$$\ddot{x}_1(t) + 0.01\dot{x}_1(t) + x_1(t) = 0, \quad (3.1)$$

$$\ddot{x}_2(t) + 0.01\dot{x}_2(t) + \sin x_2(t) = 0. \quad (3.2)$$

Equation (3.1) is a linear DE, while (3.2) is a nonlinear differential equation. We now determine the qualitative behavior of the solutions of (3.1) and (3.2).

Since the first equation is a linear equation with the eigenvalues having negative real part ($\Re(\lambda_{1,2}) = -1/200$), the domain of attraction is the whole plane. This means, for any choice of initial state of the system, the system state variables will always converge to the origin. This is confirmed by the explicit solution of (3.1)

$$x_1(t) = \exp(-t/200)C \sin(\omega_1 t + \phi),$$

where ω_1 is the imaginary part of the eigenvalue, the constants C and ϕ are determined by initial conditions. Clearly, $\lim_{t \rightarrow \infty} x_1(t) = 0, \forall C, \phi$.

Now equation (3.2) is examined. Despite its apparent simplicity, there exists no closed-form solution to this equation. The difficulty in finding closed-form solutions to nonlinear differential equations² has stimulated the search for other methods which allow the analyst to obtain a qualitative characteristics of a solution without actually having to solve the equation.

For the moment, this approach will not be pursued, instead the domain of attraction of this system will be found. This is done by integrating the equation backwards in time [128]. The domain of attraction³ is the region which includes the origin, see Fig. 3.1. If the initial state of the system was chosen inside the region, the system states will eventually converge to the origin, otherwise the origin will never be reached. \square

It is evident that for small deviations from the origin, equations (3.1) and (3.2) are equivalent ($\sin x \approx x$); as the deviations grow in magnitude, the difference in the behavior becomes more expressed. This example concludes the notes on qualitative difference between linear and nonlinear models.

²Only in some exceptional cases there exist closed-form solutions to nonlinear systems [127].

³The Bendixson theorem indicates that this domain is open.

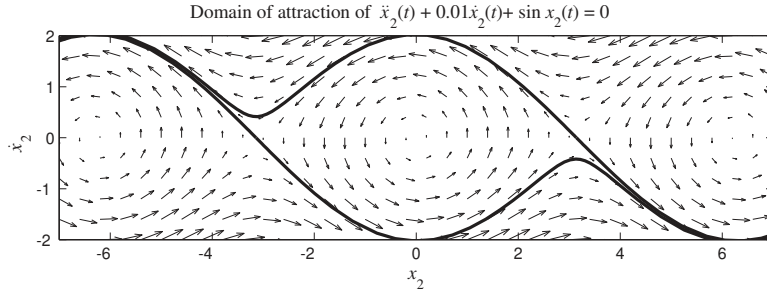


Figure 3.1: Domain of attraction of system (3.2)

Appreciating the importance of proper modeling of power system components, we first present the nonlinear and then linearized equations describing the basic components of power systems.

Modeling of Synchronous Machines

Synchronous machines are one of the most important power system components. They are also among the oldest pieces of electrical equipment in use. We commence by considering the equations describing a synchronous machine.

Depending on the nature of a study, several models of a synchronous generator, having different levels of complexity, can be utilized [74], [88]. In the simplest case, a synchronous generator is represented by a second-order differential equation, while studying fast transients in the generator's windings would require the use of a more detailed model, e.g., 7th order model.

In this project, fast dynamics of synchronous generators and the network are neglected and the generators are modeled by the two-axis model [107], i.e., it is assumed that the dynamical characteristics of a generator can be accurately represented by four differential equations, see (3.3)–(3.6).

$$\frac{d\delta_i}{dt} = \omega_i - \omega_s \quad (3.3)$$

$$M_i \frac{d\omega_i}{dt} = T_{M,i} - (E'_{q,i} - X'_{d,i} I_{d,i}) I_{q,i} - (E'_{d,i} + X'_{q,i} I_{q,i}) I_{d,i} - D_i (\omega_i - \omega_s) \quad (3.4)$$

$$T'_{do,i} \frac{dE'_{q,i}}{dt} = -E'_{q,i} - (X_{d,i} - X'_{d,i}) I_{d,i} + E_{fd,i} \quad (3.5)$$

$$T'_{do,i} \frac{dE'_{d,i}}{dt} = -E'_{d,i} - (X_{q,i} - X'_{q,i}) I_{q,i} \quad (3.6)$$

In the equations above, the following symbols are used to denote:

- δ_i : The rotor shaft angle of the i^{th} generator. Normally this angle is expressed in radians or degrees.
- ω_i, ω_s : The rotor angular velocity of the i^{th} generator. This velocity is commonly expressed in radians per second or per unit. ω_s is the synchronous speed of the system which usually takes two values $\omega_s = 100\pi, (120\pi)$ radians per second.
- M_i : The shaft inertia constant of the i^{th} generator which has the units of seconds squared.
- $T_{M,i}$: The mechanical torque applied to the shaft of the i^{th} generator.
- $E'_{q,i}, E'_{d,i}$: These symbols denominate the transient EMF's of the machine in the q and d axes, respectively.
- $I_{q,i}, I_{d,i}$: Are the equivalent currents of the synchronous machine in the q and d axes, respectively.
- D_i : The damping coefficient of the i^{th} generator.
- $T'_{do,i}, T'_{qo,i}$: Are transient time constants of the open circuit and a damper winding in the q -axis. These time constants are commonly expressed in seconds.
- $X_{q,i}, X_{d,i}, X'_{q,i}, X'_{d,i}$: These four symbols stand for the synchronous reactance and transient synchronous reactance of the i^{th} machine.

Sometimes equation (3.6) is eliminated yielding the third-order model of the synchronous generator. In the equations above, the index i runs from 1 to n , where n is the number of synchronous generators in the system. In our case studies, the number of synchronous machines does not exceed 2; yet in many studies this number may exceed several hundred.

Modeling the excitation system

Control of the excitation system of a synchronous machine has a very strong influence on its performance, voltage regulation, and stability [34]. Not only is the operation of a single machine affected by its excitation, but also the behavior of the whole system is dependent on the excitation system of separate generators. For example, inter-area oscillations are directly connected to the excitation of separate generators [71]. These are only a few arguments justifying the necessity for accurate and precise modeling of the excitation system of a synchronous machine. This subsection therefore presents the modeling principles of the excitation system. A detailed treatment of all aspects of the modeling is far beyond the scope of the thesis; we only synoptically present a literature survey on the subject.

There are different types of excitation systems commercially available in power industry. However, one of the most commonly encountered models is the so-called “IEEE Type DC1” excitation system. The main equations describing this model are listed below.

$$T_{E,i} \frac{dE_{fd,i}}{dt} = - (K_{E,i} + S_{E,i}(E_{fd,i})) E_{fd,i} + V_{R,i} \quad (3.7)$$

$$T_{A,i} \frac{dV_{R,i}}{dt} = -V_{R,i} + K_{A,i} R_{f,i} - \frac{K_{A,i} K_{F,i}}{T_{F,i}} E_{fd,i} + K_{A,i} (V_{ref,i} - V_i) \quad (3.8)$$

$$T_{F,i} \frac{dR_{f,i}}{dt} = -R_{f,i} + \frac{K_{F,i}}{T_{F,i}} E_{fd,i} \quad (3.9)$$

In these equations, the parameters and variables used are:

- $T_{E,i}, K_{E,i}, E_{fd,i}, S_{E,i}$: Time constant, gain, field voltage, and saturation function of the excitor.
- $V_{R,i}, T_{A,i}, K_{A,i}$: Exciter input voltage, time constant and gain of the voltage regulator (amplifier), respectively.
- $V_{ref,i}, V_i$: The reference and actual voltage of the i^{th} node.
- $R_{f,i}, K_{F,i}, T_{F,i}$: Transient gain reduction circuit parameters—state, gain, and time constant.

A block diagram of the exciter given by equations (3.7)–(3.9) is shown in Fig. 3.2. As is evident from (3.7)–(3.9), each excitor of the type DC1 adds three state variables to the state matrix.

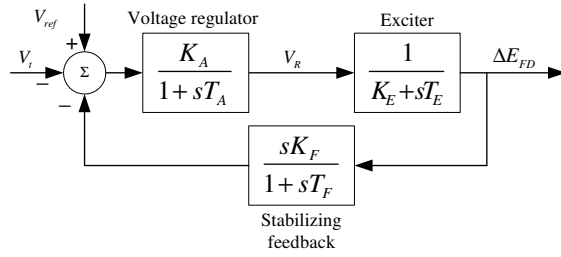


Figure 3.2: IEEE Type DC1 exciter system with saturation neglected

Modeling the turbine and governor

The number of poles of a synchronous generator and the speed of the prime mover determine the frequency of the ac current produced by the generator. In order to control the primer mover, turbine with associated controls are used in power systems. There exist two types of turbines—hydro and steam turbines. Only steam turbines will be presented here.

There are several models of the steam turbines in operation in power systems. We confine ourselves to exhibiting the simplest first-order models of the turbine and speed governor. The equations which model the dynamics of these devices are shown below [107].

$$T_{CH,i} \frac{dT_{M,i}}{dt} = -T_{M,i} + P_{SV,i} \quad (3.10)$$

$$T_{SV,i} \frac{dP_{SV,i}}{dt} = -P_{SV,i} + P_{C,i} - \frac{1}{R_i} \left(\frac{\omega_i}{\omega_S} \right). \quad (3.11)$$

The model (3.10)–(3.11), corresponds to a steam turbine with no reheater. The variables and parameters of equations (3.10)–(3.11) are given in [107]. While being important pieces of power system equipment, the dynamics of the turbine and governor are normally much slower⁴ than that of the exciter. This fact is often used as an argument for neglecting the dynamics of these devices.

⁴In [107] the following figures are given: $T_{SV} = 2$ sec. and $T_{CH} = 4$ sec. On the other hand, T_A is approximately 10 to 100 times smaller.

Asynchronous Generators

It is known that the essential dynamical properties of an asynchronous generator can be accurately described by the following model [73]

$$\begin{aligned}
\frac{1}{\omega_s} \frac{d\psi_{ds}}{dt} &= -\frac{r_s x_{rr}}{D} \psi_{ds} - \psi_{qs} + \frac{r_s x_m}{D} \psi_{dr} + v_{ds} \\
\frac{1}{\omega_s} \frac{d\psi_{qs}}{dt} &= \psi_{ds} - \frac{r_s x_{rr}}{D} \psi_{qs} + \frac{r_s x_m}{D} \psi_{qr} + v_{qs} \\
\frac{1}{\omega_s} \frac{d\psi_{dr}}{dt} &= -\frac{r_r x_{ss}}{D} \psi_{dr} + \frac{r_r x_m}{D} \psi_{ds} - \frac{\omega_s - \omega_r}{\omega_s} \psi_{qr} + \tilde{v}_{dr} \\
\frac{1}{\omega_s} \frac{d\psi_{qr}}{dt} &= -\frac{r_r x_{ss}}{D} \psi_{qr} + \frac{r_r x_m}{D} \psi_{qs} + \frac{\omega_s - \omega_r}{\omega_s} \psi_{dr} + \tilde{v}_{qr} \\
\frac{d\omega_r}{dt} &= \frac{\omega_s}{2H} (T_m - T_e), \tag{3.12}
\end{aligned}$$

where $x_{ss} = x_s + x_m$, $x_{rr} = x_r + x_m$, $D = x_{ss}x_{rr} - x_m^2$, $T_e = x_m(\psi_{qs}\psi_{dr} - \psi_{ds}\psi_{qr})/D$. x_r and x_s stand for the rotor and stator leakage reactances, respectively. x_m and ω_r signify the magnetizing reactance and the mechanical rotor angular frequency. The state variables ψ_{ds} , ψ_{qs} , ψ_{dr} , and ψ_{qr} are the d and q components of the stator and rotor flux linkages per second. [Note that the explicit dependence of the state variables on time is suppressed for notational ease.] r_s and r_r are the stator and rotor resistances, respectively. $\omega_s = 2\pi f_0$, where f_0 is the steady-state grid frequency (50 or 60 Hz.) Finally, v_{ds} (\tilde{v}_{dr}) and v_{qs} (\tilde{v}_{qr}) denote the d and q components of the stator (rotor) voltage. Unless otherwise specified, all the quantities are given in per unit. For more details on the model (3.12), the reader can refer to [73].

Neglecting the asynchronous generator's stator dynamics, i.e., assuming that $\omega_s^{-1} d\psi_{ds}/dt = 0$, $\omega_s^{-1} d\psi_{qs}/dt = 0$ and that the stator resistance is negligibly small, the following model of the asynchronous generator is obtained [23]:

$$\begin{aligned}
\frac{d\psi_{dr}}{dt} &= \omega_s \left[-\frac{r_r x_{ss}}{D} \psi_{dr} + \frac{r_r x_m}{D} v_{qs} + \frac{\omega_s - \omega_r}{\omega_s} \psi_{qr} + \tilde{v}_{dr} \right] \\
\frac{d\psi_{qr}}{dt} &= \omega_s \left[-\frac{r_r x_{ss}}{D} \psi_{qr} - \frac{r_r x_m}{D} v_{ds} \omega_s - \frac{\omega_s - \omega_r}{\omega_s} \psi_{dr} + \tilde{v}_{qr} \right] \\
\frac{d\omega_r}{dt} &= \frac{\omega_s}{2H} (T_m - T_e). \tag{3.13}
\end{aligned}$$

Introducing the constants $v_{dr} = \omega_s \tilde{v}_{dr}$, $v_{qr} = \omega_s \tilde{v}_{qr}$, $a_1 = r_r x_m \omega_s / D$, $a_2 = r_r x_{ss} \omega_s / D$ and denoting the state variables $x_1 = \psi_{dr}$, $x_2 = \psi_{qr}$, $x_3 = \omega = \omega_r - \omega_s$, we arrive at

the reduced-order model of the asynchronous generator:

$$\begin{aligned}\frac{dx_1}{dt} &= -a_2x_1 + x_2x_3 + a_1v_{qs} - v_{dr} \\ \frac{dx_2}{dt} &= -a_2x_2 - x_1x_3 - a_1v_{ds} - v_{qr} \\ \frac{dx_3}{dt} &= c_1 + c_2(v_{ds}x_1 + v_{qs}x_2)\end{aligned}\quad (3.14)$$

where $c_1 = \omega_s T_m / (2H)$ and $c_2 = -a_1 / (2Hr_r)$.

The steady state of the asynchronous generator is characterized by the equilibrium point $x^* = [x_1^*, x_2^*, x_3^*]'$ which renders the right-hand side of (3.14) zero⁵. There are 2 such points:

$$\begin{aligned}x_1^* &= \frac{1}{2a_2c_2v_s^2} [v_{qs} [c_2p_3 \pm p_4] - 2a_2c_1v_{ds}] \\ x_2^* &= \frac{-1}{2a_2c_2v_s^2} [c_2p_3 \pm p_4 + 2a_2c_1] \\ x_3^* &= \frac{1}{2c_1} [c_2p_3 \pm p_4],\end{aligned}\quad (3.15)$$

where the constants p_1, \dots, p_4 are defined as follows: $p_1 = v_{ds}v_{qr} - v_{qs}v_{dr}$, $p_2 = v_{ds}v_{dr} + v_{qs}v_{qr}$, $p_3 = a_1v_s^2 + p_1$, and $p_4 = \sqrt{c_2^2p_3^2 + 4a_2c_1c_2p_2 - 4a_2^2c_1^2}$. One of the points is asymptotically stable, while the second is unstable. For convenience of the analytical explorations presented in this section, the stable equilibrium point of the model (3.14) is translated to the origin by means of the change of coordinates $\xi_1 := x_1 - x_1^*$, $\xi_2 := x_2 - x_2^*$, $\xi_3 := x_3 - x_3^*$. This operation yields the model:

$$\begin{aligned}\dot{\xi}_1 &= -a_2\xi_1 + x_3^*\xi_2 + x_2^*\xi_3 + \xi_2\xi_3 \\ \dot{\xi}_2 &= -a_2\xi_2 - x_3^*\xi_1 - x_1^*\xi_3 - \xi_1\xi_3 \\ \dot{\xi}_3 &= c_2v_{ds}\xi_1 + c_2v_{qs}\xi_2.\end{aligned}\quad (3.16)$$

Note that the model (3.16) can be decomposed into two parts: linear and nonlinear. That is,

$$\dot{\xi} = \begin{bmatrix} -a_2 & x_3^* & x_2^* \\ -x_3^* & -a_2 & -x_1^* \\ c_2v_{ds} & c_2v_{qs} & 0 \end{bmatrix} \xi + \begin{bmatrix} \xi_2\xi_3 \\ -\xi_1\xi_3 \\ 0 \end{bmatrix}, \quad (3.17)$$

⁵In this thesis the prime denotes the transposition operator, unless explicitly stated otherwise.

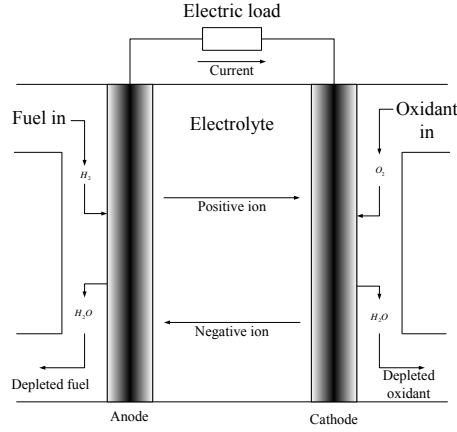


Figure 3.3: Simplified schematic diagram of a fuel cell

where ξ denotes the vector $[\xi_1, \xi_2, \xi_3]'$. The system (3.17) can be put in a more compact form

$$\dot{\xi} = A\xi + g(\xi). \quad (3.18)$$

For simplicity, sometimes the vector field $(A\xi + g)$ will also be denoted by $f(\xi)$ in this thesis.

3.2 Modeling of Solid Oxide Fuel Cells

A fuel cell is an electrochemical device that oxidizes fuel without combustion to directly convert the chemical energy of the fuel cell into electrical energy [9]. In simple terms, the fuel cell produces electric power by feeding a hydrogen-rich gaseous fuel to porous anode as an oxidant (air) is supplied to the cathode. The electrochemical reactions taking place at the electrodes result in electric current injected to the external circuit. Figure 3.3 schematically shows a simplified diagram of a fuel cell. The operational principle of fuel cells was discovered by the British amateur physicist W. Grove already in 1839. However, the commercial potential of the fuel cell technology was only recognized in the 1960's when fuel cells were successfully applied in the space industry. For example, the alkaline fuel cells belonging to the first generation of fuel cells were used in the Apollo space vehicles. Solid oxide fuel cells belong to the second generation of fuel cells. They are characterized by high operating temperatures (600 – 1000°C), use of ceramic electrolyte, the absence of external reformer, and the use of relatively cheap

catalysts. The high operating temperatures of SOFC result in a high temperature exhaust which can be utilized to increase the overall efficiency of the process. In recent years, the combined use of SOFC and a small-scale gas turbine (GT) or “microturbine” has been actively discussed. Analysis and experiments show that very high efficiencies (over 80%) can be achieved if the hot exhaust from the fuel cell is used to power a gas turbine [9]. It is argued in [9] and [126] that the capacity of the microturbine should be at most one third of the capacity of the SOFC/GT system. The technical and economical advantages of SOFC/GT systems make them attractive energy sources for distributed generation.

In addition to generating electric power at high efficiency, the SOFC/GT based distribution generation can also provide ancillary services such as load following and regulation. The technical feasibility of load following functionality of SOFC/GT systems is investigated in [135]. The numerical experiment results provided in [135] indicate that the fuel cell response times are significantly greater than those of the GT used in that study. This result implies that the GT rather than the fuel cells should be deployed in load following. The active power set-point of the fuel cell should only be adjusted when it is needed to substantially alter the net output of the SOFC/GT system. In this chapter, the main emphasis is placed upon the control challenges of the fuel cell rather than the dynamic properties of the microturbine; therefore, no dynamic model of the microturbine are developed. The presence of the microturbine will be indirectly accounted for by modeling the voltage deviations caused by the operation of the microturbine in the analyses presented here.

Fuel cell systems have to be interfaced with the distribution grid by means of a power converter, since the fuel cells produce dc power which has to be converted to ac. Normally, a forced-commutated voltage source inverter (VSI) is utilized for interfacing a fuel cell system. It is known that a VSI can provide fast and precise control of the voltage magnitude and reactive power output of the SOFC/GT system [85]. We, therefore, assume that the fuel cell power plant is equipped with a VSI, whose internal voltage control loops ensure an accurate control of ac voltage magnitude; it is also assumed that the converter losses can be neglected and that the time constants of the control are small enough to not be taken into account here.

Figure 3.4 depicts a one-line diagram of the fuel cell power plant along with its power conditioning unit (VSI). In this figure, $V_{fc} \angle \theta_{fc}$ denotes the ac voltage of the VSI. Although not mentioned explicitly, we assume that the fuel cell plant is connected to the distribution grid via a transformer which is represented in Fig. 3.4 by its leakage reactance X_l ; thus, $V_s \angle \theta_s$ is the voltage of secondary winding of the transformer representing the bus voltage of the fuel cell. In this case, the active

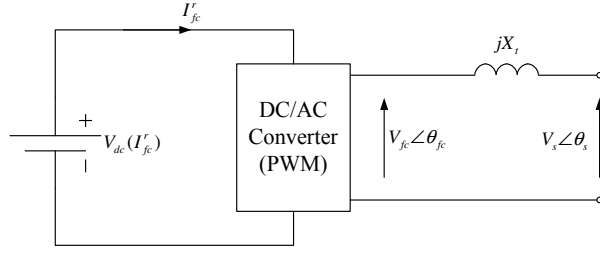


Figure 3.4: One-line diagram of a fuel cell-driven power plant.

power generated by the fuel cell is given by the following expression:

$$\begin{aligned}
 P_{fc} &= \frac{kmV_{dc}V_s}{X_t} \sin(\theta_{fc} - \theta_s) \\
 &= \frac{V_{fc}V_s}{X_t} \sin(\theta_{fc} - \theta_s), \tag{3.19}
 \end{aligned}$$

where k is a constant defined by the configuration of the VSI, V_{dc} is the dc voltage of the fuel cell, and m stands for the amplitude modulation index of the VSI. The voltage source inverter is operated in such a mode that the voltage V_s is kept constant for all times. That is, when an external disturbance is encountered which might cause a variation of V_s , the VSI controls the modulation index m to keep V_s constant, based on the typical control strategy of ac/dc converters. Equation (3.19) suggests that the output power of the fuel cell will change when m and/or angle θ_s vary. For instance, faults on the distribution grid might cause voltage magnitude variations as well as jumps in the phase angle θ_s . Thus, variations of V_{fc} and $\angle\theta_s$ can be seen as unwanted disturbances which should be attenuated by the control of the fuel cell in order to provide a constant active power output. Thus, it would be of interest to design an auxiliary controller which ensures a smooth output power regulation that is insensitive to small variations of m and angle of the distribution grid voltage.

We commence the design of such a controller by a closer examination of the controlled object, i.e., the fuel cell power plant.

Linearized model of SOFC

Making the following assuming that: (i) the fuel cell gases are ideal;(ii) it is sufficient to define only one single pressure value in the interior of the electrodes; (iii)

the fuel cell temperature is stable at all times; and (iv) Nernst's equation is applicable, the main equations describing the slow dynamics of a solid oxide fuel cell can be written as follows [135], [94]:

$$\frac{dI_{fc}^r}{dt} = \frac{1}{T_e} [-I_{fc}^r + I_{ref}] \quad (3.20a)$$

$$\frac{dq_{H_2}^{in}}{dt} = \frac{1}{T_f} \left[-q_{H_2}^{in} + \frac{2K_r}{U_{opt}} I_{fc}^r \right] \quad (3.20b)$$

$$\frac{dp_{H_2}}{dt} = \frac{1}{\tau_{H_2}} \left[-p_{H_2} + \frac{1}{K_{H_2}} [q_{H_2}^{in} - 2K_r I_{fc}^r] \right] \quad (3.20c)$$

$$\frac{dp_{H_2O}}{dt} = \frac{1}{\tau_{H_2O}} \left[-p_{H_2O} + \frac{2K_r}{K_{H_2O}} I_{fc}^r \right] \quad (3.20d)$$

$$\frac{dp_{O_2}}{dt} = \frac{1}{\tau_{O_2}} \left[-p_{O_2} + \frac{1}{K_{O_2}} \left[\frac{1}{\tau_{HO}} q_{H_2}^{in} - 2K_r I_{fc}^r \right] \right] \quad (3.20e)$$

$$I_{ref} = \begin{cases} q_{H_2}^{in} \frac{U_{max}}{2K_r}, & \text{if } \tilde{I} > q_{H_2}^{in} \frac{U_{max}}{2K_r} \\ q_{H_2}^{in} \frac{U_{min}}{2K_r}, & \text{if } \tilde{I} < q_{H_2}^{in} \frac{U_{min}}{2K_r} \\ \tilde{I} = P_{ref}/V_{ref}, & \text{otherwise,} \end{cases} \quad (3.21)$$

where I_{fc}^r is the fuel cell current; $q_{H_2}^{in}$ stands for the hydrogen input flow; and p_{H_2} , p_{O_2} , p_{H_2O} denote the partial pressures of hydrogen, oxygen, and water, respectively. The time constants T_e , T_f , τ_{H_2} , τ_{H_2O} , τ_{O_2} , designate the electrical response time of the fuel cell, fuel processor response time, response times of hydrogen, water, and oxygen flows, respectively. K_{H_2} , K_{H_2O} , and K_{O_2} , denote the valve molar constants for hydrogen, water, and oxygen. The auxiliary constants U_{opt} , U_{max} , and U_{min} stand for the optimal, maximum, and minimum fuel utilization, respectively. Finally, $K_r = N_0/(4F)$. The numerical values of the aforementioned constants can be found in [135] and [94].

The dc voltage across the stack of the fuel cells is governed by the Nernst equation, i.e.,

$$V_{dc} = N_0 \left[E_0 + \frac{RT}{2F} \log \left(\frac{p_{H_2} p_{O_2}^{1/2}}{p_{H_2O}} \right) \right] - r I_{fc}^r, \quad (3.22)$$

where r , R , T , E_0 , and N_0 are the ohmic loss of the fuel cell, universal gas constant, absolute temperature, the ideal standard potential, and the number of fuel cells in series in the stack. The active (dc) power produced by the fuel cell is then given by the following relation:

$$P_{fc} = V_{dc} I_{fc}^r. \quad (3.23)$$

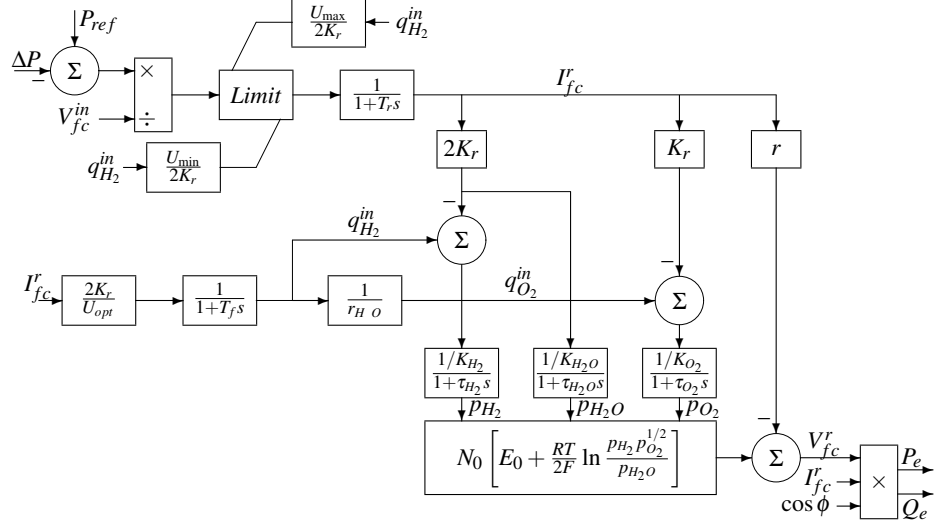


Figure 3.5: SOFC system block diagram

The dynamic equations (3.20) of the fuel cell are linear; the only nonlinearities in these expressions are in the stack voltage and the active power equations. The block diagram of the SOFC plant with its basic auxiliary controls is shown in Fig. 3.5.

To obtain the complete linear model, equations (3.19), (3.22), and (3.23) have to be linearized about the equilibrium point. The resulting linear model contains 5 state variables and can be represented by

$$\dot{x}(t) = Ax(t) + Bu(t) \quad (3.24)$$

$$y(t) = Cx(t) + Du(t), \quad (3.25)$$

where $x = [\Delta I_{fc}^r, \Delta q_{H_2}^{in}, \Delta p_{H_2}, \Delta p_{H_2O}, \Delta p_{O_2}]'$ (here, a prime denotes transposition). For convenience of notation, in the remainder of the chapter, the symbol Δ is omitted for simplicity, but small deviations from the equilibrium are assumed. Also, the explicit dependence of the plant states, inputs, and outputs on time is suppressed for simplicity of notation. The state matrix $A \in \mathbb{R}^{5 \times 5}$ can be easily extracted from the dynamic equations (3.20); $B \in \mathbb{R}^{5 \times 3}$; $C \in \mathbb{R}^{1 \times 5}$; and $D \in \mathbb{R}^{1 \times 3}$ are the input, output, and direct feedthrough matrix (their numerical values are given in the Appendix). The input vector and the output are denoted by $u = [\Delta m, \Delta \theta_s, \Delta P_{ref}]'$ and $y = P_{fc}$, respectively.

3.3 Algebraic Constraints in Power Systems

As was briefly explained in Section 3.1 on page 20, the power systems are described by a set of differential and algebraic equations. The origins of the differential equations have already been discussed, while those of the algebraic equations are the main subject of this section.

The main equations relating the algebraic variables of the power system are given below.

$$0 = V_i e^{j\theta_i} + (R_{s,i} + jX'_{d,i})(I_{d,i} + jI_{q,i})e^{j(\delta_i - \frac{\pi}{2})} - [E'_{d,i} + (X'_{q,i} - X'_{d,i})I_{q,i} + jE'_{q,i}]e^{j(\delta_i - \frac{\pi}{2})} \quad (3.26)$$

$$0 = -P_i - jQ_i + V_i e^{j\theta_i} (I_{d,i} - jI_{q,i})e^{-j(\delta_i - \frac{\pi}{2})} + P_{L,i}(V_i) + jQ_{L,i}(V_i) \quad (3.27)$$

$$0 = -P_i - jQ_i + P_{L,i}(V_i) + jQ_{L,i}(V_i) \quad (3.28)$$

$$0 = -P_i - jQ_i + \sum_{k=1}^n V_i V_k Y_{i,k} e^{j(\theta_i - \theta_k - \alpha_{i,k})} \quad (3.29)$$

In equations (3.26)–(3.29), the following notation is adopted:

- V_i, θ_i The magnitude and phase angle of the i^{th} node.
- P_i, Q_i The active and reactive power injection in the i^{th} node.
- $P_{L,i}, Q_{L,i}$ The active and reactive power of the load connected to the i^{th} node. These quantities generally are nonlinear functions of the node voltage.
- $Y_{i,k} e^{j\alpha_{i,k}}$ The complex admittance of the branch connecting the i^{th} and k^{th} nodes.
- $R_{s,i}$ The resistance of the stator of i^{th} generator.

The rest of the variables and parameters have been introduced earlier in this chapter. The number of the algebraic equations is dependent on the topology network, though the structure of the equations is generic and always corresponds to that shown in this section.

It is preferable to eliminate as many algebraic variables as possible and deal with differential equations only, which is much simpler. In the special case of constant impedance loads, which is always the case in this thesis, it is possible to reduce the total number of algebraic variables to $2n$ equations. That is, the

only remaining variables are the complex nodal voltages. To eliminate the stator currents one has to solve equation (3.26) for $I_{q,i}$ and $I_{d,i}$. After some manipulation, the following expressions are obtained:

$$I_{q,i} = -\frac{X'_{d,i}V_i \sin(\theta_i - \delta_i) + V_i R_{s,i} \cos(\theta_i - \delta_i) + X'_{d,i}E'_{d,i} - E'_{q,i}R_{s,i}}{X'_{d,i}X'_{q,i} + R_{s,i}^2} \quad (3.30)$$

$$I_{d,i} = \frac{V_i R_{s,i} \sin(\theta_i - \delta_i) + E'_{d,i}R_{s,i} - X'_{q,i}V_i \cos(\theta_i - \delta_i) + X'_{q,i}E'_{q,i}}{X'_{d,i}X'_{q,i} + R_{s,i}^2} \quad (3.31)$$

Having done this, one can substitute equations (3.30) and (3.31) into (3.26)–(3.29). Moreover, one could reduce the number of algebraic states by eliminating the active P and reactive Q power from equations (3.26) – (3.29).

“... But in this respect hardly any other method of investigation could be said to be completely satisfactory.”
— A. A. Lyapunov
On the generality of his method.

Chapter 4

Energy Function Analysis of Mixed Power Systems

The Direct Lyapunov Method is one of the most powerful and well understood analytical tools for investigating the dynamic properties of electric power systems and other nonlinear systems. Lyapunov’s method establishes a uniform framework for the assessment of stability of the power system by analyzing an appropriate Lyapunov or energy function. The main advantages of the Lyapunov method are the possibility to perform parametric stability studies and the feasibility to conclude stability without having to solve the nonlinear differential equations describing the system. On the other hand, a practical application of the Lyapunov theory to transient stability analysis is often a nontrivial task, since finding a suitable Lyapunov function is almost always a challenge. To overcome the difficulties inherent in the classical Lyapunov theory, the so-called Extended Invariance Principle (EIP) can be considered [25]. The Extended Invariance Principle is an important extension of LaSalle’s invariance principle which is in turn an extension of Lyapunov’s direct method. A function satisfying the conditions of the Extended Invariance Principle is called an extended Lyapunov function. This chapter briefly presents the basic concepts of Lyapunov’s direct method and the Extended Invariance Principle and reports the main findings of this thesis related to the transient stability analysis of power systems with asynchronous generators.

4.1 Mathematical Preliminaries

The Direct Lyapunov Method

The Lyapunov theory is essentially based on the existence of a scalar (energy or Lyapunov) function that establishes the sufficient conditions for stability of the dynamic system in question. Furthermore, the properties of the Lyapunov function and its Lie derivative provide auxiliary information about the attraction region of a given equilibrium point. This subsection presents a rudimentary introduction to the Direct Lyapunov Method¹

Let the unforced system be described by the set of autonomous nonlinear differential equations:

$$\dot{x} = f(x), \quad (4.1)$$

where $x(t) \in U \subseteq \mathbb{R}^n$ is the vector of state variables and f stands for a continuous map from \mathbb{R}^n to \mathbb{R}^n . Without loss of generality, assume that the origin is the equilibrium point of (4.1). Then the origin of (4.1) is asymptotically stable if there exists a C^1 function $V(x)$ such that [68]

1. $V(0) = 0$,
2. $V(x)$ is positive definite $\forall x \neq 0$,
3. $\mathcal{L}_f V = \partial V / \partial x' \cdot f(x) = dV/dt < 0, \forall x$,

where $\mathcal{L}_f V$ is the Lie derivative of V along the vector field f . Thus, the stability properties of the system can be established by analyzing an appropriate Lyapunov function. If a such a function is found, than the origin of (4.1) is asymptotically stable; however, since the Lyapunov Direct Method establishes only a sufficient condition for stability of the system of interest, the actual system can be classified by the Lyapunov function as unstable, while in fact it could remain stable. On the other hand, if a positive definite function is found such that its Lie derivative is also positive definite, than the system can be immediately classified unstable.

Example: Consider the set of autonomous ordinary differential equations [108]

$$\dot{x}(t) = -x(t) + 2y(t), \quad \dot{y}(t) = -2x(t) - y^3(t) \quad (4.2)$$

and the following Lyapunov function candidate $V(x) = \|x\|^2$. The Lie derivative of V is given by the expression

$$\mathcal{L}_f V(x) = -2y^2(1 + y^2) - 2x^2.$$

¹The terms ‘Direct’ and ‘Second’ Lyapunov Method are used in this chapter synonymously.

Clearly, both V and $-\mathcal{L}_f V$ are positive definite in the whole state space, which establishes global asymptotic stability of (4.2) ‘in-the-large’. \square

Example: Consider the set of autonomous linear differential equations

$$\dot{x} = Ax, \quad (4.3)$$

where $A \in \mathbb{R}^{n \times n}$ has distinct eigenvalues $\{\lambda_i\}_1^n$. Changing the coordinates by the similarity transformation $z = Tx$, where T is the matrix of right eigenvalues of A , the system (4.3) can be transformed to diagonal form

$$\dot{z} = \Lambda z,$$

where $\Lambda = \text{diag}(\lambda_1, \lambda_2, \dots, \lambda_n)$. Let us now apply the direct Lyapunov method to investigate the stability of (4.3). Consider the Lyapunov function candidate

$$V(z) = -z'(\Lambda + \Lambda^*)z,$$

where the symbol Λ^* denotes the complex conjugate of Λ . The Lie derivative of $V(z)$ is

$$\mathcal{L}_f V(z) = -z'(\Lambda + \Lambda^*)^2 z.$$

Observe that $\mathcal{L}_f V(z)$ is at least negative semidefinite, thus the stability of (4.3) can be determined by inspecting the Lyapunov function $V(z)$ alone. Indeed, if all $\Re(\lambda_i) < 0$, then (4.3) is globally exponentially stable. If any of $\Re(\lambda_i) > 0$, then the system (4.3) is unstable, since for any ε -neighborhood of the origin there is an escape segment for the system trajectory. Therefore, it can be concluded that a linear system is stable if all the eigenvalues of its state matrix have negative real parts; and conversely: a linear system is unstable if any of the eigenvalues has positive real part. \square

Despite the fact that the Lyapunov Direct Method has proven a very useful and practical analytical tool, it is commonly recognized that finding an appropriate Lyapunov function for a problem at hand is often a complicated mathematical exercise. As a matter of fact, there is no general systematic procedure for constructing Lyapunov functions for nonlinear systems of orders greater than 2.

This and some other considerations have stimulated the research in the area of ordinary differential equations and eventually resulted in the discovery of Extended Invariance Principle [25], [100] which allows a wider class of functions to be used for the assessment of the stability properties.

4.2 Extended Invariance Principle

Consider again the set of n autonomous ordinary differential equations (4.1) describing the power system. A simplified (weak) version of the invariance principle is given by the following

Theorem 1 *Let $V : \mathbb{R}^n \rightarrow \mathbb{R}$ be a continuous function. Also, let a scalar L be a constant such that $\Omega_L = \{x \in \mathbb{R}^n \mid V(x) < L\}$ is bounded. Let $C := \{x \in \Omega_L \mid \mathcal{L}_f V(x) > 0\}$, suppose that $\sup_{x \in C} V(x) = l < L$. Define $\bar{\Omega}_l = \{x \in \mathbb{R}^n \mid V(x) \leq l\}$ and $E := \{x \in \Omega_L \mid \mathcal{L}_f V(x) = 0\} \cup \bar{\Omega}_l$. Let \mathcal{B} be the largest invariant set of (4.1) contained in E . Then, all solutions of (4.1) originating in Ω_L converge to \mathcal{B} , as $t \rightarrow \infty$. \square*

A proof of the theorem can be found in [100]. Paraphrasing the theorem, it can be said that it establishes sufficient conditions for stability of (4.1) in terms of the sets $\Omega_L, \bar{\Omega}_l, E$ and the function V : if such sets and V exist, then the system (4.1) is stable in the Lyapunov sense, provided the initial conditions are such that $x(0) \in \Omega_L$. The sets introduced in the theorem are schematically shown in Fig. 4.1. The major difference between LaSalle's invariance principle and the EIP is in the fact that the EIP allows the Lie derivative $\mathcal{L}_f V(x)$ to be greater than zero on some bounded set of nonzero measure, which implies that a significantly larger class of positive definite functions can be used as extended Lyapunov function candidates (ELFC).

A further exploration of Theorem 1 reveals that the direct application of EIP is not straightforward, since the auxiliary requirements stated in the theorem have to be fulfilled. That is, a suitable extended Lyapunov function $V(x)$ has to be found, then it has to be shown that there exist two bounded sets Ω_L and C ; in addition, the constant l has to be computed, which in itself is a complicated numerical task. Assuming that a suitable extended Lyapunov function candidate is found, verification of the other conditions of the theorem can be simplified if the methods of interval arithmetic are applied. The basic facts about interval arithmetics are gathered in Appendix A.

A preliminary study performed within this project has indicated that the development of a Lyapunov function for a power system with both synchronous and asynchronous generators is a nontrivial task; therefore, it was decided to first analyze a simple power system consisting of a single generator connected to an infinite bus and then extend the results to a larger number of generators. We therefore commence by the construction of a Lyapunov function for a single asynchronous machine-infinite bus (SAMIB) system.

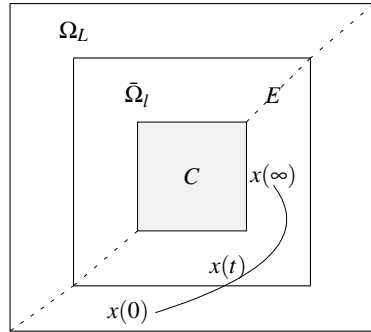


Figure 4.1: Graphical illustration of the Extended Invariance Principle. All trajectories $x(t)$ with $x(0) \in \Omega_L$ converge to the largest invariant set contained in E .

4.3 Single Asynchronous Machine-Infinite Bus System

Often DG power plants [e.g., microturbines and wind mills in a wind farm] consist of a large number of individual generators. For detailed simulations, each generator should be modeled separately; however, for the purposes pursued in this study, an aggregation of the generators should be carried out. Although being an interesting problem in its own right, the aggregation is not considered here; instead, it is assumed that such an aggregation has already been done, using an aggregation technique, e.g., that reported in [14]. That is, the DG power plant is represented by a single aggregate, whose parameters can be readily determined from the parameters of the individual generators. Fig. 4.2 shows such an aggregated DG power plant. As can be seen in the figure, this simplified system consists of an asynchronous generator denoted as AG , a step-up transformer T , a local constant impedance load LD , and two lines $L1-L2$ connecting the plant to the main grid. The short circuit capacity of the main grid is assumed to be much greater than the installed capacity of the farm. This assumption is not limiting, since the ‘stiffness’ of the main grid can be reduced by adjusting the impedance of the lines $L1$ and $L2$. The power factor correcting capacitors are included in the load LD . Figure 4.3 shows the one-line diagram of the system studied. In the figure, the impedances of the lines and the transformer are lumped into a single impedance Z_1 , thus eliminating the node 2. Let us introduce the following notation: v_∞ denotes the voltage of the main grid, v_s is the terminal voltage of the asynchronous generator, T_m and T_e are mechanical and electrical torques of the generator, respectively. Applying the

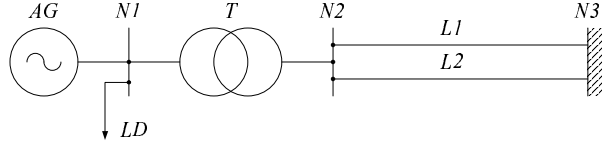


Figure 4.2: Single Asynchronous Machine Infinite Bus system

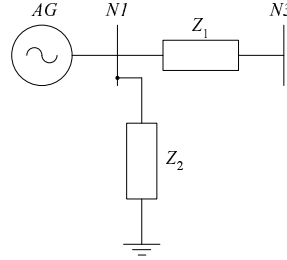


Figure 4.3: Impedance diagram of the SAMIB system

superposition principle, the relationship between v_s and v_∞ can be derived

$$v_s = \frac{Z_2}{Z_1 + Z_2} v_\infty, \quad (4.4)$$

where Z_2 is the load impedance including the phase compensation.

In order to construct a Lyapunov function for the SAMIB system, several well-known methods are tried. The next section summarizes the results of these attempts.

4.4 Transient Stability Analysis of the SAMIB System

Verification of the Energy Metric Algorithm

The Energy Metric Algorithm has been successfully used for the construction of energy functions for various nonlinear dynamic systems, including detailed power systems [47, 131]. It is therefore natural to attempt to construct a Lyapunov function for the system (3.17) using the Energy Metric Algorithm [131].

The main steps of the algorithm for constructing a Lyapunov function for (3.17) are outlined in Algorithm 1.

Algorithm 1:

1. Eliminate the time variable from the differential equations describing the system

$$\frac{d\xi_1}{d\xi_2} = \frac{-a_2\xi_1 + x_3^*\xi_2 + x_2^*\xi_3 + \xi_2\xi_3}{-a_2\xi_2 - x_3^*\xi_1 - x_1^*\xi_3 - \xi_1\xi_3} \quad (4.5)$$

$$\frac{d\xi_2}{d\xi_3} = \frac{-a_2\xi_2 - x_3^*\xi_1 - x_1^*\xi_3 - \xi_1\xi_3}{c_2v_{ds}\xi_1 + c_2v_{qs}\xi_2} \quad (4.6)$$

$$\frac{d\xi_3}{d\xi_1} = \frac{c_2v_{ds}\xi_1 + c_2v_{qs}\xi_2}{-a_2\xi_1 + x_3^*\xi_2 + x_2^*\xi_3 + \xi_2\xi_3} \quad (4.7)$$

2. Convert the differential equations to 3 one-forms ω_i by multiplying and clearing the denominator terms.
3. Reduce the one-forms to a single one-form $\omega(\xi)$ by addition and substitution of the 3 one-forms.
4. Perform line integration of $\omega(\xi)$ along some path, which for simplicity can be chosen along the ‘elbow’ path. \square

It appears however that no Lyapunov function can be constructed for the system (3.17) using the Energy Metric Algorithm. This result is summarized in the following

Proposition 1 *The model (3.17) admits no energy function constructed by Algorithm 1.* \square

Proof Consider the line integral generated by Algorithm 1.

$$\begin{aligned} V = \int_{\Gamma} & \{ a_2c_2v_{qs}\xi_2 + a_2c_2v_{ds}(\xi_1 + \xi_2) + c_2v_{ds}(\xi_1 + x_1^*)\xi_3 \\ & + c_2v_{ds}\xi_1x_3^* \} d\xi_1 + \{ c_2v_{ds}(\xi_1 + \xi_2 + x_2^*)\xi_3 \\ & + c_2v_{ds}(\xi_1 + \xi_2)x_3^* + c_2v_{qs}\xi_2(\xi_3 + x_3^*) \\ & + a_2c_2v_{qs}\xi_2 \} d\xi_2 + \{ a_2^2(\xi_1 + \xi_2) + a_2\xi_1x_3^* \\ & + a_2(\xi_1 + x_1^* - x_2^*)\xi_3 + (\xi_1 + x_1^*)\xi_3(\xi_3 + x_3^*) \\ & + \xi_1x_3^*(\xi_3 + x_3^*) \} d\xi_3, \end{aligned} \quad (4.8)$$

where Γ stands for the elbow path. The Lyapunov function candidate can be rewritten in a more compact form:

$$V(\xi) = \int_{\Gamma} \sum_{i=1}^3 \Xi_i(\xi) d\xi_i, \quad (4.9)$$

where the variables entering the equation can be readily identified from (4.8). In order to constitute a valid energy function—which is a necessary condition—the functions $\Xi_i(\xi)$ in (4.9) must fulfil the following condition²: $\partial \Xi_i(\xi) / \partial \xi_k = \partial \Xi_k(\xi) / \partial \xi_i, \forall i, k \in \{1, 2, 3\}$, which would guarantee the path independence of the integral (4.8). Direct inspection of the matrix $\partial \Xi_k(\xi) / \partial \xi_i$ shows that the symmetry requirements are not fulfilled³:

$$\partial \Xi_k(\xi) / \partial \xi_i = \begin{bmatrix} h_{11} & 0 & 0 \\ c_2 v_{ds} x_3^* & h_{22} & 0 \\ h_{31} & 0 & h_{33} \end{bmatrix}, h_{31} > 0, \forall \xi. \quad (4.10)$$

This observation completes the proof. \square

Now a few auxiliary observations are due, which are formulated in the form of corollary and conjecture.

Corollary 1 *The [empirical] existence of a stable equilibrium of the SAMIB system, for instance the equilibrium given by (3.15), and the converse Lyapunov theorems imply that there must exist a valid Lyapunov function for the model (3.18). However, the structure of the Lyapunov function will necessarily differ from that generated by Algorithm 1.* \square

Conjecture 1 *The non-existence of a Lyapunov function in the form (4.8) for a single generator suggests that no Lyapunov function of this type can be found for a multimachine power system. On the other hand, it is possible to use a quadratic Lyapunov functions for the estimation of the attraction region of a multimachine power system; however, it can also be problematic due to the possible conservatism of the estimates.* \square

It should however be stated that the quadratic Lyapunov functions can be quite useful if other applications are considered, such as the design of Control Lyapunov functions.

²For details, the reader is referred to Appendix B.

³In the equation above the elements h_{ii} are not shown as they are irrelevant.

Verification of the First Integral of Motion Algorithm

The first integral of motion has been successfully used in power system applications for generating Lyapunov functions [95]. To facilitate the presentation, the essential steps of the construction of a Lyapunov function using this technique are highlighted in the following

Algorithm 2:

1. Define the quantity dt as is shown below

$$dt = \frac{d\xi_1}{-a_2\xi_1 + x_3^*\xi_2 + x_2^*\xi_3 + \xi_2\xi_3} \quad (4.11)$$

$$= \frac{d\xi_2}{-a_2\xi_2 - x_3^*\xi_1 - x_1^*\xi_3 - \xi_1\xi_3} \quad (4.12)$$

$$= \frac{d\xi_3}{c_2v_{ds}\xi_1 + c_2v_{qs}\xi_2} \quad (4.13)$$

2. Perform line integration of the separate pairs (4.11)–(4.13) along the system's post-fault trajectory.
3. Identify the energy function as the function obtained in the previous step. \square

Let us now show that Algorithm 2 cannot be applied to generate a Lyapunov function for (3.17).

Proposition 2 *The model (3.17) admits no Lyapunov function constructed by Algorithm 2.* \square

Proof The necessary and sufficient condition for the existence of a Lyapunov function generated by Algorithm 2 is the following equality

$$\text{Trace } \nabla(A\xi + g) = 0, \quad (4.14)$$

where ∇ denotes the gradient of the vector field $A\xi + g$. As can be easily verified, in the present case the equality (4.14) does not hold. \square

Verification of Krasovskii's method for the SAMIB system

Another well-known method for the construction of Lyapunov functions is due to Krasovskii [68]. The mathematical machinery of Krasovskii's method is fairly simple and is summarized in the following theorem [19]:

Theorem 2 Let $f(\xi)$ be differentiable w.r.t. ξ and let $f(0) = 0$; then the origin is: (a) stable if the matrix $H = \partial f' / \partial \xi + \partial f / \partial \xi'$ is negative semidefinite in some neighborhood \mathcal{N} of the origin, (b) asymptotically stable if H is negative definite in \mathcal{N} , or (c) asymptotically stable in the large if H is negative definite for all ξ and $f'f$ is radially unbounded. \square

Let us now show that Krasovskii's method fails to yield a Lyapunov function for the SAMIB system. This statement is formulated in the following

Proposition 3 The model (3.17) admits no Lyapunov function constructed by the method of Krasovskii. \square

Proof Clearly, the conditions of Theorem 2 are fulfilled for the system (3.17), i.e., $(A\xi + g(\xi))(0) = 0$ and $(A\xi + g(\xi))$ is continuously differentiable in the entire state space. Moreover, the function $\|(A\xi + g(\xi))\|_2^2 = (A\xi + g(\xi))'(A\xi + g(\xi))$ is radially unbounded, i.e., $\lim_{\|\xi\| \rightarrow \infty} \|(A\xi + g(\xi))\|_2^2 = \infty$.

Let us now determine the sign definiteness of the matrix H . Omitting the algebra, this matrix can be written in the following form

$$H = \left[\begin{array}{c|c|c} -2a_2 & 0 & c_2v_{ds} + \xi_2 + x_2^* \\ \hline 0 & -2a_2 & c_2v_{qs} - \xi_1 - x_1^* \\ \hline c_2v_{ds} + \xi_2 + x_2^* & c_2v_{qs} - \xi_1 - x_1^* & 0 \end{array} \right]$$

The application of Sylvester's criterion indicates that H in this particular case is negative definite if and only if its determinant is negative. However, the determinant is nonnegative for all $\xi \in \mathbb{R}^3$, as (4.15) shows.

$$|H| = 2a_2((c_2v_{ds} + \xi_2 + x_2^*)^2 + (c_2v_{qs} - \xi_1 - x_1^*)^2) \quad (4.15)$$

Therefore, H is sign indefinite, which implies that $f'f$ does not qualify as a valid Lyapunov function. This concludes the proof. \square

The Existence of a Quadratic Lyapunov Function

As was already stated in Corollary 1, for any dynamic system [with differentiable vector field] possessing a stable equilibrium there exists an appropriate Lyapunov function in some neighborhood of the equilibrium.

A naïve reasoning of this statement applied to the present system (3.17) may include the following line of argumentation. Since the vector field $(A\xi + g)$ in our

case can be directly decomposed into a linear and nonlinear part, and the 2-norm of the nonlinear part vanishes as $\|\xi\|_2$ approaches the origin, i.e.,

$$\lim_{\|\xi\|_2 \rightarrow 0} \|g(\xi)\|_2 / \|\xi\|_2 = 0,$$

in some neighborhood \mathcal{N} of the equilibrium the dynamics of the linear part will dominate those of the nonlinear part⁴. Therefore, the stability of the equilibrium will be solely determined by the eigenvalues of the matrix $A, \forall \xi \in \mathcal{N}$. Therefore, if all the eigenvalues have strictly negative real parts, there should exist an appropriate quadratic Lyapunov function which can be found by solving the corresponding matrix Lyapunov equation or determined as in the example on page 36. It is however known, that in practical applications such quadratic Lyapunov functions yield overly conservative estimates of the associated attraction domain; therefore, the application of quadratic Lyapunov functions will not be pursued in this thesis. Instead, the system model will be reformulated in order to facilitate the construction of an appropriate Extended Lyapunov function.

4.5 Alternative Formulation of the System Model

Let us reformulate the model (3.13) in order to obtain an alternative representation of the asynchronous generator in the polar coordinates (E, δ) :

$$\begin{aligned} E &= \frac{x_m}{x_{rr}} \sqrt{\psi_{dr}^2 + \psi_{qr}^2} \\ \delta &= \tan^{-1}(-\psi_{qr}/\psi_{dr}). \end{aligned} \quad (4.16)$$

Then assuming for simplicity that the rotor voltages are zero and defining $T_0 = x_{rr}/(\omega_s r_r)$, $X' = x_{ss} - x_m^2/x_{rr}$ the model (3.13) transforms to the following system of equations

$$\frac{d\delta}{dt} = \omega_r - \omega_s - \frac{X_s - X'}{X'T_0E} v_s \sin(\delta + \phi) \quad (4.17)$$

$$\frac{d\omega_r}{dt} = -\frac{E}{X'M} v_s \sin(\delta + \phi) + \frac{T_m}{M} \quad (4.18)$$

$$\frac{dE}{dt} = -\frac{X_s}{X'T_0} E + \frac{X_s - X'}{X'T_0} v_s \cos(\delta + \phi). \quad (4.19)$$

⁴In most practical cases (i.e., $f \in C^1$) this decomposition can also be done as follows: $f(x) := (\partial f'/\partial x)x + \{f(x) - (\partial f'/\partial x)x\} = Ax + g(x)$.

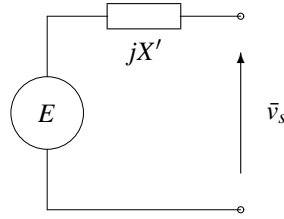


Figure 4.4: Equivalent circuit of the model (4.20)–(4.22)

In equations (4.17)–(4.19) it was assumed that $v_{qs} = v_s \cos \phi$ and $v_{ds} = v_s \sin \phi$, where v_s and ϕ are the magnitude and phase angle of the stator voltage \bar{v}_s . To simplify the notation, let us denote $\omega = \omega_r - \omega_s$ and introduce the following constants: $\eta_1 = X_s/(X'T_0)$, $\eta_2 = v_s(X_s - X')/(X'T_0)$, $\theta = \delta + \phi$, $\eta_3 = T_m/M$, and $\eta_4 = v_s/(X'M)$. To make the model more realistic, a damping term $D = T_f/M$ proportional to the friction torque T_f is added to (4.18), resulting in the following model

$$\frac{d\theta}{dt} = \omega - \frac{\eta_2}{E} \sin \theta \quad (4.20)$$

$$\frac{d\omega}{dt} = \eta_3 - \eta_4 E \sin \theta - D\omega \quad (4.21)$$

$$\frac{dE}{dt} = -\eta_1 E + \eta_2 \cos \theta. \quad (4.22)$$

It can be noticed that the model given by the equations (4.20)–(4.22) to a certain degree resembles the equations describing a single machine system with flux decay model; however, the physical meaning of the state variables of these two models is quite different [95]. Figure 4.4 shows the equivalent circuit of the model.

Construction of the Lyapunov function for the simplified SAMIB system

Construction of a suitable Lyapunov function or Extended Lyapunov function for the system (4.20)–(4.22) has proven a very challenging mathematical task, which confirmed the main conclusions from Section 4.4. Therefore, it was decided to further reduce the order of the model. To do so, we postulate that

$$\eta_1^{-1} \dot{E} \rightarrow 0, \quad (4.23)$$

which renders E an algebraic variable. This approximation can be justified by the following argument.

Consider again the differential equation describing the time evolution of E , i.e., (4.22). Let us now solve the equation, assuming that θ is an unknown function of time. The solution is given by the expression

$$E(t) = E_0 \exp(-\eta_1 t) + \exp(-\eta_1 t) \eta_2 \int_0^t \exp(\eta_1 \tau) \cos \theta(\tau) d\tau. \quad (4.24)$$

Taking the absolute value of both sides of (4.24) and noting that $\exp(\eta_1 \tau) \cos \theta(\tau)$ is dominated by $\exp(\eta_1 \tau)$, the following inequality can be obtained

$$|E(t)| \leq E_0 \exp(-\eta_1 t) + \exp(-\eta_1 t) \eta_2 \left| \int_0^t \exp(\eta_1 \tau) d\tau \right|. \quad (4.25)$$

Evaluating the integral in (4.25), the estimate of $E(t)$ reduces to

$$|E(t)| \leq E_0 \exp(-\eta_1 t) + \frac{\eta_2}{\eta_1} (1 - \exp(-\eta_1 t)). \quad (4.26)$$

Clearly, for large values of η_1 , the internal voltage $E(t)$ is mainly determined by the quotient η_2/η_1 . According to [106], for the typical parameter values of wind turbines in the range 500 kW to 1 MW, the values of η_1 are in the range [11.1, 28.9]. Recalling that η_2 is linearly proportional to the terminal voltage of the asynchronous generator, we conclude that variations $E(t)$ follow closely the variations in the terminal voltage.

Thus, assuming

$$E = \frac{\eta_2}{\eta_1} \cos \theta,$$

we arrive at the following second-order model:

$$\dot{\theta} = \omega - \eta_1 \tan \theta \quad (4.27)$$

$$\dot{\omega} = \eta_3 - \frac{\eta_2 \eta_4}{2\eta_1} \sin(2\theta) - D\omega. \quad (4.28)$$

Consider the following new energy function candidate obtained by numerous trial-and-error experiments

$$V(\theta, \omega) = \frac{\omega^2}{2} - \eta_3 \theta - \frac{\eta_2 \eta_4}{4\eta_1} \cos(2\theta) + V_0, \quad (4.29)$$

where V_0 is an arbitrary constant. In some neighborhood of (θ_0, ω_0) , the function V is locally positive definite. The Lie derivative of V along the planar vector field (4.27)–(4.28) is given by the expression

$$\mathcal{L}_f V(\theta, \omega) = \eta_1 \eta_3 \tan \theta - \eta_2 \eta_4 \sin^2 \theta - D\omega^2. \quad (4.30)$$

The function $\mathcal{L}_f V$ suggests that there are sets in the $\delta - \omega$ plane where the Lie derivative is positive; the boundedness of these sets needs to be checked, in order to verify that (4.29) fulfills the conditions of Theorem 1, i.e., that it is an Extended Lyapunov function. We will use interval arithmetics to numerically perform the verification.

Construction of the Lyapunov function for the full SAMIB system

Let us now relax the assumption (4.23) and derive a new energy function for the full model (4.20)–(4.22) and consider the following new Lyapunov function candidate

$$V(\theta, \omega, E) = \frac{\eta_2}{2\eta_4} \omega^2 - \frac{\eta_2 \eta_3}{\eta_4} \theta - \eta_2 E \cos \theta + \frac{\eta_1}{2} E^2 + V_0. \quad (4.31)$$

The Lie derivative of (4.31) is given by

$$\mathcal{L}_f V(\theta, \omega, E) = -\frac{\eta_2 D}{\eta_4} \omega^2 - \eta_2^2 \sin^2 \theta + \frac{\eta_2^2 \eta_3}{\eta_4 E} \sin \theta - \dot{E}^2. \quad (4.32)$$

Direct inspection of (4.32) reveals that large deviations of E from the equilibrium point can result in positive $\mathcal{L}_f V$. This observation would severely affect the use of conventional energy function methods; however, it is less restrictive for the Extended Invariance Principle. Technically, it is only necessary to assure that the set $\{(\theta, \omega, E) \in \mathbb{R}^3 : \mathcal{L}_f V > 0\}$ is bounded. Apparently, $\mathcal{L}_f V$ is finite in the whole state space, except for the manifold $(\theta, \omega, 0)$ ⁵. For obvious reasons, it is also desirable to ensure that the set on which $\mathcal{L}_f V > 0$ is as small as possible. As before, the properties of $\mathcal{L}_f V$ should be checked numerically.

Construction of the Lyapunov function for the three-bus power system

The construction of the energy function for the three-machine power system presented in this subsection is based on the so-called “State Function Method” [108].

⁵On the manifold $E = 0$, the function (4.31) is not analytic; however, the model of asynchronous generator itself is invalid on this manifold. Therefore, the state space U of the generator should be restricted such that $E = 0$ is excluded from it.

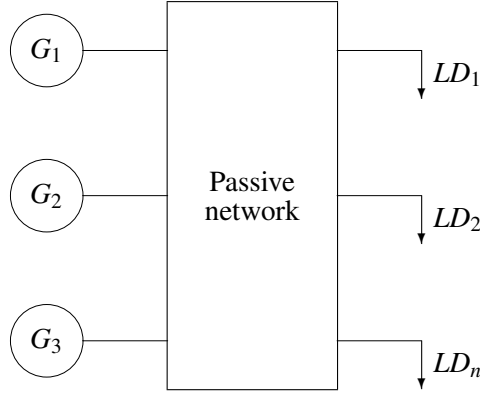


Figure 4.5: Simple three-machine power system.

The development of the energy function is mainly due to [60]; however, the analysis and interpretation of the energy function are made by the author and are novel.

The simple multimachine power system consists of two synchronous machines (a generator and a motor) and one asynchronous generator, which are schematically shown in Fig. 4.5. The electrical machines are interconnected in the passive network whose transfer conductances are assumed to be negligibly small. The model of the asynchronous generator is slightly changed in order to conform to the model of a synchronous generator. That is, equation (4.20) is differentiated w.r.t time and equation (4.21) is substituted into it, which is followed by shifting the stable equilibrium of the three-machine system to the origin. More details can be found in [60]. Thus, the power system is modeled by the following set of equations:

$$\begin{aligned} M_1 \ddot{x}_1 &= -D_1 \dot{x}_1 - E_1 B_{12} [(E_2^o + x_4) \sin(x_{12} + \delta_{12}^o) - E_2^o \sin \delta_{12}^o] \\ &\quad + E_1 E_3 B_{13} [\sin(x_{13} + \delta_{13}^o) - \sin \delta_{13}^o] \end{aligned} \quad (4.33)$$

$$\begin{aligned} M_2 \ddot{x}_2 &= -K_1(x) \dot{x}_1 - (D_2 + K_1(x) + K_3(x)) \dot{x}_2 - K_3(x) \dot{x}_3 - K_4(x) \dot{x}_4 \\ &\quad - E_1 B_{12} [(E_2^o + x_4) \sin(x_{12} + \delta_{12}^o) - E_2^o \sin \delta_{12}^o] \\ &\quad + E_3 B_{23} [(E_2^o + x_4) \sin(x_{23} + \delta_{23}^o) - E_2^o \sin \delta_{23}^o] \end{aligned} \quad (4.34)$$

$$\begin{aligned} M_3 \ddot{x}_3 &= -D_3 \dot{x}_3 - E_1 E_3 B_{13} [\sin(x_{13} + \delta_{13}^o) - \sin \delta_{13}^o] \\ &\quad - E_3 B_{23} [(E_2^o + x_4) \sin(x_{23} + \delta_{23}^o) - E_2^o \sin \delta_{23}^o] \end{aligned} \quad (4.35)$$

$$\begin{aligned} \dot{x}_4 &= T_2^{-1} (1 - x_m B_{22}) x_4 + K_a M_2^{-1} [\cos \delta_{12}^o - \cos(x_{12} + \delta_{12}^o)] \\ &\quad + K_b M_2^{-1} [\cos \delta_{23}^o - \cos(x_{23} + \delta_{23}^o)], \end{aligned} \quad (4.36)$$

where the states x_{ik} are defined as $x_i - x_k$. M_i and D_i are the inertia constant and the damping of machine i , respectively. E_k and T_2 denote the transient EMF of machine k and the ‘open circuit time constant’ of the asynchronous generator; B_{ik} is the (i, k) ’s element of the reduced network matrix of the power system. The functions K_a , K_b , and K_1, \dots, K_4 are defined as follows.

$$K_a = \frac{x_m}{T_2} B_{12} E_1 M_2$$

$$K_b = \frac{x_m}{T_2} B_{23} E_3 M_2$$

$$K_1(x) = K_a \frac{\cos(x_{12} + \delta_{12}^0)}{x_4 + E_2^0} \quad (4.37)$$

$$K_3(x) = K_b \frac{\cos(x_{23} + \delta_{23}^0)}{x_4 + E_2^0} \quad (4.38)$$

$$K_4(x) = -K_a \frac{\sin(x_{12} + \delta_{12}^0)}{(x_4 + E_2^0)^2} + K_b \frac{\sin(x_{23} + \delta_{23}^0)}{(x_4 + E_2^0)^2}. \quad (4.39)$$

In the equations above, the state variables with superscript ‘0’ denote the steady state values of the corresponding state.

Defining the new constant matrices M, M_s, C, C_s, D_c , the variable matrix D_v , the new variables σ , and the vector-valued function $f(\sigma)$ as follows,

$$M_s = \text{diag}(M_1, M_2, M_3), \quad M = \text{diag}(M_s, 1), \quad D_c = \text{diag}(D_1, D_2, D_3, 1)$$

$$C_s = \begin{bmatrix} 1 & -1 & 0 \\ 1 & 0 & -1 \\ 0 & 1 & -1 \end{bmatrix}, \quad C = \begin{bmatrix} C_s & 0 \\ 0 & 1 \end{bmatrix}, \quad A = \begin{bmatrix} I_3 & 0 \\ 0 & 0 \end{bmatrix}, \quad \sigma = Cx,$$

$$D_v = \begin{bmatrix} 0 & 0 & 0 & 0 \\ -K_1(x) & K_1(x) + K_3(x) & -K_3(x) & -K_4(x) \\ 0 & 0 & 0 & 0 \\ 0 & 0 & 0 & 0 \end{bmatrix}$$

$$f(\sigma) = \begin{bmatrix} E_1 B_{12} [(E_2^0 + x_4) \sin(\sigma_1 + \delta_{12}^0) - E_2^0 \sin \delta_{12}^0] \\ E_1 E_3 B_{13} [\sin(\sigma_2 + \delta_{13}^0) - \sin \delta_{13}^0] \\ E_3 B_{23} [(E_2^0 + x_4) \sin(\sigma_3 + \delta_{23}^0) - E_2^0 \sin \delta_{23}^0] \\ f_5(\sigma) \end{bmatrix}$$

$$f_5(\sigma) = T_2^{-1} (1 - x_m B_{22}) \sigma_4 + K_a M_2^{-1} [\cos \delta_{12}^0 - \cos(\sigma_1 + \delta_{12}^0)] \\ + K_b M_2^{-1} [\cos \delta_{23}^0 - \cos(\sigma_3 + \delta_{23}^0)],$$

equations (4.33)–(4.36) can be put in matrix form:

$$A\ddot{x} + M^{-1}(D_c + D_v)\dot{x} + M^{-1}C'f(\sigma) = 0. \quad (4.40)$$

The energy function is sought in the following form:

$$V(x, \dot{x}) = \int_0^{\dot{x}} QA\dot{x}d\dot{x} + \int_0^x QM^{-1}C'f(Cx)dx. \quad (4.41)$$

The unknown nonsingular matrix Q is the main design parameter which has to be determined. The key idea is to find such a matrix Q that the function (4.41) satisfies the associated curl equations and the Rayleigh dissipation function $\dot{x}'(QM^{-1}(D_c + D_v))\dot{x} \geq 0$, which will ensure that the line integrals in (4.41) are path independent and the Lie derivative of V is non-positive definite.

It is shown in [60] that for some $m > 0$, $l \geq -m/\text{Trace}(M_S)$, the matrix Q defined as

$$Q = \begin{bmatrix} mM_S + lM_S 1M_S & 0 \\ 0 & mT_2/x_m \end{bmatrix}$$

satisfies the curl equations associated with V . Thus, the following energy function is obtained

$$\begin{aligned} V(x, \dot{x}) = & \frac{1}{2}\dot{x}'_+ [mM_1 + lM_1 1M_1]\dot{x}_+ \\ & + m [E_1 B_{12} \{ (E_2^0 + \sigma_4) \{ \cos \delta_{12}^0 - \cos(\sigma_1 + \delta_{12}^0) \} - \sigma_1 E_2^0 \sin \delta_{12}^0 \} \\ & + E_1 E_3 B_{13} \{ \cos \delta_{13}^0 - \cos(\sigma_2 + \delta_{13}^0) - \sigma_2 \sin \delta_{12}^0 \} \\ & + E_3 B_{23} \{ (E_2^0 + \sigma_4) \{ \cos \delta_{23}^0 - \cos(\sigma_3 + \delta_{23}^0) \} - \sigma_3 E_2^0 \sin \delta_{23}^0 \} \\ & + (2x_m)^{-1} (1 - x_m B_{22}) \sigma_4^2], \end{aligned} \quad (4.42)$$

where $x_+ = [x_1, x_2, x_3]'$. It can be shown that the Lie derivative of (4.42) is given by the expression:

$$\begin{aligned} \mathcal{L}_f V(x, \dot{x}) = & -\frac{1}{2}\dot{x}'_+ (QM^{-1}(D_c + D_v) + (D_c + D_v)'M^{-1}Q)\dot{x}_+ \\ = & -\frac{1}{2}\dot{x}'_+ (QM^{-1}D_c + D'_c M^{-1}Q)\dot{x}_+ \\ & -\frac{1}{2}\dot{x}'_+ (QM^{-1}D_v + D'_v M^{-1}Q)\dot{x}_+ \\ = & -\frac{1}{2}\dot{x}'_+ R_c x_+ - \frac{1}{2}\dot{x}'_+ R_v(x) x_+. \end{aligned} \quad (4.43)$$

In order to apply (4.43) for stability studies, its properties should be clarified. In particular, the sign definiteness of $\mathcal{L}_f V$ should be determined, which can be done by a closer examination of matrices R_c and $R_v(x)$. Clearly, $R_c \succcurlyeq 0$, which however does not guarantee that $\mathcal{L}_f V$ is non-positive. In [60], it was assumed that $E_2(t)$ could be linearized around the post-fault equilibrium and conditions were derived which would assure positive definiteness of $R_c + R_v$. However, it should be noted that the assumption on small changes in $E_2(t)$ might be unrealistic, since $E_2(t)$ heavily depends on the terminal voltage of the asynchronous generator; should the terminal voltage change, $E_2(t)$ will also change in fractions of a second.

Let us denote the maximum and the minimum eigenvalue of R_c and $R_v(x)$ by λ_{\max} and λ_{\min} , respectively

$$\lambda_{\max} = \max\{\lambda(R_c)\} = 2m \max\{D_1, D_2, D_3, T_2 x_m^{-1}\} \quad (4.44)$$

$$\lambda_{\min} = \min\{\lambda(R_v(x))\} = 2m (K_1(x) + K_3(x)). \quad (4.45)$$

It is important to note that both λ_{\min} and λ_{\max} depend linearly on the arbitrary constant m , implying that both equalities (4.44) and (4.45) hold for any choice of m . Therefore, in general, the negative definiteness of $\mathcal{L}_f V$ in (4.43) cannot be ascertained by the choice of m .

Recalling the inequalities from Appendix B,

$$\begin{aligned} x' R_c x &\leq \lambda_{\max} \|x\|^2 \\ x' R_v(x) x &\geq \lambda_{\min} \|x\|^2, \end{aligned}$$

the best and the worst-case scenarios can be considered:

Best case The system dynamics evolve in the [nonempty] null space $\mathcal{N}_{R_v} = \ker R_v$ of the matrix R_v , or alternatively $\lambda_{\max} + \lambda_{\min} > 0 \forall x$. Then, the time derivative of V is at least nonpositive, which guarantees that $(R_c + R_v) \succcurlyeq 0$, thus rendering V a valid energy function.

Worst case If $\exists [\tau_1, \tau_2] : (R_c + R_v)(\tau) \prec 0$ for all $\tau \in [\tau_1, \tau_2]$ and $\tau_1 \neq \tau_2$, then $\mathcal{L}_f V(\tau) > 0$, which invalidates the energy function candidate V given by expression (4.42).

Obviously, the realization of either the best or the worst case scenarios cannot be asserted without running a time domain simulation, which makes the direct use of V questionable. However, in the framework of the Extended Invariance Principle, V can constitute a valid extended Lyapunov function if the conditions of Theorem 1

are fulfilled. Thus, EIP lays a solid theoretical basis for the use of the function (4.42) for transient stability analysis, which would be impossible in the framework of the conventional invariance principle.

4.6 Use of Interval Arithmetics for Set Inversion

As was stated in the preceding section, in order to assess whether or not a given function qualifies as a valid Extended Lyapunov function, the conditions of Theorem 1 have to be checked, i.e., the set C has to be bounded and the constants l and L have to be computed. As this verification involves operations on sets, the use of interval arithmetics can be attempted, since it offers tools that are able to directly manipulate sets of numbers.

In more precise terms, the verification procedure reduces to the inversion of the Lie derivative of the Extended Lyapunov function candidate; in other words, we will seek the set $C = \{x | \mathcal{L}_f V(x) \subset \mathbb{R}_+\} = (\mathcal{L}_f V)^{-1}(\mathbb{R}_+)$. If C is bounded and $l = \sup_{x \in C} V < L$, then V qualifies as an Extended Lyapunov function.

In the work reported in this chapter, the so-called SIVIA (Set Inversion Via Interval Arithmetics) algorithm was adopted to perform the set inversion [61]. The essential steps of SIVIA are summarized below.

1. Choose a [multidimensional] box $[x]$ enclosing the state-space domain of interest. That is, we choose the domain that might contain C . Usually, this is some [small] neighborhood of the stable post-fault equilibrium.
2. Partition $[x]$ into a set of non-overlapping boxes, i.e., $[x] = \bigcup [x]_i$.
3. Perform the test $\forall i, [\mathcal{L}_f V]_i([x]_i) \subset \mathbb{R}_+ \Rightarrow [x]_i \subset C$
4. Perform the test $\exists i : [\mathcal{L}_f V]_i([x]_i) \cap \mathbb{R}_+ = \emptyset \Rightarrow [x]_i \cap C = \emptyset$.
5. Form the union of all boxes in step (3), which yields the set C .

The major advantage of SIVIA is its ability to find *all* sets of interest in the given domain of the state space.

4.7 Numerical Examples

In this section the theoretical foundations presented in the previous sections will be further explored by means of numerical examples. The main aim of the examples

Table 4.1: Parameters of the equivalent model of the wind farm. All values are given in per unit on the base of the generator

$H, [s]$	r_r	r_s	x_s	x_r	x_m	v_s
4	0.0073	0	0.1248	0.0884	1.8365	$0 + j1$

is to illustrate the use of the proposed extended Lyapunov functions determining the attraction region of simple power systems.

Example: Consider a wind farm consisting of 10 wind turbines. The total installed capacity of the farm is 10 MW. It is also assumed that the turbines have been aggregated in one equivalent turbine having the parameters shown in Table 4.1. The damping term D is set to 0.05 p.u.

It has been shown in Section 4.4 that for any model having the structure (3.17), certain commonly known Lyapunov functions cannot be constructed; therefore, the wind turbine model will be reformulated in the polar coordinates and an Extended Lyapunov function will be sought.

With these parameters, the model (4.20)–(4.22) can be written as follows

$$\begin{aligned}\dot{\theta} &= \omega - 9.9816E^{-1} \sin \theta \\ \dot{\omega} &= 365.21 - 1877.68E \sin \theta - 19.635\omega \\ \dot{E} &= -11.173E + 9.9816 \cos \theta\end{aligned}$$

Numerically, the corresponding simplified second-order model (4.27)–(4.28) is

$$\dot{\theta} = \omega - 11.173 \tan \theta \quad (4.46)$$

$$\dot{\omega} = 365.21 - 838.729 \sin(2\theta) - 19.635\omega. \quad (4.47)$$

Using expression (4.29), the Extended Lyapunov function candidate and its Lie derivative can be readily computed as

$$V = \frac{1}{2}\omega^2 - 365.21\theta - 419.36 \cos(2\theta) + 456.69 \quad (4.48)$$

$$\mathcal{L}_f V = 4080.5 \tan \theta - 18742.3 \sin^2 \theta - 19.635\omega^2. \quad (4.49)$$

The boundedness of the set C for (4.49) is checked with the help of the SIVIA algorithm. The results of set inversion are shown in Fig. 4.6. As can be seen in the figure, C has multiple components, one of which is bounded. In practice, it suffices for V to have a single bounded component of C to qualify as an Extended Lyapunov

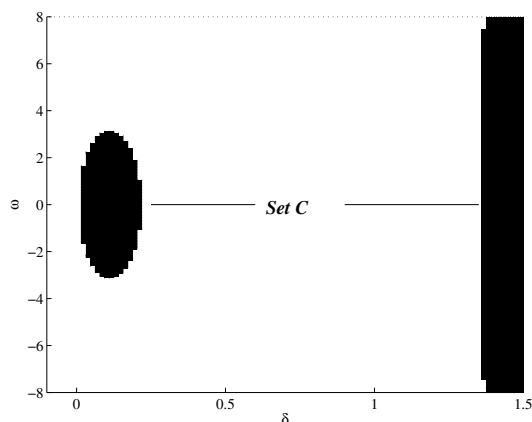


Figure 4.6: Set C found by the SIVIA algorithm. Only two components of C are shown.

function. In the case of the second-order model it is relatively easy to find the set C by direct inspection of the level curves of $\mathcal{L}_f V$; however, in general the direct inspection can be complicated, especially if C has multiple components. Fig. 4.7 shows the level curves of the Lyapunov function (4.48) and its Lie derivative. In the figure, the interiors of the level curves labeled with ‘0’ show the set C , while the sets bounded by the level curves with labels ‘35’ and ‘346’ designate the sets $\bar{\Omega}_l$ and Ω_L , respectively.

It should be noted that the performance of SIVIA was significantly improved by reformulating the Lie derivative

$$\begin{aligned} \mathcal{L}_f V &= \eta_1 \eta_3 \tan \theta - \eta_2 \eta_4 \sin^2 \theta - D\omega^2 \\ &= \tan \theta \left(\eta_1 \eta_3 - \frac{\eta_2 \eta_4}{2} \sin(2\theta) \right) - D\omega^2, \end{aligned}$$

which is easily explained by recalling the basic properties of interval arithmetics (A.2)–(A.4). In this example interval arithmetics not only was used to determine the boundedness of the set C , but also to estimate the constant $l = \sup V$ on this set. The constant l was found to be numerically equal to 35.

In the present case study, the constant $L = 346$ was computed by evaluating V at the nearest unstable equilibrium point. It is interesting to note that L could also be

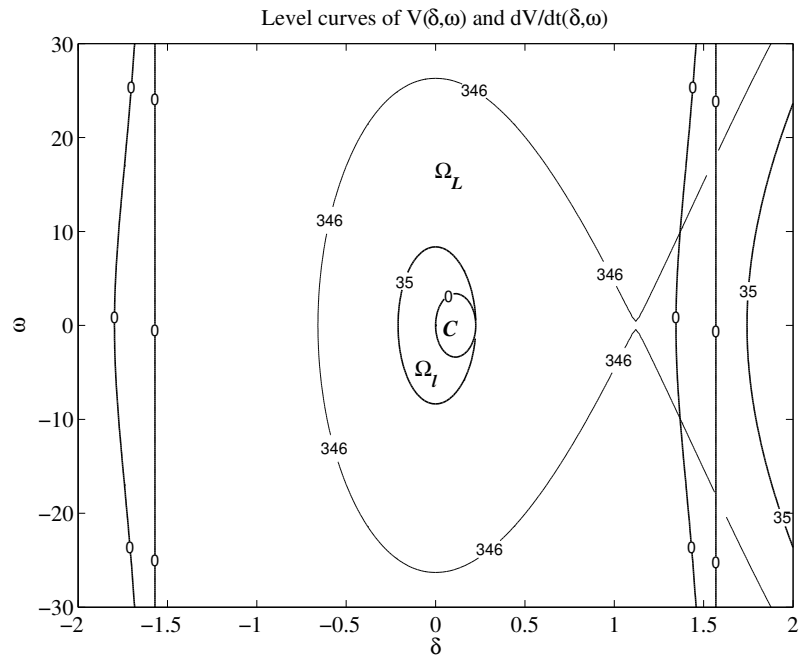
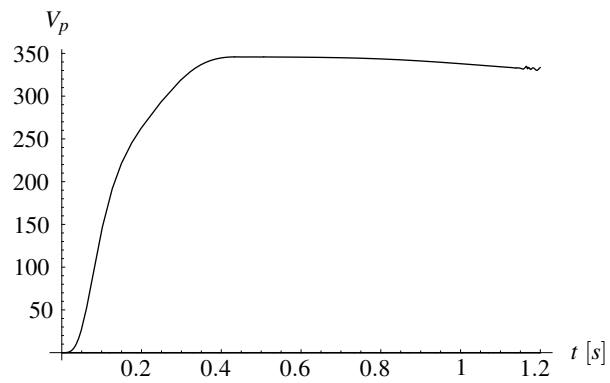
Figure 4.7: Level curves of V and $\mathcal{L}_f V$ 

Figure 4.8: Potential energy curve vs. time for the system (4.46)–(4.47). The potential energy was computed for a hypothetical fault on the transmission system, which resulted in a 60% voltage drop at the terminals of the asynchronous generator.

Table 4.2: System parameters for 3-machine power system. All values are given in per unit, except δ_0 and T_2 . With minor modifications, the parameters values are similar the values in [60].

	M	D	x'_d	E_0	$\delta_0[\text{rad}]$	x_m	T_2 [s]	$\text{slip}(0)$
G_1	0.0132	0.0132	0.15	1.48	0.3	—	—	0
G_2	0.004	0	0.137	1	0.2	2.15	0.235	-0.0193
G_3	0.065	0.0325	0.15	1.05	0	—	—	0

determined by applying the argument of the PEBS method with the potential energy defined as $V_p = -\eta_3\theta - \eta_2\eta_4/(4\eta_1)(\cos(2\theta + 2\theta_0) - \cos(2\theta_0))$, see Fig. 4.8.

Since the conditions of Theorem 1 are fulfilled, it can be concluded that the function (4.48) is an Extended Lyapunov function and all trajectories initiated in Ω_L will eventually converge to the largest invariant set contained in the union of $\bar{\Omega}_i$ and $\{x \in \Omega_L : \mathcal{L}_f V = 0\}$.

Example: Let us now consider the three-machine power system. The power system consists of one synchronous generator G_1 , one asynchronous generator G_2 , and a synchronous motor G_3 which are interconnected by 3 power lines connected in a star. The one-line diagram of the power system is shown in Fig. 4.9. The parameters of the generators are shown in Table 4.2. The power lines have the following reactances in per unit: $Z_1 = j0.2$, $Z_2 = j0.1$, and $Z_3 = j0.1$. The synchronous frequency was set to 120π . In this example a bolted⁶ three-phase fault is applied to the terminals of G_3 which is then cleared. The main purpose of this example is to further explore and validate the extended Lyapunov function (4.42) and its Lie derivative (4.43).

A series of nonlinear time-domain experiments were performed on the three-machine power system in MATLAB. Some of the results from the experiments will be presently discussed. It is instructive to begin inspection of the numerical results by observing the state $x_4 = E_2 - E_{2,0}$ and the phase portraits of the electrical machines, see Fig. 4.10–4.14.

The simulations in this example confirm that the state variable x_4 does deviate significantly from its steady state. For instance, in the present case under the fault, E_2 reduced to approximately 25% of its steady state value, see Fig. 4.10. Physically, this is easily explained by the fact that the asynchronous generator does not have an excitation winding to support E_2 during the fault. Therefore, E_2 can be

⁶To be exact, the fault reactance was $j10^{-5}$ p.u.

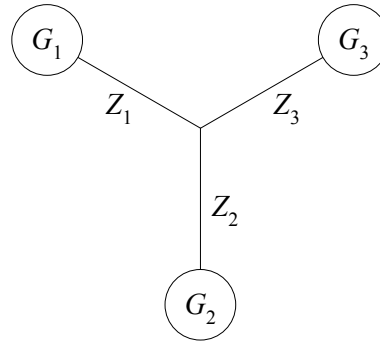
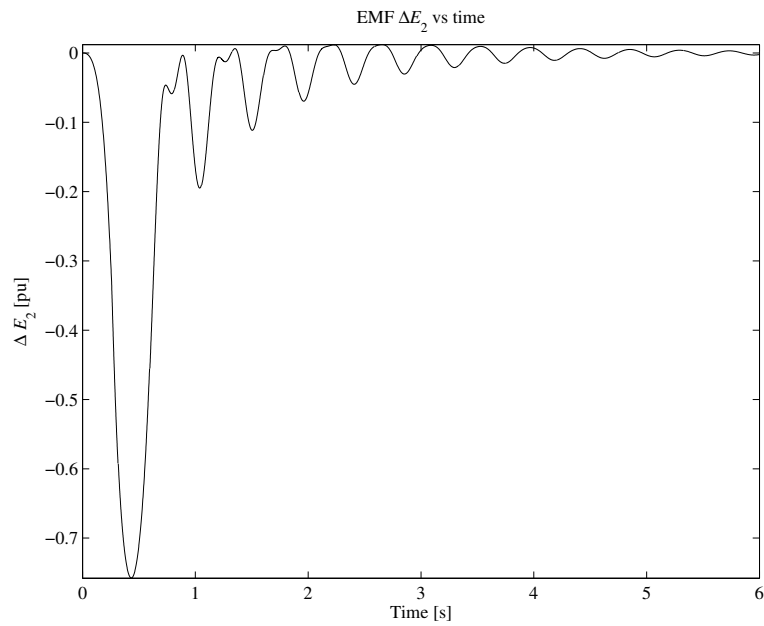


Figure 4.9: Three-machine power system

Figure 4.10: The deviation of state variable, ΔE_2 , i.e., the EMF of the asynchronous generator as a function of time

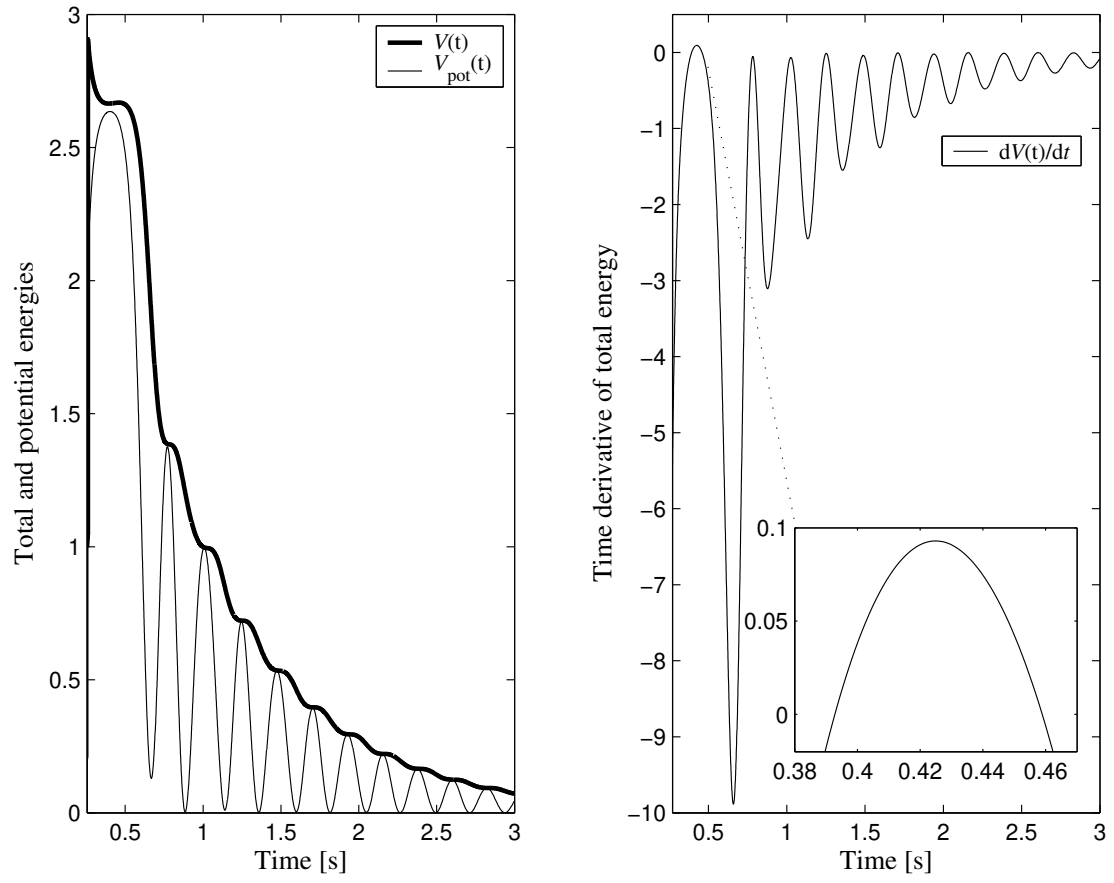
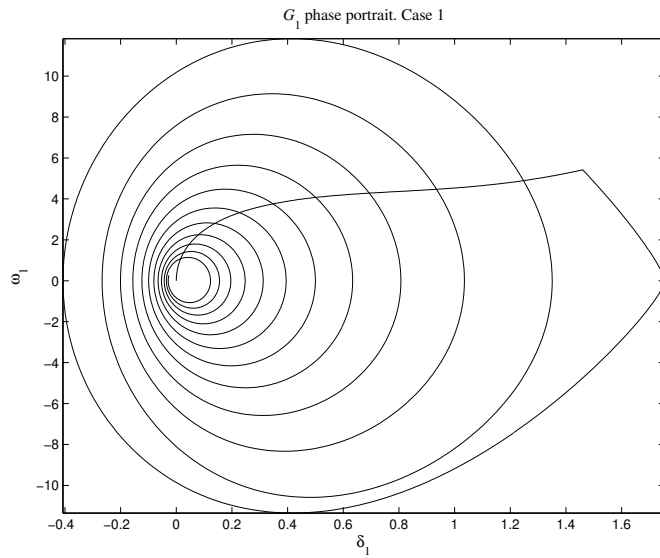
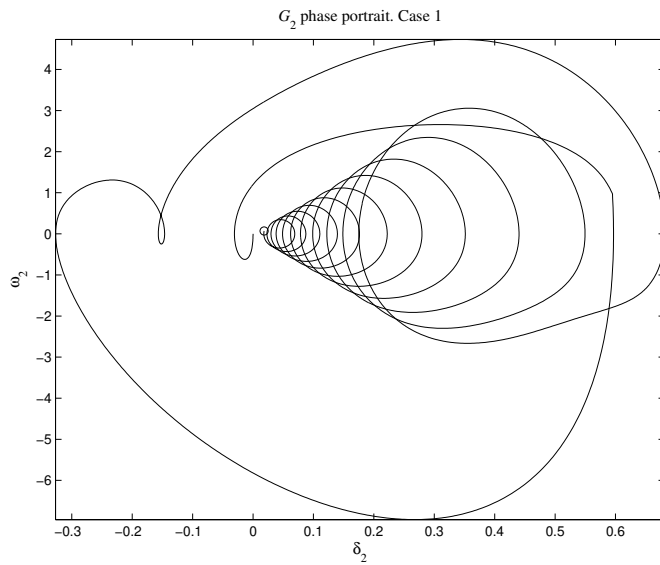
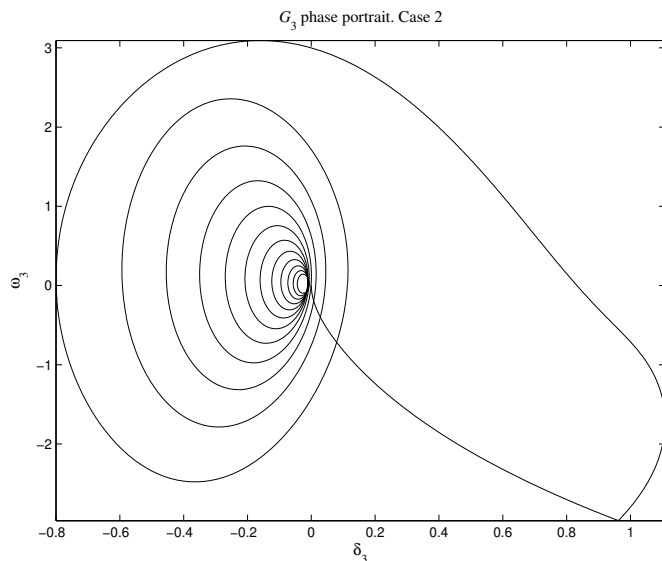


Figure 4.11: The total $V(t)$ and potential $V_p(t)$ energies of the 3-machine power system and the Lie derivative $\mathcal{L}_f V(t)$ of $V(t)$

Figure 4.12: Phase portrait of G_1 Figure 4.13: Phase portrait of G_2

Figure 4.14: Phase portrait of G_3

expected to fall rapidly as its terminal voltage decreases. This reduction in the magnitude of E_2 has an important implication – an increase of the absolute values of the variables $\{K_i(x)\}_1^4$, see (4.37)–(4.39). As a consequence, λ_{\min} in (4.45) increases in magnitude, which in turn results in positive $\mathcal{L}_f V(x)$. Thus, strictly speaking, from the view point of the classical invariance principle, the positive definite function (4.42) is neither a Lyapunov nor an energy function, since the measure of the set on which $\mathcal{L}_f V > 0$ is nonzero, as Fig. 4.11 shows. The conditions of Theorem 1 were in this example verified numerically, using both interval arithmetics and the conventional real analysis.

A comparison of the critical clearing time computed by the step-by-step method and the extended Lyapunov function, reveals that the estimates are not overly conservative. For instance, for this example the step-by-step methods yields $t_{cc} = 0.25$ s, while the Direct method suggests $t_{cc} = 0.241$ s. That is, the error in the estimate in this case does not exceed 3.6% \square

4.8 Summary

This chapter reports preliminary results of a study concerned with the questions related to the transient stability of power systems with asynchronous generators. In this study the asynchronous generators represent a large-scale wind farm consisting of fixed-speed wind turbines with fixed pitch. For a better understanding of the dynamic properties of the asynchronous generators, it is assumed that the necessary turbine aggregation has been carried out and the farm can be readily represented by a single asynchronous machine connected to an infinite bus via a transmission system.

The objective of the study was to develop a framework for studying the transient stability of the asynchronous generators similar to that of synchronous generators. That is, an attempt was made to apply a Lyapunov/energy function method to the simple power system with an asynchronous generator.

Detailed analysis was performed in order to verify the existence of a proper Lyapunov function for the system at hand. It was demonstrated analytically that three commonly known method for construction Lyapunov functions cannot yield a Lyapunov function for the SAMIB system. Even though it does not imply that an appropriate Lyapunov function does not exist, it does indicate that the construction of such a function might be a very difficult mathematical task. This fact suggests that other analytical tools should be used for the stability studies of the power system with asynchronous generators.

The Extended Invariance Principle was found capable of constructing a function that could be used in the stability studies reported in this chapter. In particular, an extended Lyapunov function was found for a simple power system. The use of Extended Invariance Principle allows a larger class of functions to be applied for stability studies of power systems; however, this comes at the expense of having to perform certain operations on sets of reals. To overcome the difficulty of manipulating the sets, the utility of interval arithmetics is proposed.

Numerical examples are used to illustrate the application of Extended Invariance Principle and interval arithmetics for system stability analysis of a simplified model of a wind farm consisting of fixed-speed wind turbines and a model of a three-machine power system.

Part II

Voltage Stability

“The actual science of logic is conversant at present only with things either certain, impossible, or entirely doubtful, none of which (fortunately) we have to reason on. Therefore the true logic for this world is the calculus of Probabilities, which takes account of the magnitude of the probability which is, or ought to be, in a reasonable man’s mind.”

— James Clerk Maxwell (1850)

Chapter 5

Assessment of Voltage Stability of Uncertain Power Systems

This chapter presents an application of interval arithmetics to voltage collapse analysis. The problem of calculating the power system critical loading conditions and determining the maximal loadability of a power system in a nondeterministic setting are treated. The methodology for assessment of voltage stability in deterministic power systems is well-established in the literature; however, voltage stability analysis of nondeterministic power systems has not yet received much attention. In this chapter, the uncertain power system parameters such as, for instance, loads and partly controllable generation are treated as intervals and the analysis is performed using the framework of interval arithmetics. The voltage stability problem is restated in terms of an interval-valued optimization problem and is solved by applying the Generalized Newton method.

Numerical experiments are performed in order to demonstrate the technicalities of the proposed methodology. For the examples presented, the numerical results are found to be reliable and nonconservative.

5.1 Introduction

Reliable assessment of voltage stability of an electric power system is essential for its operation and control. To accommodate the need for accurate analysis of voltage stability a number of analytical and computational tools have been developed [28], [58]. Typically, two voltage stability problems are analyzed:

1. Determination of the maximum loadability problem and

2. Computation of the critical loading of the power system [67].

In the former case, a loading scenario is assumed and the maximum power transfer to the load buses is computed. In the latter case, a minimum system loading is sought that would render the power system voltage unstable, i.e., the loading that would cause voltage collapse. Such a loading is referred to as critical system loading. From the standpoint of the system operator, the power system should be controlled in such a way that the critical loading is prevented. A recent paper reported a new method for the assessment of voltage stability in power systems with probabilistic nodal loading model [67].

It is shown in the literature that the voltage stability analysis problem can be reduced to a constrained optimization problem, see [28] and references therein. This consideration allows well-established techniques from optimization theory to be used in voltage stability analysis (VSA) studies. Typically, the direct optimization of a certain objective function is performed, which yields the critical points which are the solutions to either the maximum loadability or critical loading problem. Alternatively, the continuation method is used to solve the optimization problem [28], [67].

In all of the aforementioned publications, it is implicitly assumed that the power system is deterministic, with possibly one exception—the system loading which, in some cases, is assumed to be uncertain. While in some power systems this cannot be considered a problem, there are power systems which contain significant amounts of uncontrollable energy sources such as, for example, large wind farms and for these power systems the uncertainty in power generation can be significant. As the voltage stability is—to a certain extent—a local problem, the uncertainty in the power system parameters need to be explicitly accounted for. This chapter presents a methodology for addressing the issue of uncertainty in the power system generation. The uncertain parameters of a power system are represented by intervals, i.e., it is explicitly assumed that although uncertain, the parameters are bounded. The VSA problem is reformulated in the form of an interval-valued optimization and then solved using the methods of interval arithmetics.

5.2 Voltage Stability Formulation

System Modeling

In power systems analysis it is customary to model the network components with the help of differential-algebraic equations which—in the general case—have the

following form [28]

$$\begin{bmatrix} \dot{x} \\ 0 \end{bmatrix} = \begin{bmatrix} f(t, x, y, \lambda, p) \\ g(t, x, y, \lambda, p) \end{bmatrix} = F(z, \lambda, p). \quad (5.1)$$

In equation (5.1), the vector $x \in \mathbb{R}^n$ typically represents the state variables of the various power system devices and their respective controls; $y \in \mathbb{R}^m$ is the vector of algebraic variables which normally represent nodal voltages and angles of the load buses. Finally, the vectors $\lambda \in \mathbb{R}^l$ and $p \in \mathbb{R}^k$ stand for the set of slowly varying parameters e.g., system loading variations and the set of control parameters, respectively. It is assumed that the system operator does not have direct control over the parameters λ , as opposed to the parameters p which can directly or indirectly be altered by the operators. The vector-valued functions f and g are defined as $f : \mathbb{R} \times \mathbb{R}^n \times \mathbb{R}^m \times \mathbb{R}^l \times \mathbb{R}^k \rightarrow \mathbb{R}^n$ and $g : \mathbb{R} \times \mathbb{R}^n \times \mathbb{R}^m \times \mathbb{R}^l \times \mathbb{R}^k \rightarrow \mathbb{R}^m$. For convenience, let us introduce the variable $z = (x', y')'$. Without significant loss of generality, it is assumed in this chapter that the parameters p are kept constant and equal numerically to some $p = p_o$.

It is commonly assumed that the variable z evolves on such a manifold \mathcal{M} that the mapping $D_y g$ remains bijective for all time [54]. If this is the case, then the system (5.1) can be shown to have a unique solution and the algebraic equations can be eliminated by means of the Implicit Function Theorem [104]. In this chapter it is assumed that $D_y g \in \mathcal{M}$ along all system trajectories.

Depending on the nature of the VSA studies, either the conventional power-flow equations or the complete set of differential-algebraic equations (5.1) are used in the analysis and simulations. Nevertheless, as is reported in the literature, in many practical cases the load-flow equations alone might be inappropriate for the needs of rigorous voltage stability analysis [29], [30].

Voltage Collapse

The operational principles of power systems are such that at an given time instant, the power system is subjected to the action of various perturbations. For the convenience of analysis, the perturbations can be subdivided into two categories: slow and fast. All the systems considered in this chapter are assumed to be perturbed by slow variations in the parameters λ . As the parameter vector λ alters, the equilibrium point (z_*, λ_*) of (5.1) moves in some domain $\Omega \subset \mathbb{R}^{n+m} \times \mathbb{R}^l$. Upon approaching a local maximum of loading, the system (5.1) undergoes a local saddle-node bifurcation, which is characterized by a unique zero eigenvalue of the

Jacobian matrix $D_x f(z_*, \lambda_*)$ and the transversality conditions

$$D_x f \cdot v = D'_x f \cdot w' = 0 \quad (5.2)$$

$$w' D_\lambda f = 0 \quad (5.3)$$

$$w' \cdot D_x^2 f \cdot v = 0. \quad (5.4)$$

In equation (5.3), the variables v and w stand for the normalized right and left eigenvectors corresponding to the zero eigenvalue of $D_x f$. Note that the Jacobians $D_x f, D_\lambda$ and Hessian $D_x^2 f$ in equations (5.2)–(5.4) are evaluated at the equilibrium (z_*, λ_*) .

In order to ensure a reliable and proper operation of power systems, the current equilibrium should not approach the local bifurcation point. Moreover, a certain voltage stability margin should be identified [possibly based on practical experience] and power system operated within this stability margin. On the other hand, because of certain economical and environmental considerations, many power systems are presently operated in a proximity to their stability limits. Thus, it becomes an important task to reliably determine the local loadability limit for a given power system.

There exists a dual problem to the aforementioned one, namely, the determining of the minimal load increase that causes a system bifurcation. This problem is commonly referred to as ‘minimum distance to collapse.’

Both these problems can be reformulated as optimization problems in which the loading λ is maximized and the distance $\|\lambda - \lambda_o\|$ is minimized, respectively. That is, the maximum loadability problem reduces to the optimization of the objective function

$$\begin{aligned} \min_{\lambda, z} J_1(\lambda, z) &= -\lambda \\ \text{s.t. } F(z, \lambda) &= 0 \end{aligned} \quad (5.5)$$

while, the critical system loading can be computed by optimizing the following objective function

$$\begin{aligned} \min_{\lambda, z, w} J_2(\lambda, z, w) &= \|\lambda - \lambda_o\|^2 \\ \text{s.t. } (F(\lambda, z)', w' D_z F(\lambda, z))' &= 0. \end{aligned} \quad (5.6)$$

Analytical Tools for VSA

Normally the constrained optimization problems (5.5)–(5.6) are solved either directly by applying the Lagrange multipliers technique or using the so-called the continuation method. The direct method is less expensive numerically and only yields the set (λ_*, z_*, w_*) . The latter technique is essentially based on repetitive computation of the system equilibria as the parameter λ (usually a scalar) is varied and thus is more expensive numerically, as compared to the direct method. The direct method is applied for all optimization tasks treated in this chapter.

In the discussion above, all the variables and parameters have been assumed known exactly, which in certain situations might not be entirely true. For instance, in power systems with substantial penetration levels of distributed generation utilizing uncontrollable energy sources, for instance wind energy, the power produced at a given time instant is not known in advance. On the other hand, the actual loading of a small power system also is to some extent uncertain. In large power systems, the various loads are normally aggregated, which reduces the impact of the load uncertainty on the stability analysis. Nevertheless, the voltage instability phenomenon is considered to be a local one making a general discussion on the suitability of aggregation of large loads a nontrivial task. It is therefore of interest to develop a VSA technique capable of accounting for uncertainties in the system parameters. One of possible alternatives is to use intervals arithmetics to perform the constrained optimization tasks (5.5)–(5.6).

5.3 Application of Interval Arithmetics to Voltage Collapse Analysis

Let us reformulate the two constrained optimization problems (5.5)–(5.6) stated in Section 5.2 placing emphasis on the fact that some of the parameters are now treated as intervals. That is, now it is assumed that both λ and z are uncertain, but bounded quantities. Then, the objective functions J_1 and J_2 in (5.5)–(5.6) become

$$\begin{aligned} \min_{[\lambda],[z]} J_1([\lambda],[z]) &= -[\lambda] \\ \text{s.t. } F([\lambda],[z]) &= 0 \end{aligned} \quad (5.7)$$

$$\begin{aligned} \min_{[\lambda],[z],[w]} J_2([\lambda],[z],[w]) &= \|[\lambda] - \lambda_o\|^2 \\ \text{s.t. } (F([\lambda],[z])', w' D_z F([\lambda],[z]))' &= 0. \end{aligned} \quad (5.8)$$

To solve either of (5.5) or (5.6), the method of Lagrange multipliers can be applied.

A series of experiments was performed and it was observed that the so-called naïve Newton method was able to yield acceptable results for the problems in which the interval parameters had relatively small uncertainties. To enhance the numerical properties of the optimization, the Generalized Newton method (GN) was implemented, in which the Newton iterate is given by the expression [48]:

$$[u_{k+1}] = u_k \cap [\check{u}_k - D_u \mathcal{F}^{-1}(u_k) \cdot \mathcal{F}(\check{u}_k)], \quad (5.9)$$

where $[u_k] = [z_k] \times [\lambda_k] \times [w_k]$ and \mathcal{F} is the Lagrangian defined as

$$\mathcal{F} = \|[\lambda] - \lambda_o\|^2 + s'_1 F([u]) + s'_2 D'_z F \cdot w, \quad (5.10)$$

$D_u \mathcal{F}$ stands for the gradient of the Lagrangian evaluated at $[u_k]$, and s_1 and s_2 are the respective Lagrange multipliers. The variables u are treated as unknown intervals, the active power P_1 and P_2 are assumed to be known intervals. All the computations are performed in MATLAB with the help of the package INTLAB [105].

Numerical Experiments

To exemplify the ideas presented in the preceding sections and facilitate the discussion on the results obtained, a simple power system is chosen¹. The power system consists of a slack node, three transmission lines, and two PV nodes, see Fig. 5.1. The relevant parameters of the system are shown in the figure. It is assumed that the [aggregate] generators connected to nodes $N1$ and $N2$ maintain the voltage magnitude of the respective nodes constant, while the voltage angles are considered to be state variables. For simplicity the dynamics of the generators and loads are neglected. The net active power injected into the nodes $N1$ and $N2$ are the differential between the local generation and consumption. It is also assumed that the net active powers are uncertain, i.e., $P_i = [P_i, \bar{P}_i]$, $i = 1, 2$. In a real power system this uncertainty can be attributed to either variable loads or generation, or both. The power system is described by the following set of equations:

$$F = \begin{bmatrix} \lambda_1 P_1 + V_1 V_2 \sin(\delta_2 - \delta_1) - V_1 \sin(\delta_1) \\ \lambda_2 P_2 + V_1 V_2 \sin(\delta_1 - \delta_2) - V_2 \sin(\delta_2) \end{bmatrix} \quad (5.11)$$

Let us now solve the maximul loadability problem and also find the critical loading of this simple power system.

¹This power system was originally introduced and studied in [82].

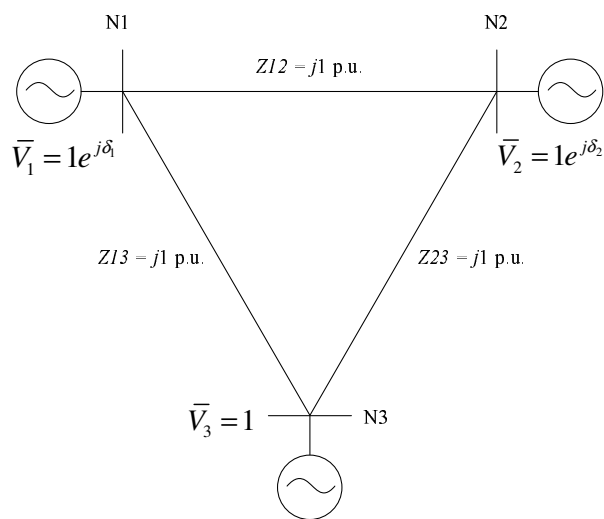


Figure 5.1: Three-bus power system

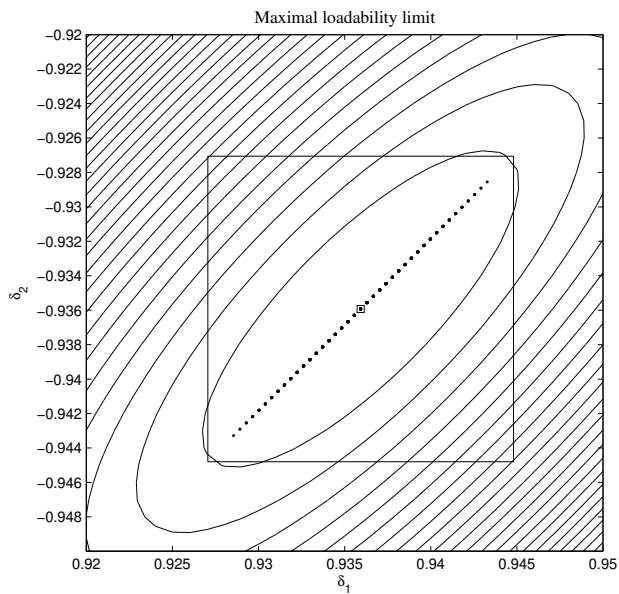


Figure 5.2: Variation of the loadability limit in $\delta_1 - \delta_2$ plane

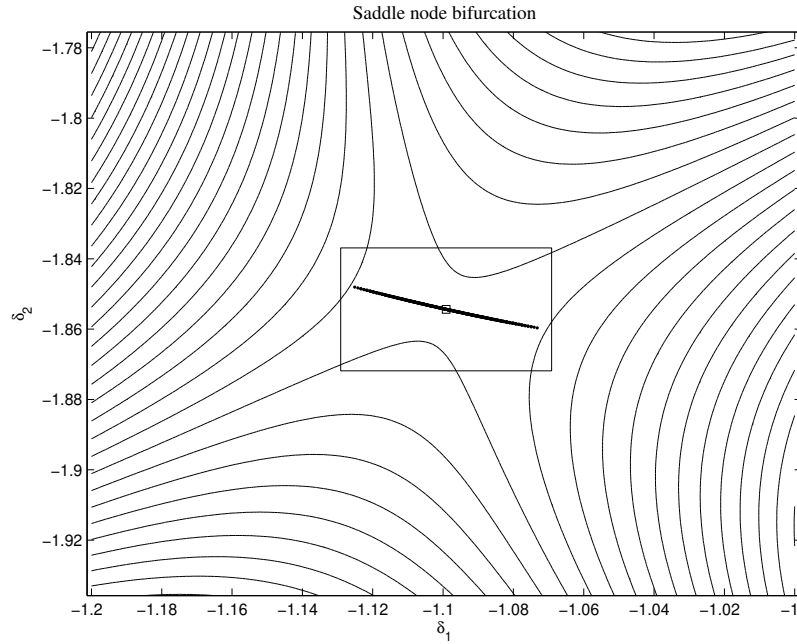


Figure 5.3: Variation of the Saddle-node bifurcation point in $\delta_1 - \delta_2$ plane

Due to the uncertain P_1 and P_2 , the critical points of the system assume certain values which can be computed by a repetitive use of either the direct method i.e., minimizing (5.5) [or (5.6)] for various combinations $(p_1, p_2) : p_1 \in [P_1], p_2 \in [P_2]$ or by using the continuation method. However, both these methods can be quite expensive numerically. Alternatively, the objective function (5.7) [or (5.8)] can be minimized only once yielding the desired result directly. That is, upon minimizing the interval-valued objective functions, we can directly find such an enclosure $[u_*]$ that contains the set of *all* values which the critical points of interest assume for the parameters $[P_1]$ and $[P_2]$.

In the first experiment the following numerical values are chosen $[P_1] = [0.5 \pm 5 \cdot 10^{-3}]$ and $[P_2] = [-0.5 \pm 5 \cdot 10^{-3}]$ and a local minimum of (5.7) is sought. This optimization problem was solved and the following numerical values were obtained: $[\lambda_1] = [3.4903, 3.5504]$, $[\lambda_2] = [3.4903, 3.5504]$. Fig. 5.2 further illustrates the results of the optimization. In the figure, the large box encloses the subset of the $\delta_1 - \delta_2$ plane that is guaranteed to contain all critical points corresponding the maximal loadability of the system for all $p_1 \in [P_1]$ and $p_2 \in [P_2]$.

To verify the interval computations and assess the conservatism of results, the objective function (5.5) was minimized on the grid $(p_1, p_2) : p_1 \in [P_1], p_2 \in [P_2]$ and plotted in Fig. 5.2. As is seen in the figure, the enclosure is computed correctly and indeed contains all the values that the critical point assumes on $[P_1] \times [P_2]$.

The second experiment is conducted on the same system, but in this case the critical loading conditions are identified; that is, the objective function (5.8) is now minimized. Assuming the same values of $[P_1]$ and $[P_2]$, the optimization is solved and the results are depicted in Fig. 5.3. Again, the enclosure $[u_*]$ is found that contains all the values that the critical point assumes on $[P_1]$ and $[P_2]$. In particular, $[\lambda_1] = [-0.4408, -0.3807], [\lambda_2] = [3.2610, 3.3211]$. That is, based on the results obtained, it can be concluded that the power system under consideration will remain voltage stable if the load at node $N1$ is not greater than $\sup [\lambda_1] \cdot [P_1]$ and the load at node $N2$ does not exceed the value $\inf [\lambda_2] \cdot [P_2]$. The dotted line in Fig. 5.3 shows the enclosure $[u_*]$ (large box) and the movement of the critical point (saddle node) as the function of $(p_1, p_2) : p_1 \in [P_1], p_2 \in [P_2]$. Direct inspection of Fig. 5.3 indicates that the enclosure is not exceedingly conservative.

5.4 Summary

This chapter considers an application of interval arithmetics to voltage stability analysis. In particular, the problem of calculating the power system critical loading conditions and determining the maximal loadability of a power system in an uncertain setting are treated. The application of the method presented in this chapter allows the power system operator to assess the location of critical points of interest directly without having to perform repeated optimization of the corresponding objective function in order to account for the system uncertainties.

Numerical experiments are performed in order to demonstrate the technicalities of the proposed methodology. The numerical results are found to be reliable and nonconservative.

Part III

Power System Load Modeling and Identification

*“A basic rule in estimation is not to estimate
what you already know.”*
— A quotation from [113]

Chapter 6

Identification and Modeling of Aggregate Power System Loads

This chapter addresses some theoretical and practical issues relevant to the problem of modeling and identification of aggregate power system load. Two identification techniques are developed in the theoretical framework of stochastic system identification. The identification techniques presented in this chapter belong to the family of output error models; both techniques are based on well-established equations describing load recovery mechanisms having a commonly recognized physical appeal. Numerical experiments with artificially created data were first performed on the proposed techniques and the estimates obtained proved to be asymptotically unbiased and achieved the corresponding Cramér-Rao lower bound. The proposed techniques were then tested using actual field measurements taken at a paper mill, and the corresponding results were used to validate a commonly used aggregate load model.

The results reported in this chapter indicate that the existing load models satisfactorily describe the actual behavior of the physical load and can be reliably estimated using the identification techniques presented herein.

6.1 Introduction

Nccurate models of power system loads are essential for analysis and simulation of the dynamic behavior of electric power systems [5]. Having accurate models of the loads that are able to reliably reflect underlying phenomena of the physical loads is important for the purposes of designing auto-

matic control systems and optimization of their configuration. More importantly, the dynamic properties of power system loads have a major impact on system stability [5, 66, 122]. In particular, previous work on the subject of voltage stability reported in the literature indicates that the parameters of both static and dynamic loads have significant impact on voltage stability of the power systems [53, 122]. On the other hand, the impact of power system load models on inter-area oscillations is discussed in [5], demonstrating the influence that load parameters have on the dominant system eigenvalues. This dependence reveals the link between the effectiveness of power system damping controllers (e.g., power system stabilizers or PSS) and the correctness of the eigenstructure of the system, which is dependent on the load model.

To be able to predict the behavior of a system, reliable models of system components are needed that faithfully reflect the dynamical behavior of the actual physical components of the system. Most of the power system components can be satisfactorily modeled by considering the physical laws which govern the respective components. There are, however, some cases when power system modeling is quite a complicated exercise. Modeling power system loads is one of them. It is known that at high voltage levels, the power system loads have to be aggregated in order to obtain manageable models suitable for analysis and simulations [5]. Depending on the load type (e.g. lighting, motor load, heating, etc.), the parameters of the aggregate load model may vary in a wide range. When the parameters of all load components are well known, the parameters of the aggregate load models can be readily determined. If the parameters of separate loads are not known or the load structure is known, but the proportion of various load components is not, deriving an aggregate load becomes more difficult.

It can be argued that in the absence of precise information about a power system load, one of the most reliable ways to obtain an accurate model of the load is to apply an identification technique. That is, if field measurements of load quantities (e.g., the voltage and current/power) adequately describing its behavior are available, then a dynamic and/or static equivalent of the load can be obtained by analyzing functional relationships between these quantities.

The current chapter is concerned with theoretical and numerical aspects of identification of an aggregate model of power system loads. Identification of both linear and nonlinear models of a power system load is treated. Two identification techniques are presented that belong to the so-called family of output error models. First, the estimation of the load parameters using a linear model is presented, which is followed by the presentation of a nonlinear identification technique. The statistical properties of the proposed identification methods are studied both numerically

and analytically. Thus, artificially created data are analyzed numerically and the variance of the obtained estimates is compared with the corresponding Cramér-Rao lower bound. Then, in order to benchmark the identification techniques and validate the analytical load models, field measurements taken at a paper mill were used. The results obtained indicate that the load models describe the actual behavior of the load with high accuracy. Moreover, it is shown that the load model parameters can be accurately identified using the proposed techniques.

6.2 Aggregate Models of Power System Loads

In general, obtaining detailed models of power system loads is a more complicated task than modeling a particular power system component, such as, for instance, a synchronous machine. The problem is two-fold:

- (a) Loads are time variant and stochastic;
- (b) In most cases, at high voltage levels the loads must be aggregated.

The latter is due to the large number and types of loads connected at the transmission system level, which makes the consideration of each separate load numerically impractical and provides no insight into the system analysis. The time variance of loads can be accounted for by the explicit modeling their dynamic behavior by differential and/or difference equations.

Power system load aggregation can be performed in two ways:

- (i) Analytically, by lumping similar loads and then using pre-determined values for each parameter of the load (e.g. [3] and [4]) or
- (ii) Selecting a load model and then performing parameter estimation using an appropriate identification technique.

Static load models

Due to the importance of adequate load modeling, a large number of various static models of power system loads have been developed. Despite this diversity, in principle, they all serve one common goal: to reflect the voltage and possibly frequency dependence of the active and reactive components of the loads. For example, in [4]

the following standard load models used for dynamic studies in established stability programs (e.g., EPRI's LOADSYN and ETMSP packages) are suggested:

$$P = P_0 \left[P_{a1} \left[\frac{V_L}{V_0} \right]^{K_{pv1}} [1 + K_{pf1}(f - f_0)] + (1 - P_{a1}) \left[\frac{V_L}{V_0} \right]^{K_{pv2}} \right] \quad (6.1)$$

$$Q = P_0 \left[Q_{a1} \left[\frac{V_L}{V_0} \right]^{K_{qv1}} [1 + K_{qf1}(f - f_0)] \right. \\ \left. + [1 + K_{qf2}(f - f_0)] \left[\frac{Q_0}{P_0} - Q_{a1} \right] \left[\frac{V_L}{V_0} \right]^{K_{qv2}} \right] \quad (6.2)$$

where V_L and f are the load bus voltage and frequency, respectively. In equations (6.1)–(6.2), K_{pv1} and K_{pv2} represent the voltage exponents for frequency dependent and frequency independent active power load; K_{qv1} and K_{qv2} stand for the voltage exponents for the uncompensated and compensated reactive power load; K_{pf1} and K_{qf1} are the frequency sensitivity coefficients for active and uncompensated reactive power load; K_{qf2} is the frequency sensitivity coefficient for reactive compensation; and P_{a1} and Q_{a1} represent the frequency dependent fraction of active load and reactive load coefficient of uncompensated reactive load to active power load, respectively. V_0 , P_0 , and Q_0 denote the nominal values of the load voltage and active and reactive power of the load. It is important to note that in the models above some fraction of the load is explicitly modeled as a function of bus voltage, while the other fraction is as an explicit function of frequency.

The usefulness of a load model is directly related to the correctness of the parameters of the model. The parameters can be obtained in two ways: pre-determined values can be chosen based on the load type, or the parameters can be estimated based on field measurements. The latter is more expensive but it is preferable, since it can yield more accurate values of the load parameters.

The estimation of the parameters of a static load is relatively simple, as the load model does not involve dynamical variables; in this case, the task of parameter estimation is practically reduced to curve fitting. References [35] and [132] report successful attempts to estimate static load parameters using a modified algorithm of Broyden, Fletcher, Goldfarb, and Shanno (BFGS) and a least squares technique, respectively. It should however be noted that the application of any gradient-based optimization routine can potentially lead to hitting a local optimum of the associated objective function, and thus obtaining inaccurate parameter values.

Dynamic load models

Nonlinear Dynamic Load Models

The impact that loads have on the dynamics of a power system has stimulated significant research efforts directed towards proper modeling of certain characteristics of power system loads. In many cases the use of static load models may be inappropriate due to their failure to accurately reflect the influence of the load on system stability [4], [81]; hence, since some loads do exhibit dynamical behavior (e.g., motor loads), these are represented by means of dynamical models.

It has been shown in [5] and [53] that the following models of aggregate loads can successfully capture the dominant nonlinear steady-state behavior of the load as well as load recovery and overshoot:

$$\begin{aligned} \dot{x}(t) &= -\frac{x(t)}{T_p} + P_0 \left[\frac{V_L(t)}{V_0} \right]^{N_{ps}} - P_0 \left[\frac{V_L(t)}{V_0} \right]^{N_{pt}} \\ P_d(t) &= \frac{x(t)}{T_p} + P_0 \left[\frac{V_L(t)}{V_0} \right]^{N_{pt}} \end{aligned} \quad (6.3)$$

$$\begin{aligned} \dot{z}(t) &= -\frac{z(t)}{T_q} + Q_0 \left[\frac{V_L(t)}{V_0} \right]^{N_{qs}} - Q_0 \left[\frac{V_L(t)}{V_0} \right]^{N_{qt}} \\ Q_d(t) &= \frac{z(t)}{T_q} + Q_0 \left[\frac{V_L(t)}{V_0} \right]^{N_{qt}} \end{aligned} \quad (6.4)$$

In the equations above $P_d(t)$ and $Q_d(t)$ are the active and reactive power demand of the load, P_0 , Q_0 , and V_0 stand for the nominal active, reactive power and voltage, respectively; the parameters T_p and T_q denote the time constant of the load internal state variables $x(t)$ and $z(t)$; and the exponents N_{ps} , N_{qs} , N_{pt} , and N_{qt} are the steady state and transient voltage indices. Observe that neglecting the frequency dependence in the static load model (6.1)–(6.2), the nonlinear load model (6.3)–(6.4) is equivalent to this model in steady state, i.e., for $\dot{x}(t) = 0$.

In the remainder of the chapter, the following notation will be used $y(t) := P_d(t)$ and $\theta = [N_{ps}, N_{pt}, T_p^{-1}]' = [\theta_1, \theta_2, \theta_3]'$. In general, for a given load the exponents θ_1 and θ_2 are not known exactly; however, similarly to the case of static load models, average values for many load types have been pre-determined. For example, [5] gives the following lower and upper bounds for these indices:

$$0 \leq \theta_1 \leq 3, \quad 0.5 \leq \theta_2 \leq 2.5. \quad (6.5)$$

For simplicity, henceforth, the voltage V_0 , active and reactive power P_0, Q_0 will be assumed to be known values. Thus, the system voltage can be normalized and denoted by: $V(t) := V_L(t)/V_0$. In the subsequent sections of this chapter only the model of active power (6.3) will be considered. The reactive power model given by (6.4) can be treated in exactly the same manner.

It should be noted that the load models (6.3)–(6.4) are linear in the states; the nonlinearities enter the equations as inputs and outputs. Thus, strictly speaking, the model in the identification procedure discussed here should be referred to as a “Hammerstein-Wiener” model structure [42]. However, since these models are actually used in stability analysis of power systems, where load voltage magnitudes are treated as either algebraic or state variables, the model is typically referred to as a nonlinear model in this context. For this reason, and for the simplicity of the comparisons between the two different load models discussed here, the present model is referred to as a “nonlinear model” in the remainder of the chapter.

Linear Dynamic Load Models

When studying the behavior of a system in a small proximity of a given operating point, the original nonlinear model can be approximated by a linear counterpart. That is, the nonlinear system can be linearized around the equilibrium point. Since the functions $V^{\theta_1}(t)$ and $V^{\theta_2}(t)$ are smooth for a smooth $V(t)$, the right-hand sides of (6.3) can be expanded in a Taylor series, resulting in the linearized model of the load [53]:

$$\begin{aligned}\Delta\dot{x}(t) &= -\theta_3\Delta x(t) + P_0(\theta_1 - \theta_2)\Delta V(t) \\ &= -A(\theta)\Delta x(t) + B(\theta)\Delta V(t) \\ \Delta y(t) &= \theta_3\Delta x(t) + P_0\theta_2\Delta V(t) \\ &= A(\theta)\Delta x(t) + D(\theta)\Delta V(t).\end{aligned}\tag{6.6}$$

In principle, to obtain a rough estimate of the system behavior, pre-determined values of the steady state and transient voltage indices can be used in simulations. However, as the transmission systems become more stressed, it becomes important to have more accurate estimates of the indices, since they directly influence important system characteristics such as damping; that is, incorporation of inaccurate load characteristics in power system simulation models can lead to overestimation of system damping [81].

As in the case of static load models, the load characteristics can be identified based on field measurements. The use of identification techniques can yield accurate estimates of load parameters, provided certain care has been exercised when selecting input signals and setting up the measurement circuits. These and related questions are treated in more detail in the next section.

6.3 System Identification

System identification can be defined as a collection of techniques which aim at extracting a mathematical model of a given process by analyzing relations between the input and output quantities of the process. Modern system identification has developed into a mature engineering discipline which is intensively applied in many branches of modern engineering. In this chapter, only identification techniques that are relevant to the problem at hand will be reviewed; for a detailed treatment of system identification theory and practice the reader is referred to [79, 80, 89].

AutoRegressive Moving Average with eXternal input (ARMAX) method

In its simplest form, the procedure of process identification may be formulated as follows:

Given two vectors u, y find three sets of parameters $a_i, b_k, c_l, i = 1, 2, \dots, n; k = 1, 2, \dots, m; l = 1, 2, \dots, p$ of a transfer function such that the model output \hat{y} best fits the measured data y , being subjected to the same excitation signal u .

The desired parameters can be found as shown below. Assume that the process can be described by the model (6.7)

$$\underbrace{y(t) + a_1y(t-1) + \dots + a_ny(t-n)}_{A(q)y(t)} = \underbrace{b_1u(t-1) + \dots + b_mu(t-m)}_{B(q)u(t)} + \underbrace{e(t) + c_1e(t-1) + \dots + c_pe(t-p)}_{C(q)e(t)} \quad (6.7)$$

or introducing the backward shift operator q , equation (6.7) can be cast in the form

$$A(q)y(t) = B(q)u(t) + C(q)e(t), \quad (6.8)$$

with the parameter vector

$$\theta = [a_1, \dots, a_n, b_1, \dots, b_m, c_1, \dots, c_p]^T.$$

Equation (6.8) can be reshaped by introducing $\hat{y}(t|\theta)$ —an estimate of $y(t)$:

$$C(q)\hat{y}(t|\theta) = B(q)u(t) + [C(q) - A(q)]y(t) \quad (6.9)$$

and further rearrangement of (6.9) yields:

$$\hat{y}(t|\theta) = B(q)u(t) + [1 - A(q)]y(t) + [C(q) - 1] \underbrace{[y(t) - \hat{y}(t|\theta)]}_{\varepsilon(t|\theta)} \quad (6.10)$$

$$= \phi'(t|\theta)\theta. \quad (6.11)$$

Minimization of the prediction error $\varepsilon(t|\theta)$ will yield the desired result—the parameter θ , i.e., the parameters a_i, b_k , and c_l . Once an objective function has been chosen, the minimization can be done in many ways. If the analyst has decided that the objective function should be a quadratic function in θ , e.g., $1/2\varepsilon(t|\theta)'\varepsilon(t|\theta)$, then the optimization results in the closed form solution:

$$\hat{\theta} = \left[\frac{1}{N} \sum_{t=1}^N \phi(t)\phi'(t) \right]^{-1} \frac{1}{N} \sum_{t=1}^N \phi(t)y(t) \quad (6.12)$$

State space identification methods

Now suppose that a model of the process is given by the state space model:

$$\begin{cases} x(t+1) = Ax(t) + Bu(t) + v(t) \\ y(t) = Cx(t) + Du(t) + w(t), \end{cases} \quad (6.13)$$

where $v(t)$ and $w(t)$ are the process and measurement noise [118]. The following statistical characteristics are given:

$$\begin{aligned} \mathcal{E}[v(t_1)v'(t_2)] &= R_1(\theta)\delta_{t_1,t_2} \\ \mathcal{E}[v(t_1)w'(t_2)] &= R_{12}(\theta)\delta_{t_1,t_2} \\ \mathcal{E}[w(t_1)w'(t_2)] &= R_2(\theta)\delta_{t_1,t_2}, \end{aligned} \quad (6.14)$$

where R are covariance matrices. The aim of the identification is to obtain the matrices A, B , and C such that the response of model (6.13) best fits the measured data.

The task is solved in several steps which involve solving a Riccati equation associated with (6.13) and (6.14):

$$P = APA' + R_1 - [APC' + R_{12}] [CPC' + R_2]^{-1} [CPA' + R'_{12}]. \quad (6.15)$$

Note that in (6.15) the argument of matrices $R(\theta)$ is suppressed for conciseness.

Having found P , one should compute the Kalman gain as

$$K = [APC' + R_{12}] [CPC' + R_2]^{-1} \quad (6.16)$$

Next, one-step ahead predictions are calculated which can be further used for the unknown parameter determination:

$$\begin{aligned} \hat{x}(t+1|t) &= A\hat{x}(t|t-1) + Bu(t) + K\tilde{y}(t) \\ y(t) &= C\hat{x}(t|t-1) + \tilde{y}(t). \end{aligned} \quad (6.17)$$

Subspace identification methods

Subspace identification methods are relatively new; however, they have already proven to be a sound alternative to well-established identification algorithms.

The power of the subspace algorithms lies in the following facts:

- They provide a clear link to the “old” identification methods
- They are of intrinsic Multi-Input-Multi-Output (MIMO) nature
- They allow the engineer to robustly estimate a possible order of the plant (done through inspection of singular values of the identified model)
- They allow for a lucid geometrical interpretation which actively connects human’s intuition [93].

Recent research [40] indicates that the use of subspace identification techniques can be utilized for the model-free Linear Quadratic Gaussian (LQG) controller design, which can be viewed as a very useful feature enabling the user to obtain an LQG controller without the need for identification of a process model.

Subspace identification methods exploit the so-called orthogonal projections of “the future outputs onto past and future inputs and the past outputs”. Mathematically the task of system identification is solved in several steps [40].

Step 1

Given two measurements u_i and y_k , $i, k = 1, 2, \dots, N$, form the input matrices for the ‘past’ and ‘future’ signals:

$$U_1 = \begin{bmatrix} u_0 & u_1 & \cdots & u_{k-1} \\ u_1 & u_2 & \cdots & u_k \\ \vdots & \vdots & \vdots & \vdots \\ u_{BH-1} & u_{BH} & \cdots & u_{BH+k-2} \end{bmatrix}, \quad (6.18)$$

$$U_2 = \begin{bmatrix} u_{BH} & u_{BH+1} & \cdots & u_{BH+k-1} \\ u_{BH+1} & u_{BH+2} & \cdots & u_{BH+k} \\ \vdots & \vdots & \vdots & \vdots \\ u_{BH+FH-1} & u_{BH+FH} & \cdots & u_{BH+FH+k-2} \end{bmatrix}, \quad (6.19)$$

where k is the number of columns¹, BH and FH stand for the backward and forward prediction horizons (number of data samples used for backward/forward prediction), respectively. According to [93], the prediction horizons must be “large enough”. U_1 and U_2 denote matrices containing the ‘past’ and ‘future’ signals. In a similar manner matrices Y_1 and Y_2 for the output y_k are formed.

Step 2

Define the new matrix $W_1 = [Y_1', U_1']'$ and then calculate the matrices L_w and L_u :

$$Y_2 / \begin{bmatrix} W_1 \\ U_2 \end{bmatrix} = Y_2 [W_1' U_2'] \begin{bmatrix} W_1 W_1' & W_1 U_2' \\ U_2 W_1' & U_2 U_2' \end{bmatrix}^\dagger \begin{bmatrix} W_1 \\ U_2 \end{bmatrix} \quad (6.20)$$

$$= L_w W_1 + L_u U_2 \quad (6.21)$$

In equation (6.20), the operator ‘ \dagger ’ is understood as the Moore-Penrose pseudo-inverse. For any square nonsingular matrix R , its pseudo-inverse $R^\dagger = R^{-1}$. If R is a non-square matrix and the following holds: $R^\dagger R R^\dagger = R^\dagger$, $R R^\dagger R = R$, $(R^\dagger R)' = R^\dagger R$, $(R R^\dagger)' = R R^\dagger$, then R^\dagger is the pseudo-inverse of R .

Step 3

The procedure terminates by computing the singular value decomposition (SVD) of L_w and estimating of the future output \hat{x}_1 [45]:

$$L_w = [U_a \ U_b] \begin{bmatrix} S_a & 0 \\ 0 & S_b \end{bmatrix} \begin{bmatrix} V_a' \\ V_b' \end{bmatrix}, \quad (6.22)$$

where U_a, U_b are the output singular vectors, V_a, V_b are the input singular vectors, and S_a, S_b are the singular values of the matrix L_w .

$$\hat{x}_1 = S_a^{1/2} V_a' W_1. \quad (6.23)$$

Concluding remarks on system identification

The main reasons for using identification techniques in power systems are the uncertain nature of the power system and ageing of power system components.

¹In [40], it is noted that k has to approach infinity in order to attain unbiased estimates.

Of course, it is preferable to explore every possibility of developing models of the system based on physical insights in order “not to estimate what we already know” [113]. Often a combination of modeling based on physical insights and system identification yields best results.

Power System Load Identification

In the context of this chapter, the load voltage and load power comprise the pair of input and output signals. It can be noticed that both models (6.3) and (6.4) describe the dynamic behavior of a load as functions of the nodal voltage in a noise-free environment i.e., the presence of noise is not reflected in the models. Hence, to account for the presence of noise in the measurements and since no information is available regarding the noise model, an output error model is chosen, which is known to be robust and have a plausible physical interpretation. To simplify notation, two new functions $u_1(\theta)$ and $u_2(\theta)$ are introduced:

$$\begin{aligned} u_1(\theta) &:= P_0 V^{\theta_1}(t) - P_0 V^{\theta_2}(t) \\ u_2(\theta) &:= P_0 V^{\theta_2}(t) \end{aligned}$$

Now, the model (6.3) can be reformulated in a stochastic framework as:

$$\begin{aligned} \dot{x}(t) &= -\theta_3 x(t) + u_1(\theta) \\ y(t) &= \theta_3 x(t) + u_2(\theta) + e(t) \\ &= \hat{y}(t) + e(t). \end{aligned} \tag{6.24}$$

In the equation above, the term $e(t)$ represents white Gaussian noise with known statistics. Similar arguments apply to the model of reactive power.

Model discretization

Since measurements used in system identification are collected at predefined instants of time, the continuous-time load equations (6.24) should be converted to discrete-time counterparts. In this work, the discrete-time description of the load equations is based on the Zero-Order Hold method (ZOH) and is obtained as follows [124]:

$$x(k\ell + \ell) = F(\theta)x(k\ell) + H(\theta)u_1(k\ell) \tag{6.25}$$

$$y(k\ell) = \theta_3 x(k\ell) + u_2(k\ell) + e(k\ell) \tag{6.26}$$

where $\ell := t_{k+1} - t_k, \forall k \in \mathcal{I} \subseteq \mathbb{N}$, stands for the sampling interval, and the variables $F(\theta)$ and $H(\theta)$ are:

$$F(\theta) := \exp(-\theta_3 \ell), \quad (6.27)$$

$$\begin{aligned} H(\theta)u_1(k\ell) &= \int_{k\ell}^{k\ell+\ell} \{\exp(\theta_3(k\ell + \ell - \tau))u_1(\tau)\} d\tau \\ &= (1 - F(\theta))\theta_3^{-1}u_1(k\ell). \end{aligned} \quad (6.28)$$

In equation (6.28), it is assumed that the input function $u_1(\tau)$ is constant and equal to $u_1(k\ell)$ for $k\ell \leq \tau \leq k\ell + \ell$.

Several numerical experiments conducted in the framework of this thesis confirmed that ZOH discretization yields the least error as compared with other methods such as, for instance, the forward Euler and the trapezoidal methods. Thus, ZOH is used here to discretize the nonlinear equations (6.24).

Prediction Error for the Nonlinear Load Model

The discretized equations can be utilized as a basis for the prediction of future outputs of the dynamic system, i.e.,

$$\begin{aligned} qx(k\ell) - F(\theta)x(k\ell) &= H(\theta)u_1(k\ell) \\ x(k\ell) &= (q - F(\theta))^{-1}H(\theta)u_1(k\ell) \\ y(k\ell|\theta) &= \theta_3 \{(q - F(\theta))^{-1}H(\theta)u_1(k\ell)\} + u_2(k\ell)e(k\ell) \\ &= \frac{1 - F(\theta)}{q - F(\theta)}u_1(k\ell) + u_2(k\ell) + e(k\ell) \\ &= \hat{y}(k\ell|\theta) + e(k\ell). \end{aligned} \quad (6.29)$$

In equation (6.29), the symbol q denotes the forward shift operator. It is interesting to observe that the predicted value of the system output $\hat{y}(k|\theta)$ at time k equals the sum of the pre-filtered input function $u_1(k)$ and input function $u_2(k)$. Finally, the prediction error is defined as the difference between the predicted and actual output of the system

$$\varepsilon(k|\theta) = y(k) - \hat{y}(k|\theta), \quad \forall k \in \mathcal{I}. \quad (6.30)$$

Prediction Error for the Linear Load Model

Similarly to the nonlinear load model, let us assume that the dynamic response of the load can be satisfactorily described by a linear output error model, i.e.,

$$\Delta y(t) = A(\theta)\Delta x(t) + D(\theta)\Delta V(t) + e(t). \quad (6.31)$$

Applying the ZOH method to linearized load model (6.6), one readily obtains the discrete load model:

$$\begin{aligned} \Delta x(k\ell + \ell|\theta) &= F(\theta)\Delta x(k\ell) + \Gamma(\theta)\Delta V(k\ell) \\ \Delta y(k\ell|\theta) &= A(\theta)\Delta x(k\ell) + D(\theta)\Delta V(k\ell) + e(k\ell), \end{aligned} \quad (6.32)$$

where (6.32), $\Gamma(\theta) = H(\theta)P_0(\theta_1 - \theta_2)$, where $F(\theta)$ and $H(\theta)$ are defined as in (6.27) and (6.28), respectively.

Eliminating the state variable $\Delta x(k\ell)$, the discretized output error model (6.32) can be rewritten in the form of a transfer function:

$$\begin{aligned} \Delta y(k\ell|\theta) &= \frac{\theta_3\Gamma(\theta)}{q - F(\theta)}\Delta V(k\ell) + e(k\ell) \\ &= P_0\frac{1 - F(\theta)}{q - F(\theta)}(\theta_1 - \theta_2)\Delta V(k\ell) + e(k\ell) \\ &= \Delta\hat{y}(k\ell|\theta) + e(k\ell). \end{aligned} \quad (6.33)$$

The prediction error for the linearized model is formulated as the difference between the measured output $\Delta y(k\ell)$ and the predicted output $\Delta\hat{y}(k\ell)$:

$$\varepsilon(k|\theta) = \Delta y(k\ell) - \Delta\hat{y}(k\ell|\theta), \quad \forall k \in \mathcal{I}. \quad (6.34)$$

Minimization of the Prediction Error

Ideally, in a noise-free environment the prediction error is zero at all times, if both load model and the values of the parameter vector θ are known exactly. In practice, however, this is not achievable due to the fact that these conditions are not satisfied; moreover, field measurements always contain noise. Therefore, in the best case scenario, one can hope for keeping the prediction error reasonably small, which

can be accomplished by formulating an optimization problem in which certain objective function—often a 2-norm of the prediction error vector—is minimized by varying the parameter vector θ over the feasible parameter space. We thus follow the system identification tradition and define the optimization problem as

$$\theta^* = \arg \min_{\theta \in \Omega} \frac{1}{2N} \|\varepsilon(\theta)\|_2^2. \quad (6.35)$$

In the expression above, N is the number of data samples, θ^* and Ω stand for the optimal parameter vector and the feasible parameter space defined by (6.5), respectively.

The success of prediction error minimization depends on a number of factors, namely,

- (i) The optimization technique applied
- (ii) The availability of a reasonable initial vector θ_0 , and
- (iii) The properties of the objective function.

While the first two factors in most practical cases can be relatively easy overcome, non-convexity of the objective function can in general represent a significant challenge for all gradient-based optimization techniques. In order to avoid the traps of local minima, a robust minimization technique capable of finding the global optimum has been applied in the work reported in this chapter. A brief description of this optimization method as well as the techniques used to determine the variance of the estimates are given below.

Adaptive Simulated Annealing

Simulated annealing (SA) can be defined as a family of general-purpose constrained optimization algorithms whose operational principles imitate the process of crystal formation in solids during gradual cooling [92], [119].

The key idea behind SA algorithms is the analogy with the thermodynamical process of cooling of a substance and subsequent formation of regular crystals. It has been discovered that when slowly cooled, the molecules of the substance tend to assume spatial positions which minimize the total potential energy of the substance. Analogously, in SA optimization routines a certain objective function represents the potential energy of the substance, the parameters to be optimized can be thought of as the molecules of the substance. The analogy is completed by introducing an artificial parameter that represents the temperature of the substance.

The invention of SA is credited to Metropolis [83]; however, its widespread use was initiated by Kirkpatrick's work [70]. Simulated annealing algorithms have already been applied to a large number of optimization problems such as power system planning and dynamic security assessment, spectral analysis estimation, signal detection, image processing and many other.

The main strength of SA algorithms lies in the fact that they are capable of finding the global optimum of a given objective function. This is achieved by introducing the so-called acceptance probability which allows avoiding local optima. The simplest implementation of an SA algorithm involves the following steps.

- Selection of an initial guess θ_0 of the parameter vector θ .
- Formulation of the objective function $J(\theta)$ and temperature schedule $T_k(\Delta J_k, k)$, where k is the iteration number. Evaluation of the objective function at θ_0 .
- Setting the so-called generating probability function, i.e., the function that will govern the formation of random perturbations to the current parameter vector θ .
- Setting the acceptance probability which is described by the Boltzmann distribution $p_k(\Delta J_k, T_k)$.
- Generation of r perturbations $\theta^{(r)}$ in proximity to θ_0 and computing the corresponding $\Delta J_k^{(r)} = J_k^{(r)} - J_k$. If $\theta^{(r)}$ yields an increase of the objective function, it is accepted as the new parameter vector, i.e., $\theta \leftarrow \theta^{(r)}$, otherwise it is accepted with the probability $p_k^{(r)} = \exp(\Delta J_k^{(r)} / T_k)$.
- Selection of a stopping criterion and checking if the stopping criterion is satisfied.
- The iteration number is increased and the temperature is reduced.

It is known that simulated annealing algorithms are statistically guaranteed to find global optima, provided the temperature schedule, generating probability function, and acceptance probability are properly chosen [111]. It should however be noted that simulated annealing has some drawbacks, one of which is slow convergence rate.

Several modifications have been made to the basic SA algorithms in an attempt to improve its performance. One of the most successful SA variations was developed by L. Ingber [59] and termed *Adaptive Simulated Annealing* (ASA). Due to a

new temperature schedule with T_k decreasing exponentially in time and utilization of re-annealing ASA performs significantly better than the basic SA algorithm and algorithms based on Cauchy annealing.

The reasonable performance of ASA combined with the ability to locate global optima make its use suitable for the optimization tasks studied in this chapter.

Cramér-Rao Lower Bound for the nonlinear load model

Determination of an optimal θ^* satisfying (6.35), constitutes the first step of the load identification procedure presented in this chapter. The second step involves the computation of the variance of the estimates to assess the “quality” of the proposed identification procedure. The variance of the estimates depends on several factors, among which the most important for the application discussed here are the number of data samples available, the variance of noise $e(t)$, the model of the load, and the input signal.

To assess the minimum variance of the unknown parameters, the so-called Cramér-Rao Lower Bound (CRLB) is often used. By definition, CRLB is an inverse of the Fisher Information Matrix (*FIM*)

$$FIM = \mathcal{E} \left(\left(\frac{\partial \ln L(\theta, N)}{\partial \theta} \right)' \frac{\partial \ln L(\theta, N)}{\partial \theta} \right), \quad (6.36)$$

where N is the number of data samples available and $\mathcal{E}(\xi)$ is the expected value of ξ . The maximum likelihood function $\ln L(\theta, N)$ is defined in terms of the corresponding probability density function $L(\theta, N)$ as follows:

$$\begin{aligned} L(\theta, N) &= \frac{(2\pi)^{-N/2}}{\sqrt{\det(W)}} \exp \left[-\frac{1}{2} [y - \hat{y}]' W^{-1} [y - \hat{y}] \right] \\ &= \frac{(2\pi)^{-N/2}}{\sqrt{\det(W)}} \exp \left[-\frac{1}{2} \|y - \hat{y}\|_{W^{-1}}^2 \right] \end{aligned} \quad (6.37)$$

In equation (6.37), W is a symmetric matrix representing the covariance of white Gaussian noise $e(t)$. This matrix can be used as an instrument to accentuate reliable parts of the measured data y . Often it is assumed that $W = \sigma^2 I_N$, where I_N is the identity matrix and σ^2 is the variance of $e(t)$. Without significant loss of generality, in the remainder of this chapter it is assumed that $W \equiv I_N$, which renders the two norms $\|\cdot\|_2$ and $\|\cdot\|_{W^{-1}}$ equivalent.

The derivation of CRLB for the parameter vector θ requires the computation of the gradient of the maximum likelihood function, which is equivalent to the

gradient of the objective function in (6.35). The gradient is computed as follows: (for notational simplicity the argument θ is suppressed in the following)

$$\begin{aligned} \frac{1}{2N} \frac{\partial \|\varepsilon(\theta)\|_2^2}{\partial \theta} &= \frac{1}{2N} \frac{\partial (\varepsilon' \varepsilon)}{\partial \theta} \\ &= \frac{1}{2N} \left[\frac{\partial \varepsilon'}{\partial \theta} \varepsilon + (\varepsilon' \otimes I_n) \frac{\partial \varepsilon}{\partial \theta} \right] \\ &= \frac{1}{N} \frac{\partial \varepsilon'}{\partial \theta} \varepsilon, \end{aligned} \quad (6.38)$$

where the Jacobian matrix $\partial \varepsilon' / \partial \theta$ is defined by

$$\frac{\partial \varepsilon'}{\partial \theta} = \begin{bmatrix} \frac{\partial \varepsilon_1}{\partial \theta_1} & \frac{\partial \varepsilon_2}{\partial \theta_1} & \cdots & \frac{\partial \varepsilon_n}{\partial \theta_1} \\ \frac{\partial \varepsilon_1}{\partial \theta_2} & \frac{\partial \varepsilon_2}{\partial \theta_2} & \cdots & \frac{\partial \varepsilon_n}{\partial \theta_2} \\ \frac{\partial \varepsilon_1}{\partial \theta_3} & \frac{\partial \varepsilon_2}{\partial \theta_3} & \cdots & \frac{\partial \varepsilon_n}{\partial \theta_3} \end{bmatrix} \quad (6.39)$$

and the partial derivatives are

$$\begin{aligned} \frac{\partial \varepsilon_k}{\partial \theta_1} &= \frac{F(\theta) - 1}{q - F(\theta)} P_0 V^{\theta_1}(k) \ln V(k) \\ \frac{\partial \varepsilon_k}{\partial \theta_2} &= \frac{1 - q}{q - F(\theta)} P_0 V^{\theta_2}(k) \ln V(k) \\ \frac{\partial \varepsilon_k}{\partial \theta_3} &= \ell F \frac{1 - q}{(q - F(\theta))^2} u_1(k). \end{aligned} \quad (6.40)$$

It should also be noted that for the load model adopted in this chapter, i.e., that given by (6.25)–(6.26), the CRLB explicitly depends on both the input signal $V(k)$ and the sampling interval ℓ . Moreover, by direct inspection of equations (6.39) and (6.40), one can immediately conclude that for $V(k) \equiv 1 \forall k$, the matrix $\partial \varepsilon' / \partial \theta$ loses rank and as a result *FIM* becomes singular indicating that the variance of θ is infinite; that is, the parameters θ are not identifiable, when the voltage is at steady state ($V(t) = V_0$).

It should be noted that the Jacobian (6.39) can be utilized to enhance the identification procedure by excluding the parameters θ_i that are weakly identifiable or non-identifiable [27], [57]. That is, one can use the algorithm proposed in [27] to determine which load parameters θ_i cannot be reliably identified from the available field measurements. This can be done in the following 5 steps.

1. Decompose $\partial \varepsilon' / \partial \theta := V \Lambda V'$.
2. Inspect the eigenvalues of the Jacobian, i.e., the diagonal elements of the matrix Λ . Determine the number ρ which is equal to the number of eigenvalues of the Jacobian which are greater than some threshold value. This number indicates the number of identifiable parameters.
3. Partition $V := V_1 \oplus V_2$, where $V_1 \in \mathbb{R}^{N \times \rho}$ consists of the first ρ columns of matrix V .
4. Factorize V_1' to obtain the orthonormal basis of the range space of V_1' , the upper triangular matrix R , and the permutation matrix P , i.e., $V_1' P := QR$.
5. Use P to determine the parameters θ_i that should not be identified but rather set to some (approximate) values which are known beforehand.

The study reported in [27] indicates that this algorithm allows a significant reduction of the variance of the estimates of the ρ parameters even when the exact values of the non-identifiable parameters are unknown. A more detailed description of the algorithm and its applications can be found in [27], [57]. Numerical experiments conducted in the framework of this study show that for the typical values of the load parameters the Jacobian matrix is always well-conditioned implying that all 3 parameters are identifiable; thus this algorithm is not applied in the case study discussed here.

6.4 Application Examples

Artificial data

In order to investigate the statistical properties of the identification procedure presented in this chapter, a series of experiments is conducted using artificially created data. Thus, in this section, the following issues are addressed:

- It is shown numerically that the estimates are asymptotically unbiased, which would not have been the case if an unreasonable predictor was chosen.
- A rough estimate of the magnitude of bias that can be expected for the linearized model (6.33) is obtained, which is a basic issue in system identification that has not yet been addressed in the current literature in load modeling.

- The adequacy of the optimization routine, i.e. an adaptive simulated annealing algorithm, used in the chapter is demonstrated, as the method is able to locate the global minimum of the objective function in all experiments.

The data vector $y(t_k)$ is generated with the help of a model with known parameters θ ; the output $y(t_k)$ is then corrupted by Gaussian noise having known statistics, i.e., $e(t) \sim \mathcal{N}(0, \sigma^2 I)$ and the identification procedure is applied. The estimates of the parameter vector θ are analyzed in this case to assess the performance of the proposed technique.

The main goal of the numerical experiments in this section is to investigate the asymptotic behavior of the variance of the estimates $\hat{\theta}(N)$. In other words, the following relation has to be verified numerically:

$$\lim_{N \rightarrow \infty} \text{var } \hat{\theta}(N) = 0 \quad (6.41)$$

for both linear and nonlinear load models. In expression (6.41) the operator var is defined as $\text{var } \xi = \mathcal{E}(\xi^2)$, where ξ is a stochastic variable. To study the variance of estimates, the value of N is steadily increased and for each value of N , a series of Monte-Carlo simulations is performed. The variance is then computed and plotted versus the number of samples N . In this case study, the data are generated using the discrete-time model (6.25)–(6.26). The Monte-Carlo simulations involve 30 runs for each N , and the noise has the statistics $\mathcal{N}(0, 0.0015)$ with $\theta = [1.2 \ 2.7 \ 0.3448]'$. The adaptive simulated annealing optimization routine is initialized with $\theta_0 = [0.5 \ 2.0 \ 1.7]'$; and the feasible region Ω is given by (6.5), and the additional inequality $0 \leq \theta_3 \leq 10$.

The results of the Monte-Carlo simulations are shown in Figures 6.1 and 6.2.

Several important observations can be made regarding the performance of the nonlinear model-based identification technique:

- All three parameters θ_i are accurately estimated by applying the identification algorithm to noisy data.
- The variance of the estimates decreases as the number of samples increases. This result indicates that the estimate $\hat{\theta}$ is asymptotically unbiased, i.e., equation (6.41) holds. This could be expected since minimization of (6.35) is equivalent to maximization of the maximum likelihood function, which yields asymptotically unbiased estimates [79].
- For all N the variance of the estimates is insignificantly greater than the corresponding CRLB, which implies that the proposed estimator is statistically efficient.

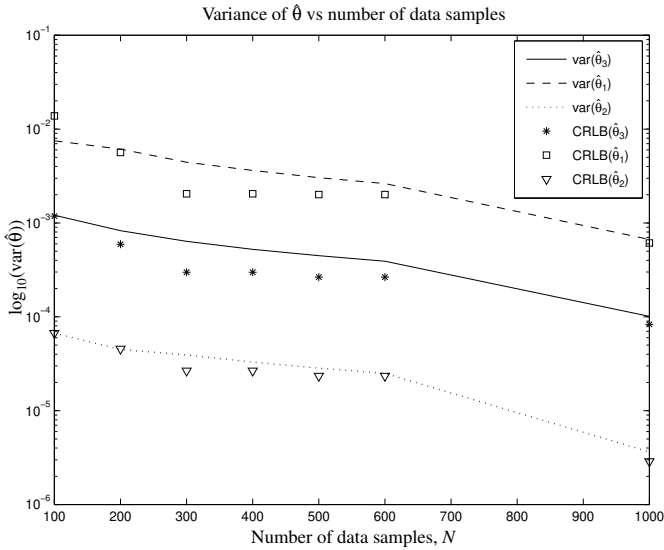


Figure 6.1: Variance of the estimated parameter vector $\hat{\theta}$ versus number of samples and the corresponding Cramér-Rao Lower Bounds for the artificial data set. Nonlinear load model

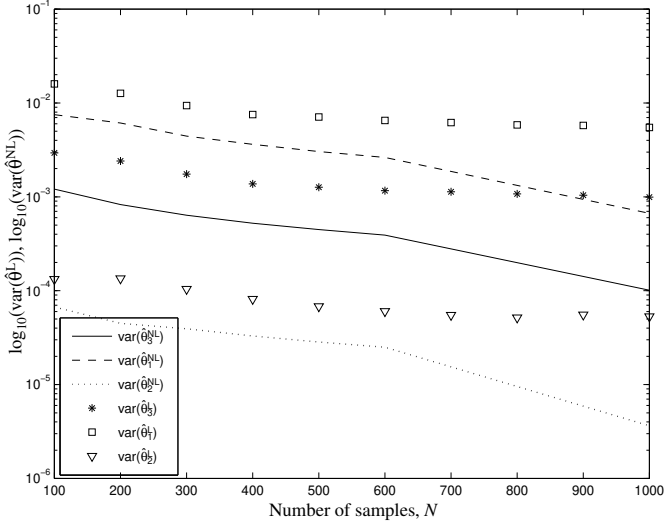


Figure 6.2: Variance of the estimates of the linear and nonlinear model parameters

Comparing the results obtained with the linear and nonlinear model-based identification methods, the following can be concluded:

- The linear model-based identification method yields estimates of the parameters $\hat{\theta}^L$ acceptable for most practical purposes, since the maximum variance for this model does not exceed 2×10^{-2} for the given level of noise and number of data samples.
- The variance of $\hat{\theta}^L$ decreases as the number of data samples increases; however, in all cases, the decrease rate is not very large.
- In all cases, the variance of the estimates $\hat{\theta}^{NL}$ obtained with the nonlinear model is smaller than that obtained with the linear model. This is due to the bias induced by the use of the linearized model. In other words, for the linear model, (6.41) does not hold.

It should therefore be expected that the use of linear model may yield reasonable estimates of the parameters θ ; however, the estimates will be biased. In general, the use of the nonlinear load model always provides more accurate estimates of the load parameters as compared to the linear model; nevertheless, in the real world applications the estimates obtained with the nonlinear model will also be biased, since the nonlinear model (6.24) is only an idealization of the actual load and thus has its limitations in terms of the accuracy of the estimates.

Application to field measurements

After verifying the adequacy of the proposed technique, it is then applied to field measurements taken at a paper mill located in the neighborhood the town of Grums, Sweden. The electrical network of the paper mill is schematically shown in Fig. 6.3; in this figure, only the part of the network relevant to the present case study is depicted. The network consists of two synchronous backup generators G1 and G3, four high-priority loads LD1–LD4, and six transformers T1–T6.

In normal conditions, the paper mill is fed by the grid denoted as NET. During the hours of high risk of having power supply interruptions (due to thunderstorms), the load LD1–LD4 are entirely fed by the backup generators.

In order to assure the proper and reliable operation of the paper mill, detailed dynamic simulations with accurate load models are needed; thus, a series of field measurements was obtained on May 15, 2001, in order to obtain aggregate models of LD1–LD4 and some other equipment. To the best knowledge of the author, the load in question mainly consists of lighting, heating devices, and electrical motors.

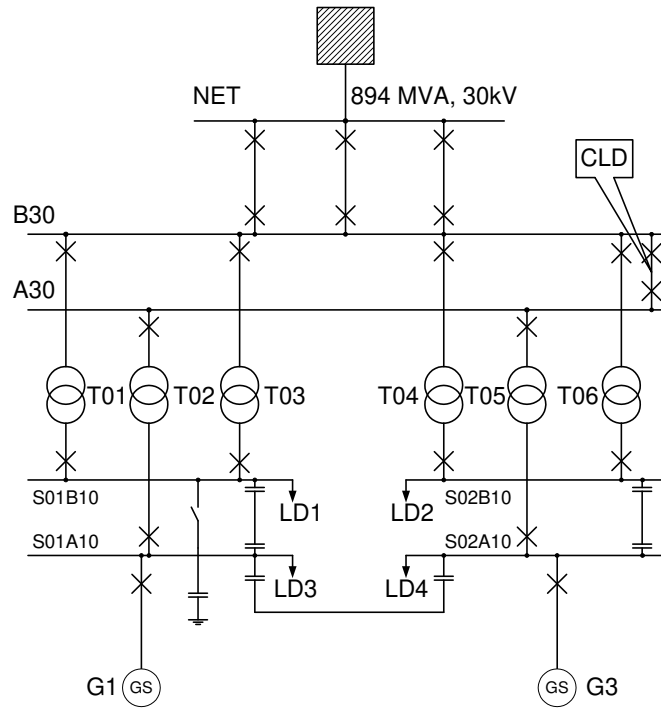


Figure 6.3: Electrical diagram of the studied part of Grums paper mill

The motors are in almost all cases equipped with power converters. The load voltage was used as the input and load current as the output. Since the load models (6.3)–(6.4) use the active P_d and reactive Q_d power signals as outputs, P_d and Q_d were synthesized off-line. The sampling rate was set to 2 kHz.

An interruption of power supply to the paper mill may result in a substantial monetary loss. It should be noted that a step-wise voltage change could cause excessive shock to the system and trigger a power interruption. Moreover, a voltage step could result in an ill-conditioned Fisher information matrix and thus estimates with a large variance. Therefore, the backup generators were used to vary the load voltage in a smooth manner in a $\pm 3\%$ range. Extensive studies reported in [132] also suggest that the variations of voltage magnitude has little effect on the success of the parameter identification procedure, as long as the magnitude variation is a few per cent of the nominal voltage.

Given the restrictions imposed in the measuring procedure as well as the costs

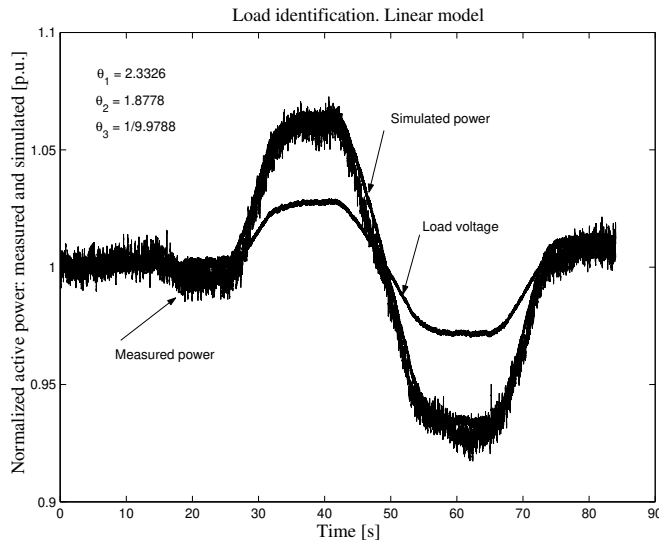


Figure 6.4: Application of the proposed identification scheme to field measurements. Estimation of the parameters of active power load. Linearized model

associated with obtaining these measurements, it was only feasible to gather one set of data at the given operating conditions. Hence, the cross-validation procedure applied here is based on a comparison between the linear (6.6) and nonlinear (6.24) load models identified using the proposed procedure and based on the same set of field measurements. Figures 6.4 and 6.5 depict the field measurements, i.e., the load voltage and active power, as well as the simulated outputs $P_d(t)$ of the linear and nonlinear models. Visual comparison of the measured and simulated power indicate that both models capture the relevant dynamics of the load; however, the nonlinear model yields better results, showing a very close match with the field measurement, as these two curves are practically indistinguishable.

Table 6.1 presents the numerical values of the parameters obtained with both linear and nonlinear system identification techniques. In the table, the error is defined as $(\hat{\theta}_i^{NL} - \hat{\theta}_i^L) / \hat{\theta}_i^{NL} \cdot 100\%$, where $\hat{\theta}_i^L$ and $\hat{\theta}_i^{NL}$, $i = 1, 2, 3$ are the estimates of the linearized and nonlinear model parameters, assuming the nonlinear model is the reference for these calculations, given the close match between this model and the actual measurements. The table reveals that the parameters identified with the linear model do not deviate significantly from those obtained with the nonlinear

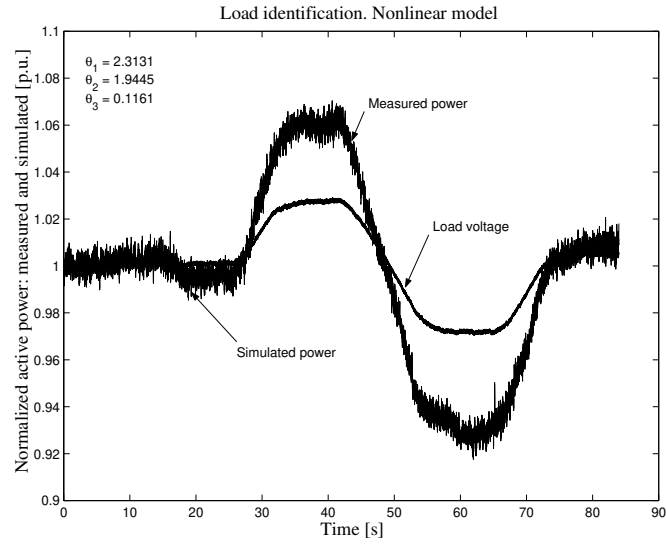


Figure 6.5: Application of the proposed identification scheme to field measurements. Estimation of the parameters of active power load. Nonlinear Identification

Table 6.1: Comparison of the load parameters identified using linear and nonlinear models

	Linear model	Nonlinear model	Error [%]
N_{ps} [p.u.]	2.3326	2.3131	-0.8430
N_{pt} [p.u.]	1.8778	1.9445	3.4302
T_p^{-1} [s]	0.1002	0.1161	13.6951

load identification technique. This is mainly due to the fact that the voltage deviation was not large and hence nonlinear effects were not very significant. However, observe that the maximum error introduced by the use of linearized model is still greater than 13%; hence, we may conclude from these results that the nonlinear model is a more accurate representation of the given aggregate load.

Notice that at different operating conditions, one would expect to obtain different values for the load parameters. However, based on the results depicted here and the fact that the load composition is not expected to change significantly for typical operating conditions, it is reasonable to expect similar trends in terms of the accuracy of the linear and nonlinear load models for representing the given aggregate load.

It is interesting to compare the values of load parameters obtained in this study with those reported in the literature. For instance, [132] cites the following value for $N_{ps} = 0.72$ for an industrial load. This value differs significantly from the one shown in Table 6.1, which can be mainly explained by a different composition of the load. The steady state and transient voltage indices determined in [66] match those of the present case study somewhat more closely; however, the time constants T_p differ significantly, which can be explained by the absence of devices having slow dynamics, e.g., OLTC in the present study.

6.5 Summary

Two power system load identification techniques are proposed in this chapter. Well established equations describing the nonlinear recovery mechanisms of load form the basis of both techniques, which are formulated in the framework of stochastic system identification theory. Specifically, a linear and nonlinear output error estimators are introduced and analyzed, and generic equations applicable to identification of aggregate models of power system loads are developed and studied in detail.

The asymptotic behavior of the estimates is studied by means of numerical experiments with artificially created data, demonstrating that the estimates are asymptotically unbiased for the nonlinear load model and their variance attains the Cramér-Rao lower bound. To avoid numerical problems associated with possible multiple minima of the objective function, a global minimization technique was utilized. The enhanced numerical features of the minimization routine enable fast convergence to the global minimum of the objective function with a probability of 1.

The theoretical foundations presented in this chapter were applied to field measurements taken at a paper mill located in the neighborhood of the town of Grums, Sweden. Both linear and nonlinear models were utilized in order to estimate the load parameters. The results show that, in principle, the linear model yields valid estimates that differ from the estimates obtained using the nonlinear model. Whenever the accuracy requirements on the numerical values of the load parameters are not stringent, linear identification can be applied for the estimation of the parameters. Alternatively, the nonlinear load modeling and identification technique presented in this thesis can be used to better model the load and obtain more accurate estimates of the load parameters.

Part IV

Qualitative Analysis of Operation, Control, and Stability of Distributed Generation

*“He was under the impression that a system description
(like the transfer function) is exactly the same
as a system in a concrete physical sense.”*

— R. Kalman [65]

On the flaws in the Wiener formulation.

Chapter 7

Design of Robust Control for Enhancing the Performance of SOFC Power Plant

This chapter presents a discussion on the load following capabilities of a power plant that consists of solid oxide fuel cells (SOFC) and microturbines. Such a power plant, in theory, is capable of operating at unprecedented efficiencies which can be above 80%. However, as the analysis in this chapter shows, the load following capabilities of this power plant can be unsatisfactory, due to certain control limitations. To enhance the load following capabilities of the power plant, attenuate possible disturbances from the distribution grid, and avoid interaction between the control functionalities of the fuel cells and the microturbines, two \mathcal{H}_∞ controllers are designed. The main emphasis in this chapter is placed upon the behavioral features of the fuel cell plant itself rather than on the studying the integrated system “fuel cell–distribution grid”. The exposition of the theoretical material in this chapter is rather axiomatic; however, this approach will certainly suffice for the practical purposes of this work. We commence by giving a brief overview of \mathcal{H}_∞ control theory.

7.1 Robust Control

Modeling of electric power systems is not a trivial task even if the engineer has succeeded in collecting all the necessary information about the power system. Aging of power equipment and uncertain load¹ complicate

¹More specifically, both the level and composition of the load at a given instant of time are uncertain. In system planning studies, power system loads can be forecasted; however, neither type

modeling, analysis, and control of electric power systems.

This feature of power systems suggests the choice of control strategy—robust control—if precise and “guaranteed” control of some quantities, e.g., active power output is required. It is quite likely that the potential of robust and optimal control techniques will have the commanding influence on power engineering; however, this time is yet to come. For this and other reasons, the foundations of \mathcal{H}_∞ control theory are presented in detail in this chapter. It is hoped that this will help in disseminating these techniques among practicing electrical engineers.

The origins of \mathcal{H}_∞ optimal control theory were established in the early 1980’s by G. Zames, see e.g., [133]. Since then it has been intensively studied by the control community. A brief introduction to this fascinating theory is given below. This section establishes the relationship between the robustness issue and \mathcal{H}_∞ -norm minimization. Most of the section makes an extensive use of frequency domain due to nice geometrical interpretations of the main concepts and follows chiefly [76]; however, time-domain solutions to the standard \mathcal{H}_∞ problem are also presented. It should be noted that the presentation is fairly general, and the theory is applicable to a large class of linear time-invariant systems, whose transfer functions or state space realizations are represented by either the capital P or G , respectively. There is however a simple relationship between these two representations. For details on the SOFC plant studied, the reader should refer to Section 3.2 and Appendix C.

The standard \mathcal{H}_∞ control problem can now be formulated. However, prior to the introduction of the \mathcal{H}_∞ theory, it is instructive to introduce the main configuration of the controlled plant and controller itself. Fig. 7.1 shows the standard block diagram of the dynamic system which is controlled by an external controller K . It should be stressed that the so-called weighting functions which are the main tools for fulfilling the control specifications are already absorbed into the plant G . At the present time, this will not be discussed, as the structure of the plant is different in the setting for the frequency and time domains.

The main purpose of the linear robust controllers in this chapter is to provide tight active power output control of the tandem SOFC–microturbines. Furthermore, the models of the SOFC is assumed be deterministic; however, the terminal voltage variations are treated as unstructured model uncertainty. The voltage variations are assumed to be caused either by the operation of the microturbines or by the disturbances on the distribution grid. Thus, in this study, the presence of the microturbines is accounted for only indirectly.

Now the problem of \mathcal{H}_∞ -controller synthesis can be stated

nor dynamical characteristics of the load are specified.

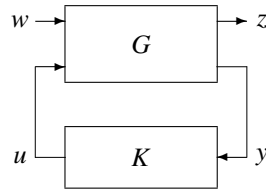


Figure 7.1: Standard diagram of the plant and controller

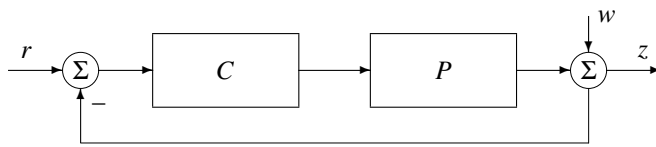


Figure 7.2: Single-input single-output plant

\mathcal{H}_∞ CONTROLLER PROBLEM FORMULATION

Given the generalized plant G , exogenous inputs w , outputs z , and control specifications, find all admissible controllers K such that the \mathcal{H}_∞ -norm of the transfer matrix from w to z is minimized, subject to the constraint that all K 's stabilize the plant G .

We commence by reviewing frequency-domain methods for \mathcal{H}_∞ controller synthesis.

Frequency domain solutions to \mathcal{H}_∞ control problem

The system to be controlled is depicted in Fig. 7.2. For simplicity, the system is assumed to be a single-input single-output (SISO) system. As the analysis is somewhat more lucid in the frequency domain, the plant studied is represented by the transfer function $P = C(sI - A)^{-1}B + D$, where A, B, C , and D are the system matrices.

In Fig. 7.2, $P(s)$ is the controlled plant, $C(s)$ is the controller, w represents a disturbance, and z is the output. The resultant transfer function from r to z is given by the expression:

$$H(s) = \frac{C(s)P(s)}{1 + C(s)P(s)} \quad (7.1)$$

The ratio $(1 + C(s)P(s))^{-1}$ is called the *sensitivity function* of the feedback system, which characterizes the sensitivity of the compensated plant to various disturbances.

Usually the sensitivity function is denoted by capital S . In the ideal case, the sensitivity function S should be zero. In practice it is, however, unrealistic to require zero sensitivity. Instead, an upper bound on the peak value of the sensitivity function is specified for a certain range of frequencies. That is, one sets an upper limit on $\|S\|_\infty$:

$$\|S\|_\infty = \sup_{\omega \in \mathbb{R}} |S(j\omega)|. \quad (7.2)$$

As is seen in (7.2), the sensitivity function is a function of frequency, assuming different values for different frequencies. As this dependence is undesirable (due to the possible magnification of noise and the influence of neglected dynamics), a weighting function $W(j\omega)$ is introduced in order to reduce the dependence.

$$\|WS\|_\infty = \sup_{\omega \in \mathbb{R}} |W(j\omega) \cdot S(j\omega)|. \quad (7.3)$$

The loop gain $L = PC$ is another quantity which plays an important role in \mathcal{H}_∞ optimization and is closely connected to robustness of the system, see Fig. 7.2.

Due to the plant uncertainties (in power systems this can be the level of loading of the system), the actual plant parameters differ from the nominal ones. To distinguish between them, the loop gain of the actual plant is denoted by L and that of the nominal plant as L_0 . Both these plants are stable if the corresponding Nyquist plots do not encircle the point $(-1, j \cdot 0)$. Following in steps of [76], it may be noted that plant is stable if the following inequality holds:

$$|L(j\omega) - L_0(j\omega)| < |L_0(j\omega) + 1|, \quad \forall \omega \in \mathbb{R}. \quad (7.4)$$

Graphical interpretation of the inequality is given by Fig. 7.3. Inequality (7.4) can be rearranged as follows:

$$\frac{|L(j\omega) - L_0(j\omega)|}{|L_0(j\omega)|} \cdot \frac{|L_0(j\omega)|}{|L_0(j\omega) + 1|} < 1, \quad \forall \omega \in \mathbb{R} \quad (7.5)$$

The complementary sensitivity function T_0 of the closed loop plant is defined as:

$$T_0 = 1 - S_0 = 1 - \frac{1}{1 + L_0} = \frac{L_0}{1 + L_0} \quad (7.6)$$

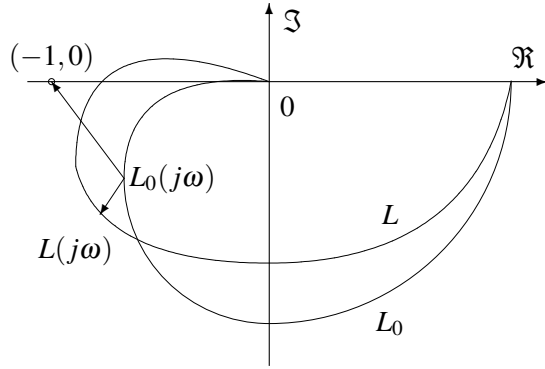


Figure 7.3: Nyquist plot of the SISO system

In equation (7.6), S_0 stands for the sensitivity function of the nominal plant. Equations (7.5)–(7.6) can be combined to produce:

$$\frac{|L(j\omega) - L_0(j\omega)|}{|L_0(j\omega)|} \cdot |T_0(j\omega)| < 1, \quad \forall \omega \in \mathbb{R}. \quad (7.7)$$

The multiplier $|L(j\omega) - L_0(j\omega)|/|L_0(j\omega)|$ is called the *relative size* of the perturbation of the gain loop L from its nominal value L_0 . If the relative size of the perturbation is bounded, we can write:

$$\frac{|L(j\omega) - L_0(j\omega)|}{|L_0(j\omega)|} \leq |W(j\omega)|, \quad \forall \omega \in \mathbb{R}, \quad (7.8)$$

where $W(j\omega)$ is the aforementioned (given) weighting function. The following expression can be obtained after simple manipulations:

$$\frac{|L(j\omega) - L_0(j\omega)|}{|L_0(j\omega)|} \frac{1}{|W(j\omega)|} |T_0(j\omega)W(j\omega)| < |W(j\omega) \cdot T_0(j\omega)|, \quad (7.9)$$

$$|W(j\omega) \cdot T_0(j\omega)| < 1, \quad \forall \omega \in \mathbb{R}. \quad (7.10)$$

The last result can be interpreted as follows: for any disturbance that is bounded by $W(j\omega)$ (inequality (7.10) holds) the closed-loop plant remains stable (inequality

(7.9) holds). Since \mathcal{H}_∞ is essentially norm minimization, the last equation should be written in terms of norm notation:

$$\|W(j\omega) \cdot T_0(j\omega)\|_\infty < 1. \quad (7.11)$$

Thus, the open loop plant remains stable for any disturbance that is bounded by equation (7.8), if inequality (7.11) holds. However, it must be explicitly stated that stability alone is not the ultimate goal. For most practical systems there are two competing requirements: stability and performance. Not all stable systems perform well, though all systems performing well must be stable, except explosive devices, of course. This consideration in some sense discourages the direct use of inequality (7.11) for an \mathcal{H}_∞ loop shaping and requires a new minimization objective. The so-called *mixed sensitivity problem* was presented in [76] to incorporate the performance specification into the \mathcal{H}_∞ controller design. In mathematical terms it is usually expressed by

$$\left\| \begin{array}{c} W_1 S V \\ W_2 U V \end{array} \right\|_\infty, \quad (7.12)$$

where W_1 and W_2 are weighting functions that are the “knobs” of the \mathcal{H}_∞ -norm minimization, S and U are the sensitivity function and input sensitivity function, respectively. The new function V is introduced to increase the design flexibility.

There is a nonunique solution to the standard \mathcal{H}_∞ -optimal regulator problem [50], [76]

$$\begin{bmatrix} X \\ Y \end{bmatrix} = Z_\lambda^{-1} \begin{bmatrix} A \\ B \end{bmatrix}, \quad (7.13)$$

where the optimal controller is $C = YX^{-1}$, normally $A = I$, $B = 0$, and Z_λ is determined from equation (7.14)

$$\begin{bmatrix} 0 & I \\ -\tilde{P}_{12}^* & -\tilde{P}_{22}^* \end{bmatrix} \begin{bmatrix} \lambda^2 I - \tilde{P}_{11} \tilde{P}_{11}^* & -\tilde{P}_{11} \tilde{P}_{21}^* \\ -\tilde{P}_{21} \tilde{P}_{11}^* & -\tilde{P}_{21} \tilde{P}_{21}^* \end{bmatrix}^{-1} \begin{bmatrix} 0 & -\tilde{P}_{12} \\ I & -\tilde{P}_{22} \end{bmatrix} = Z_\lambda^* J Z_\lambda, \quad (7.14)$$

where $(\cdot)^*$ operates as $X^*(s) = X'(-s)$ and the plant transfer matrix \tilde{P} is defined as

$$\tilde{P} = \begin{bmatrix} \tilde{P}_{11} & \tilde{P}_{12} \\ \tilde{P}_{21} & \tilde{P}_{22} \end{bmatrix} = \left[\begin{array}{c|c} W_1 V & W_1 P \\ \hline 0 & W_2 \\ \hline -V & -P \end{array} \right]. \quad (7.15)$$

Time domain solutions to \mathcal{H}_∞ control problem

Time-domain solutions to standard \mathcal{H}_∞ control problem have been in the focus of attention of control society for quite a long time and resulted in neat, compact, and

relatively “simple” expressions. Below we replicate the ones that will shortly be used in the present thesis.

Some mathematical preliminaries which will facilitate the further treatment open this subsection.

Lemma 1 *Let matrix H be defined as*

$$H \triangleq \begin{bmatrix} A & R \\ Q & -A' \end{bmatrix},$$

and suppose $H \in \text{dom}(\text{Ric})$ and $X = \text{Ric}(H)$. A, Q and $R \in \mathbb{R}^{n \times n}$ with Q and R symmetric. Then:

- 1** X is symmetric.
- 2** $\lambda_i(A + RX) < 0, \forall i$.
- 3** X satisfies the algebraic Riccati equation $A'X + XA + XRX - Q = 0$. □

A proof of the lemma and details on the notation used can be found in [36] and [134]. For now, the most important detail is that X satisfies the associated Riccati equation. This fact will be used when tackling with suboptimal \mathcal{H}_∞ controllers.

Unlike the situation with LQR, in the present case close-form solutions to the optimal \mathcal{H}_∞ control problem cannot be obtained as the optimal control requires an iterative search over the set of all admissible controllers.

Let the transfer matrix of the plant G be partitioned as

$$G = \left[\begin{array}{c|cc} A & B_1 & B_2 \\ \hline C_1 & 0 & D_{12} \\ C_2 & D_{21} & 0 \end{array} \right] \quad (7.16)$$

and the following assumptions hold

- a** (A, B_1) and (A, B_2) are stabilizable.
- b** (C_{12}, A) and (C_{21}, A) are detectable².
- c** $D'_{12} = [0, I]$.
- d** $\begin{bmatrix} B_1 \\ D_{21} \end{bmatrix} D'_{21} = \begin{bmatrix} 0 \\ I \end{bmatrix}$.

²The pair (C, A) is said to be detectable if for some L the matrix $A + LC$ is a Hurwitz matrix.

We now present closed-form *suboptimal* \mathcal{H}_∞ controllers which are given by

Theorem 3 *Let the following two matrices be defined as*

$$H_\infty \triangleq \begin{bmatrix} A & \gamma^{-2}B_1B_1' - B_2B_2' \\ -C_1'C_1 & -A' \end{bmatrix}$$

$$J_\infty \triangleq \begin{bmatrix} A' & \gamma^{-2}C_1'C_1 - C_2'C_2 \\ -B_1B_1' & A \end{bmatrix},$$

where γ is a given real number. There exists an admissible controller s.t. $\|T_{zw}\|_\infty < \gamma$ if and only if the following conditions hold:

- a $H_\infty \in \text{dom}(\text{Ric})$ and $X_\infty \triangleq \text{Ric}(H_\infty) \geq 0$.
- b $J_\infty \in \text{dom}(\text{Ric})$ and $Y_\infty \triangleq \text{Ric}(J_\infty) \geq 0$.
- c $\rho(X_\infty Y_\infty) < \gamma^2$.

In addition, if these conditions hold, one such controller is given by

$$K_{sub} = \begin{bmatrix} \hat{A}_\infty & -Z_\infty L_\infty \\ F_\infty & 0 \end{bmatrix}, \quad (7.17)$$

where the matrices $\hat{A}_\infty, F_\infty, L_\infty$ and Z_∞ are defined as

$$\begin{aligned} \hat{A}_\infty &\triangleq A + \gamma^{-2}B_1B_1'X_\infty + B_2F_\infty + Z_\infty L_\infty C_2 \\ F_\infty &\triangleq -B_2'X_\infty \\ L_\infty &\triangleq -Y_\infty C_2' \\ Z_\infty &\triangleq [I - \gamma^{-2}Y_\infty X_\infty]^{-1}. \end{aligned}$$

□

Again, a proof of the theorem can be found in [36]. It is possible to parameterize all the suboptimal controllers K_{sub} that are given by Theorem 3; here only the final result is shown. For technicalities and a proof, the reader can consult [36] or [134].

Theorem 4 *Suppose the conditions of Theorem 3 are satisfied. Then, for any choice of Q : $\|Q\|_\infty < \gamma$ and $Q \in \mathcal{RH}_\infty$, the set of all admissible suboptimal controllers with $\|T_{zw}\|_\infty < \gamma$ is*

$$M_\infty = \begin{bmatrix} \hat{A}_\infty & -Z_\infty L_\infty & Z_\infty B_2 \\ F_\infty & 0 & I \\ -C_2 & I & 0 \end{bmatrix}.$$

□

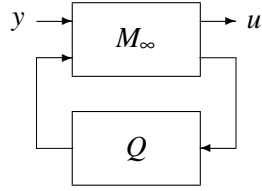
Figure 7.4: Parametrization of all suboptimal \mathcal{H}_∞ controllers

Figure 7.4 shows a schematic block diagram of the parameterized sub-optimal \mathcal{H}_∞ controllers.

To exemplify the theory presented earlier in this chapter, let us design an \mathcal{H}_∞ - controller for a single machine infinite bus (SMIB) system.

Example: Consider the SMIB system, which represents a simplified linearized model of single generator connected to an infinite bus. The classical model of the generator is used in this example; that is, the generator is modeled by equations (3.3)–(3.4). The quantities E'_q and E'_d in equations (3.4) are assumed to be constant. The parameters of the system are chosen such that the generator exhibits quite an oscillatory behavior. In this example we seek an \mathcal{H}_∞ controller that is capable of stabilizing the SMIB system by regulating the mechanical power of the generator.

$$\begin{bmatrix} \dot{\delta} \\ \dot{\omega} \end{bmatrix} = \begin{bmatrix} 0 & 100\pi \\ -0.05 & -0.01 \end{bmatrix} \begin{bmatrix} \delta \\ \omega \end{bmatrix} + \begin{bmatrix} 0 \\ 0.1 \end{bmatrix} u(t), \quad (7.18)$$

$$y = C [\delta, \omega]^T + Du, \quad C = [1, 0], \quad D = 0.$$

The following frequency-domain control specifications are set³:

Closed-loop bandwidth: $\omega_B = 12$ rad/sec.

Peak of sensitivity function: $S_{max} = 1.1$.

Steady state: Approximate integral action at low frequencies.

Obj. function: For this example, selecting $\varepsilon = 10^{-6}$, the objective functions is chosen as

$$J(S, K) = \arg \min_K \left\| \begin{bmatrix} w_P S \\ K S \end{bmatrix} \right\|_\infty, \quad w_P = \frac{0.67s + 10}{s + \varepsilon}.$$

³These control specifications are set arbitrarily for demonstration purposes only; however, these values are quite realistic.

The \mathcal{H}_∞ -norm minimization is performed with the help of the μ -toolbox in MATLAB [20], which yields the value of $\gamma = 1.08$. The resultant suboptimal controller $K(s)$ has following structure

$$K(s) = \frac{4617s^2 + 46.17s + 7.254e4}{s^3 + 4451s^2 + 3.64e4s + 0.01348}$$

The SMIB system controlled by K has the following eigenvalues: $\lambda_1 = -4443$ and $\lambda_{2,3} = -1.8044 \pm j4.3542$. The input to the \mathcal{H}_∞ optimal controller is the angle deviation of the generator's shaft and the output is the control signal $u(t)$. \square

Note: It is worth mentioning that selection of weighting functions for the design of \mathcal{H}_∞ controller synthesis plays an essential role. As yet, selection of weights in robust and optimal control is more art than science, since from case to case, different ad hoc approaches have to be tried in order to obtain "the best design." This example concludes the introduction to basics of the \mathcal{H}_∞ controller synthesis.

7.2 Application of Robust Control to the SOFC Plant

Motivation

Recent advances in the fuel cell technology significantly improved the technical and economical characteristics of modern fuel cells making them more suitable and beneficial for the decentralized use of energy generation [55]. Environmental friendliness, practically noise free operation, and very high efficiency combined with the forecasted shift to gaseous fuels make fuel cells a very sound competitor on the future electricity markets [22], [12]. In addition, it should be noted that fuel cell-based generators possess other important properties such as compact size, modularity, and controllability.

It is shown in [56] and [135] that load following and regulation comprise a substantial part of total interconnected operation services, which is likely to stimulate the owners of DG's to participate in the provision of this particular ancillary service. There are, however, some technical challenges associated with the fuel cell technology which can represent certain difficulties for these services. One of the most important challenges is the slow output power ramping [135]. Therefore, a series of questions concerning the adequacy of some fuel cell power plants for stationary operation in conventional distribution grids has to be addressed. These questions are closely related to that of the fundamental control limitations of fuel cell-driven power plants.

Thus, effective methods should be devised to overcome the control barrier imposed by the inability of some fuel cell power plants (e.g., solid oxide fuel cells, or SOFC) to ramp up the power output quickly. Physically, the inability of the SOFC power plant to ramp the output very quickly is caused by the dynamics of the fuel cell reformer which itself is slow.

One of the most economic solutions is to build an integrated system consisting of a fuel cell module and a small-scale gas turbine. Typically, the rating of the microturbine is one third of that of the fuel cell plant, which enables a more efficient use of the hot exhaust of the SOFC.

Normally, the contracts of DG owners require either maintaining a constant output power level of the DG or following the local load demand⁴.

Irrespective of the DG operation mode, the fuel cell module and the gas turbine will have different control objectives, i.e., the fuel cell will control the voltage magnitude (short-term control) and the reactive power generation, supplying a constant active power, while the gas turbine will perform load following. Here it is worth recalling that usually microturbines utilize asynchronous generators that are incapable of controlling the terminal voltage, while their active power output can be easily controlled by manipulating the mechanical torque applied to the generator. The voltage source inverter of the fuel cell plant, on the other hand, is able to accurately control the terminal voltage of the plant as well as the output power and the frequency. However, ultimately the inverter itself does not produce active power, which implies that its output power control is as effective as the power control of the fuel cell power plant.

If the contractual obligations of the DG owner require load following capabilities, then most likely it will be effective to utilize both the fuel cell system and the microturbines, since the rating of the microturbine is relatively small compared to the rating of the fuel cell. If both the fuel cell and the microturbine are deployed in the active power regulation, it is likely to result in undesirable interactions between the fuel cell system and the microturbine turbine, which can adversely affect the performance of the overall system.

To ensure the proper operation of this control scheme, undesirable interactions between the fuel cell and turbine controls should be eliminated. In order to avoid these dynamic interactions, an auxiliary controller can be designed that is able to sustain the output power of the fuel cell constant irrespective of the output power of the gas turbine.

⁴This theme will be further discussed in more detail in Chapter 8.

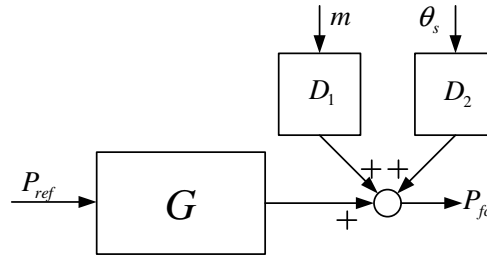


Figure 7.5: Transfer function of a fuel cell plant

In this chapter, two robust controllers are designed to achieve the aforementioned control objective. Both controllers are synthesized by solving the associated \mathcal{H}_∞ mixed sensitivity problem. In particular, the controllers are expected to enable the fuel cell power plant to reject disturbances affecting the plant's output and enhance the set-point tracking of the plant. Figure 7.6 shows the interconnection of the plant G and the controller K to be designed⁵. To validate the controller design, the performance of the fuel cell power plant compensated by each of the controllers is assessed by running several nonlinear numerical simulations.

The mixed-sensitivity S/KS optimization

According to the theory presented in the previous section [e.g., equation (7.12)], the mixed sensitivity problem can be solved by minimizing the following objective function

$$K = \arg \min_{K \in \mathcal{K}} \left\| \begin{array}{c} w_p S \\ w_u K S \end{array} \right\|_\infty. \quad (7.19)$$

In equation (7.19), S denotes the sensitivity function of the compensated plant and is defined as $S = (I - GK)^{-1}$. As usual, the performance weighting function and the input weighting function $w_p(s)$ and $w_u(s)$ are the main design mechanisms of the \mathcal{H}_∞ optimization and are used for shaping the response of the closed-loop plant. Let us consider the following two weighting functions

$$w_u = 1 \quad (7.20)$$

$$w_{p1} = \frac{0.9s + 10}{s + 10^{-5}}. \quad (7.21)$$

⁵For more details on the SOFC plant modeling, the reader should also refer to Section 3.2, Appendix C, and [135].

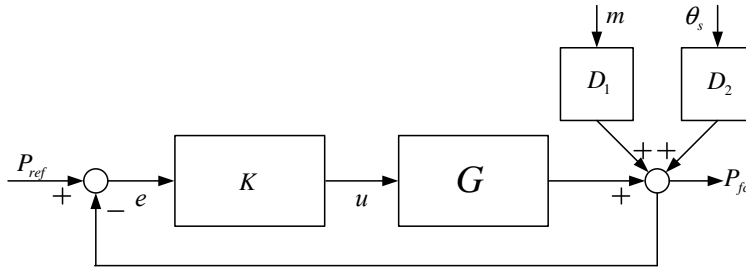


Figure 7.6: Preliminary control configuration of the fuel cell plant

This particular choice of the performance weighting function gives a peak of the sensitivity function $S = 1.1$ and the effective bandwidth of the closed loop $\omega_B = 10$ rad/s. In addition, the controller will provide an approximate integral action, thus enhancing tracking properties of the closed loop plant.

Let us now recall that the model (3.24)–(3.25) of the SOFC power plant has 3 inputs and 1 output. The inputs entering the model represent the set-point deviations and the disturbances. The exact numerical values of the disturbances [which are deviations of the terminal voltage magnitude and angle] are assumed unknown, but bounded as is shown below

$$\|\Delta m\|_2 \leq 0.1 \text{ p.u.} \tag{7.22}$$

$$\|\Delta \theta_s\|_2 \leq 20^\circ. \tag{7.23}$$

The plant’s output is the fuel cell active power injected into the distribution grid. Note that disturbances represented in such a way are fairly general, since this form can model network voltage variations due to the operation of the microturbine and any other bounded disturbances occurring on the grid.

The model (3.24)–(3.25) can be cast in the form of transfer matrix as shown in Fig. 7.5, where the plant transfer matrix $G(s)$ is defined as $G(s) = C(sI - A)^{-1}B + D$, and the output $y = G(s)P_{ref} + D_1(s)m + D_2(s)\theta_s$. In the latter expression, $D_1(s)$ and $D_2(s)$ denote the transfer functions from m and θ_s to the output y . Inspection of the transfer functions $G(s)$, $D_1(s)$, and $D_2(s)$ reveals that they share the same dynamics and therefore the disturbances m and θ_s can be transferred to the plant’s input (the argument s will be dropped in the remainder of the section for simplicity of notation).

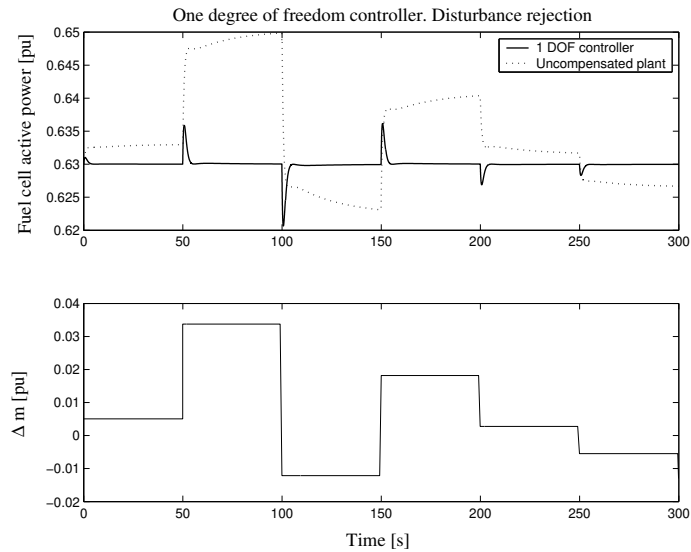


Figure 7.7: Disturbance rejection by one degree-of-freedom controller.

One-degree-of-freedom controller

An \mathcal{H}_∞ mixed sensitivity problem is solved with the help of the MATLAB's μ -Analysis and Synthesis Toolbox, resulting in a 6th order \mathcal{H}_∞ controller. The closed loop performance of the compensated plant is shown in Figs. 7.7 and 7.8. Figure 7.7 demonstrates the ability of the compensated plant to reject disturbances induced by variations in the magnitude of V_{fc} . One can see that the controller shaped by the weighting function w_{p1} , which will henceforth be called one-degree-of-freedom controller (1DOF), is capable of fast disturbance rejection. However, as Fig. 7.8 shows, the set-point tracking is unsatisfactory, as the overshoot is approximately 50%.

Two-degrees-of-freedom controller

The results obtained in the previous subsection suggest a new controller should be sought which would be able to ensure acceptable performance in terms of both disturbance rejection and tracking. One way of improving the performance of the closed-loop plant is to consider another configuration of controller. Thus, a two-

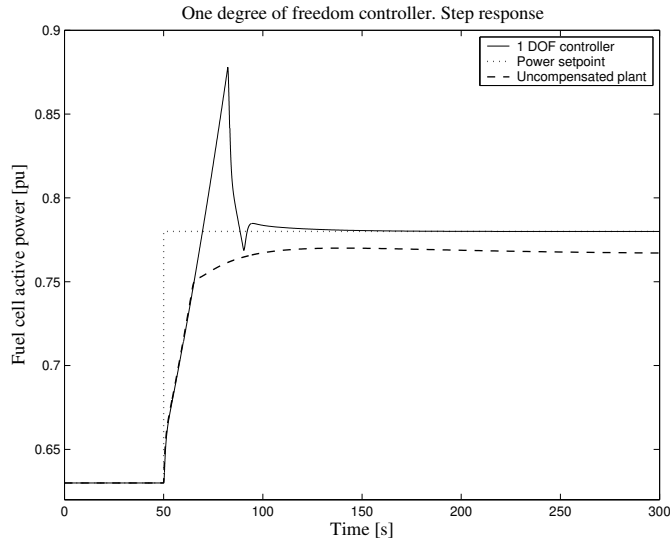


Figure 7.8: Step response by one degree-of-freedom controller.

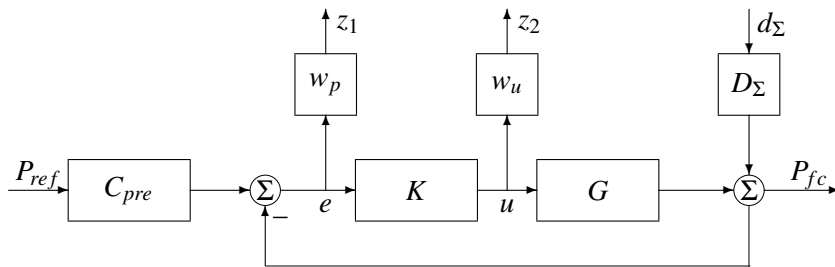


Figure 7.9: Final control configuration of the fuel cell plant

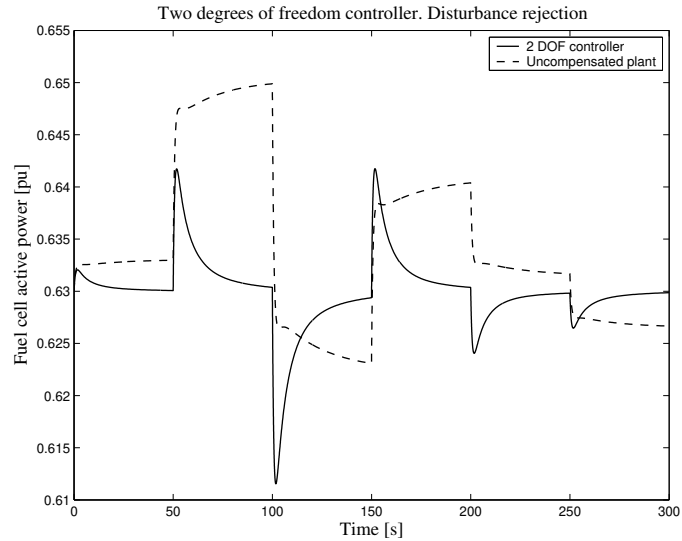


Figure 7.10: Disturbance rejection by the two degrees-of-freedom controller.

degree-of-freedom (2DOF) controller is designed. The 2DOF controller consists of 2 blocks: a compensator K and a pre-filter C_{pre} , as is shown in Fig. 7.9. The design procedure follows closely that applied to the design of the 1DOF controller; thus, the compensator block is found by solving an \mathcal{H}_∞ mixed sensitivity problem. The only new step involves the design of a pre-filter (normally a lead-lag block) whose main purpose is to improve the tracking response of the overall system. It was also decided to decrease the effective bandwidth of the closed-loop plant to $w_B = 0.08$ rad/s by modifying the performance weighting function accordingly. That is, the following w_p is used in the 2DOF controller design:

$$w_{p2} = \frac{0.9s + 0.08}{s + 10^{-5}} \quad (7.24)$$

The input weighting function w_u remains unchanged in this design. The controller is again synthesized with the help of μ -Analysis and Synthesis Toolbox in MATLAB. The pre-filter (C_{pre}) was tuned manually by the “trial-and-error” method. Satisfactory results were obtained with $C_{pre} = (2s + 1)^{-1}$.

The performance of the fuel cell power plant compensated with the 2DOF controller is depicted in Figs. 7.10 and 7.11. It can be observed in Fig. 7.10 that the

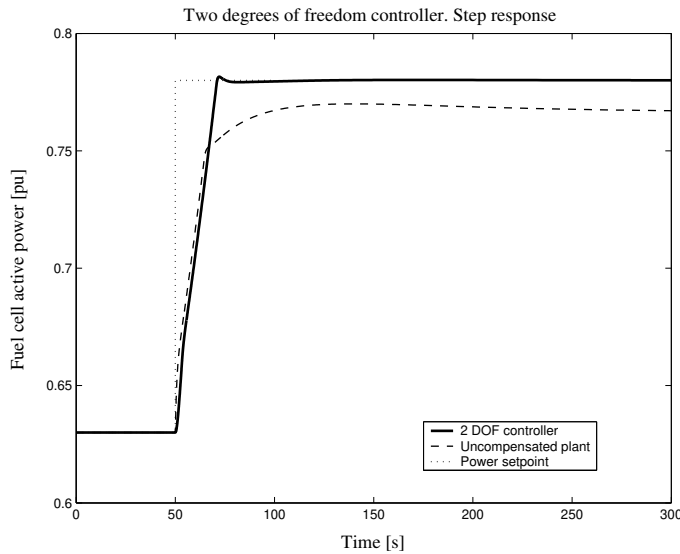


Figure 7.11: Step response of the plant with the two degrees-of-freedom controller.

reduction of the bandwidth w_B has some adverse impact on the disturbance response. Nevertheless, it can be concluded that the 2DOF controller satisfactorily rejects disturbances caused by fluctuations of the voltage V_{fc} and the output power of the fuel cell returns back to the reference value reasonably fast. On the other hand, a significant improvement of the tracking response was achieved, as Fig. 7.11 indicates, since the closed loop plant has a negligibly small overshoot, while the response time is practically unchanged. Observe also that the steady-state error of the compensated plant is eliminated by the integral action of the 2DOF controller.

7.3 Discussion

It is important to observe that neither 1DOF nor 2DOF controllers were able to significantly improve the step response of the fuel cell power plant. Even if “excessive” use of the input u signal was allowed—which normally would not be the case due to the potential risk of damaging the fuel cell—no significant improvement could be achieved in the step response of the original *nonlinear* model (3.20)–(3.21), since hard limits on the input u are built in the controls of the SOFC,

as follows from (3.21). The presence of the limits in the model is justified by the necessity to avoid under- or over-utilization of the fuel cell, which is mainly accomplished by limiting the current I_{fc}^r of the fuel cell.

The response time of a SOFC is limited by the time constants of the fuel processor, which are normally large and cannot be made smaller for a given fuel cell plant due to physical limitations imposed by the parameters of the corresponding chemical reactions. Therefore, the response time of the plant cannot be enhanced by manipulating its input, technological change in the fuel cell plant are required if the fuel cell power plant is to operate in a stand alone mode which requires load-following capabilities. Alternatively, other technical solutions should be sought; for example, the combined use of fuel cell modules and a gas turbine, or the use of an external energy storage, such as batteries, a flywheel, or a superconducting magnetic energy storage device.

Another alternative could be the use of a phosphoric acid fuel cell (PAFC) power plant which possesses significantly better load following capabilities. For instance, the commercial PAFC PC-25 according to [9]: “can be ramped at 10 kW/s up or down in the grid connected mode. The ramp rate for the grid independent mode is idle to full power in approximately one cycle or essentially one-step instantaneous from idle to 200 kW (nominal power). Following the initial ramp to full power, the unit can adjust at an 80 kW/s ramp up or down in one cycle.” It should however be mentioned that the efficiency of PAFC plants is somewhat smaller than that of SOFC/GT power plants.

7.4 Summary

In this chapter, a linearized model of a solid oxide fuel cell power plant was obtained. The linear model was used in order to design robust controllers capable of rejecting disturbances caused by fluctuations of the magnitude and/or angle of the SOFC terminal voltage, which could in real world applications be caused by either the fluctuation of the utility voltage (e.g., due to faults) or by the operation of the microturbines. Two \mathcal{H}_∞ controllers were synthesized and their performance was analyzed. To validate the performance of the controllers, nonlinear simulations of a SOFC were performed. The load following capabilities of various fuel cell power plants were briefly discussed. Apparently, further research in this area should involve numerical experiments with a more realistic model of the distribution grid and microturbines in order to assess the impact of the microturbine dynamics on the operation of the solid oxide fuel cell power plant.

“With so much new distributed generation being installed, it is critical that the power system impacts be assessed accurately.”

— A quotation from [21]

Chapter 8

Interaction Between DG and the Power System: Operation, Control, and Stability Aspects

This chapter presents qualitative analysis of the impact that distributed generation (DG) might have on the operation, control, and stability of electric power networks with large penetration ratios. The impact of DG on network losses, power quality, short circuit power, as well as on system protection and on power system stability is discussed. Based on the discussion, it can be concluded that the impact of DG to a large extent depends on the penetration level of DG in the distribution network as well as on the type of DG technology, and mode of its operation. If DG is properly sized, sited, and selected in terms of technology, it can clearly provide benefits to control, operation and stability of the power system. It should however be noted that distribution networks have traditionally a rather inflexible design (e.g., a unidirectional power flow), which in principle can cause integration problems with higher DG penetration levels or different technologies. Nonetheless, those issues can usually be solved by modifying the distribution network, including the control and/or operation approach, or by other technical means.

8.1 Introduction

Several technical, political, and environmental considerations have stimulated the relatively rapid growth of the number of various DG installations. While the total installed capacity of the distributed generation remained small, its impact on the operation of the power grid remained marginal; however,

as the installed capacity of DG increases, the impact which it has on the grid will intensify. The characterization and quantification of this impact apparently is quite a complicated engineering task, since such aspects of grid operation as voltage control, relay protection coordination, power losses, power quality, reliability, and many other will have to be simultaneously analyzed. Some of these aspects are also intimately related to the stability phenomena of the grid and therefore they will have to be explicitly addressed in the studies of the overall power system stability.

To assist in making a systematic assessment of the impact that large amounts of DG have on the operation, control, and stability of the power grid, this chapter provides basic qualitative analysis of the interaction between large amounts of distributed generation and the power network.

8.2 Historical Background

The importance of the impact that DG might have on the operation, stability, and control of the power system has already been recognized in the late 1970's. One of the most interesting publications on this subject was presented at the conference "Research needs for the effective integration of new technologies into the Electric Utility" held by the U.S. Department of Energy (DoE) in 1982 and was entitled "Impacts of new technology and generation and storage processes on power system stability and operability" [109]. Over the last two decades the number of publications discussing various areas of the interaction between DG and the utility has been gradually increasing. Historically, until the 1990's the main focus of the research was placed upon the impact that renewable power sources had on network operation, [46], [99]; however, also distributed generation in general was investigated [2]. In the late 1990's, this theme gained more interest in academia and industry, which resulted in a large number of publications [6, 7, 10, 11].

Recently, also the results of two extensive simulation case studies have been reported: (i) Simulation of interaction between wind farm and power system, by the Risø National Laboratory, Denmark [120], and (ii) DG Power Quality, Protection and reliability Case Studies Report, by GE Corporate Research and Development, USA [97].

Table 8.1: Technologies for distributed generation [13].

Technology	Typical available size p. module
1. Combined Cycle Gas T.	35 – 400 MW
2. Internal Combustion Engines	5 kW – 10 MW
3. Combustion Turbine	1 – 250 MW
4. Micro-Turbines	35 kW – 1 MW
5. Small Hydro	1 – 100 MW
6. Micro Hydro	25 kW – 1 MW
7. Wind Turbine	200 W – 3 MW
8. Photovoltaic Arrays	20 W – 100 kW
9. Solar Thermal, Central Receiver	1 – 10 MW
10. Solar Thermal, Lutz System	10 – 80 MW
11. Biomass Gasification	100 kW – 20 MW
12. Fuel Cells, PhosAcid	200 kW – 2 MW
13. Fuel Cells, Molten Carbonate	250 kW – 2 MW
14. Fuel Cells, Proton Exchange	1 – 250 kW
15. Fuel Cells, Solid Oxide	250 kW – 5 MW
16. Geothermal	5 – 100 MW
17. Ocean Energy	0.1 – 1 MW
18. Stirling Engine	2 – 10 kW
19. Battery Storage	0.5 – 5 MW

8.3 Distributed Generation Technology

One of the most essential factors influencing the interaction between the DG and grid is the technology utilized in the DG, as well as the mode of DG control and operation.

Table 8.1 provides a brief overview of the most commonly used distributed generation technologies and their typical module size. The technologies 5 – 11, 16 and 17 can be considered renewable DG. The other technologies could also be called renewable DG if they are operated with biofuels. Also fuel cells could be considered renewable DG if the hydrogen is produced using renewable energy sources, e.g. wind power.

Similarly to the centralized generation, the following three generation technologies are normally used for distributed generation: synchronous generator, asynchronous generator, and power electronic converter interface [8, 51, 62, 90]. These

DG technologies will now be briefly discussed.

Synchronous Generator

The advantageous ability of the synchronous generator—the primary generator technology for centralized generation—to produce both active and reactive power also provides benefits for distributed generation applications.

Synchronous generators are typically utilized by the following DG applications if the generation capacity exceeds a few MW: biomass, geothermal, diesel/gas engines driven generators, solar thermal generation, solar parabolic systems, solar power towers, solar dish engines, gas turbines, and combined cycle gas turbines.

Asynchronous Generator

In contrast to synchronous generators, asynchronous (induction) generators are only used for distributed generation, but not for centralized generation. An asynchronous generator is basically an induction machine which is connected to a prime-mover. When the generator is connected to the power network, the mechanical power is converted into electrical power by the action of the prime-mover that drives the machine above synchronous speed. Hence, the asynchronous generator is not capable of operating independent from a relatively strong grid. Asynchronous generators are used for many distributed generation technologies as long as the generation capacity does not exceed a few MW due to its competitive price compared to synchronous generators. Squirrel cage asynchronous generator used to be very common in the wind energy industry; however, this type of induction generator is now being gradually superseded by asynchronous generators equipped with a converter, i.e., double-fed induction generators.

Power Electronic Converter

Power converters normally use high power electronics to provide the desired power output. For example, it is quite common that wind turbines use double-fed, variable speed induction generators with an IGBT converter in the rotor circuit. Power electronic converters are also used in photovoltaic systems, fuel cells, micro turbines, Sterling engine as well as battery storage, and magnetic storage systems.

8.4 General Impact of DG on Power System Operation and Control

To make a qualitative assessment of the impact that DG has on the distribution grid, a simple example is considered. Such aspects of power system operation as voltage control, power losses, power quality, and protection system are analyzed. Based on the analysis, more generic statements are made. Clearly, there can exist distribution grids to which these statements might not apply to full extent; however, an effort is made to preserve the generality of discussion.

Difference Between Distribution and Transmission Networks

Technically speaking, distribution and transmission networks are designed for a somewhat different purposes. The main difference is that distribution systems are usually not designed for the connection of active power generators. Furthermore, distribution networks usually have a radial or loop design, rather than a meshed design typical for transmission networks. Therefore, the power flow in distribution networks usually is unidirectional and little or no redundancy exists. In addition, in transmission and urban distribution systems, the effect of line or cable resistance (R) on voltage drop is small, since its magnitude is generally much less than the reactive component (X) of the conductor impedance, i.e., $X/R > 5$. Therefore, active as well as reactive power production within the distributed generation will influence the voltage level.

It is also noteworthy mentioning that the low voltage ends of distribution systems are rarely connected to Supervisory Control and Data Acquisition (SCADA) systems. The data gathering required for the control of the distribution system as well as the distributed generation units is therefore difficult at present.

Distribution Network Operation Issues

For the explanation of the relevant operation issues, a hypothetical distribution network is used, see Fig. 8.1. Even though, the example is hypothetical, it possesses all the relevant attributes of a basic distribution grid necessary for subsequent analysis. The network is a six-bus system (B_1, \dots, B_6), with load connected to each bus (LD_1, \dots, LD_6) and three distributed generators (DG_1, \dots, DG_3) connected to buses B_2 , B_4 , and B_6 . Regarding the generation compared to the load in the system, the following cases are possible:

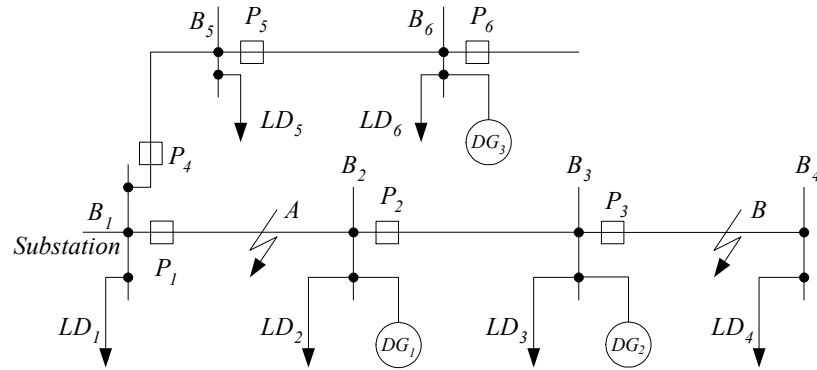


Figure 8.1: Hypothetical Distribution Network

Load case 1: The load rating at each bus is always larger than or equal to that of the distributed generator at each bus, or:

$$LD_i \geq DG_i \forall i$$

This load case is typical for DG applications such as photovoltaic (PV) systems, Sterling engines, microturbines, or small wind turbines.

Load case 2: The DG generation at least at one bus is larger than the load at the same bus, however, the total power of DG in the distribution network is less than the sum of all loads in the system, or:

$$\exists i \in N : (LD_i < DG_i) \wedge \left(\sum_{k=1}^n LD_k \geq \sum_{k=1}^n DG_k \right),$$

where $N = \{k\}_{k=1}^6$. This load case might occur if one of the DG units is a wind farm or biomass system.

Load case 3: The distributed generation at least at one bus is larger than the load at the same bus, and the sum of all DG generation in the distribution network is larger than the sum of all loads in the system, i.e.:

$$\sum_{k=1}^n LD_k < \sum_{k=1}^n DG_k$$

This load case might occur if a large wind farm is connected to the end of a distribution network. Since load centers usually are not located in areas with high

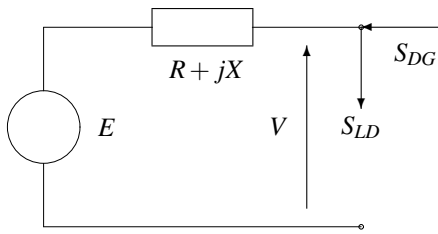


Figure 8.2: Simplified model of a power system with DG

wind speeds, the power output of a wind farm often can exceed the local power demand. Finally, it must be mentioned that the load cases within a distribution network might change over time. It is, for example, quite common that a wind farm provides a significant amount of the load in a distribution network for most of the time (Load case 2). The other two load cases, however, can also occur. Load case 1 during times with little wind and load case 3 during times with very high wind speeds and low loads, for example, during the night.

Impact on Losses

To explain the impact of DG on distribution network operation under consideration of different X/R ratios, the simplest model—a single distribution line and a load—is used.

In the model presented in Fig. 8.2, E represents the sending end voltage, V is the receiving end voltage. If we assume that the receiving voltage V as well as the load current I are known, then the following equations establish the relationship between the power produced by DG and associated reduction of losses on the line. Suppose no DG is connected. Then the power losses are

$$S_{loss} = (E - V)I^* = (E - V)(I_{LD,a} - jI_{LD,r}),$$

where $I_{LD,a}$ and $I_{LD,r}$ denote the active and reactive components of the load current. Now assume that DG producing only active power ($\cos \phi = 1$) is connected and also assume for simplicity that the voltage V at the receiving end is kept constant. Then it is easy to see that the new power losses are:

$$S_{loss}^{DG} = (E - V)(I_{LD,a} - I_{DG} - jI_{LD,r}).$$

Therefore, the presence of DG reduces the power loss by the amount

$$S_{loss} - S_{loss}^{DG} = (E - V)I_{DG}.$$

With this approximate expression, the variations of the voltage at the receiving end are not considered; however, the inclusion of the receiving voltage variations is not essential for the analysis. In summary, it can be concluded that the introduction of distributed generation reduces the current flowing through the distribution line, thus reducing the active as well as reactive power losses.

Based on three load cases defined at the beginning of this section, the following can be said:

Load case 1 DG will always result in reduced losses on all lines in the distribution network.

Load case 2 DG might lead to an increase of the losses on some lines, but the total losses within the [realistic] distribution network will be reduced.

Load case 3 DG might lead to an increase of the losses on some lines, but the total losses within the [realistic] distribution network will be reduced as long as the total DG production is less than approximately twice the total load in the distribution network.

If the DG production is larger than approximately twice the total load in the distribution network, the losses in the distribution network will be larger with DG connected than without DG. In addition, it should be noted that a power loss reduction in the distribution network entails a loss reduction in the transmission network.

Voltage Control

The voltage level in a distribution network must be kept within a certain range, as some power system equipment and customer applications function only properly if the voltage is maintained within this range. The voltage range for normal operation is defined in different national and international standards.

In a distribution system voltage fluctuations occur when the load current flowing through the resistive and reactive impedances of the lines varies. The voltage variations in distribution networks without DG are caused by the variations of the active and reactive load in the distribution network over time. The fluctuations are generally larger towards the end of the line, due to the high impedance of distribution lines. Also, the voltage fluctuations are more expressed if the load is

concentrated near the end of the (radial) system. Practically, for typical distribution lines the distance before the voltage drop exceeds the allowable fluctuation at rated current is only a few km. However, a line is normally not designed to operate at such loading levels. An in-depth analytical discussion of the impact of DG on the voltage profile in LV networks can be found in [32].

Traditionally, voltage control in distribution networks is performed in two ways:

1. The control of the source voltage at the network substation by using tap changing transformers and;
2. The control of the reactive power throughout the system, by using shunt capacitors/shunt reactors [this is very seldom done in distribution networks], series capacitors, synchronous condenser or Static VAR Compensator (SVC).

DG can influence the voltage variations in two ways:

(i) DG is operated in correlation with the local load requirements, meaning whenever the local load in the distribution network increases, the DG production increased as well, and vice versa. In this case, DG contributes to the reduction of the variations between the maximum and minimum voltage levels, compared to the situation without DG. This mode of DG operation provides no challenges to the traditional voltage control approach. This situation was thoroughly investigated in [77]. This DG control mode is well suited for photovoltaic distributed generators, if the local loading [e.g., air conditioning equipment] is naturally correlated to the solar radiation and thus the power output of the photovoltaic cells.

(ii) DG power output is controlled independently of the local loading of the area. This control mode is implemented if DG operation follows price signals, which might or might not correspond to the local load variations, or DG follows the availability of natural resources, like solar or wind power. In this case, DG might adversely affect the voltage control functionality of the network by increasing the variations between the maximum and minimum voltage level, compared to a situation without DG, since the minimum voltage level could remain (usually at a high load, no DG situation) but the maximum voltage level could increase, e.g. in low load situations with DG operating at maximum production and at a unity power factor. Generally speaking, DG can provide some challenges to the traditional voltage control. For example, during a high load situation in the hypothetical network shown in Fig. 8.1, the tap changing transformer (not shown) at the substation would increase the source voltage to keep the voltage at the end of the lines (bus B_4 and bus B_6) within the required voltage range. Now with a large DG unit at bus B_6 , but no DG at bus B_4 , the voltage at bus B_6 is raised due to DG and might reach the

overvoltage limits, while the voltage at bus B_4 could reach the lower voltage limits due to the high load. The traditional operation approach of tap changing transformer at the substation is not suitable for such situation, as it assumes a similar voltage drop on all lines downstream from the transformer.

One simple approach to solve this problem is to reduce the power output of the DG unit. This solution will be the most economic solution for the network operator but probably not for the DG owner. In case of intermittent renewable generation, particular wind power, there is a low likelihood that the maximum availability of the natural resources, e.g. very high wind speeds, correlates with very low load situation. On the Swedish island of Gotland, for example, such a situation occurs around 10 hours per year. Another, more costly solution would be the installation of a more intelligent and flexible voltage control scheme within the distribution system, based on substation automation and modern communication technology. This technology would allow sensing the voltage level at different points in the network, usually at the end of different lines. Hence, the tap changer setting at the substation could be dynamically adjusted according to the input data from the measurements. In addition, if the applied DG technology has the capability of dynamically changing the power factor it could be used to locally control the voltage. The aim would be to keep the voltage variations in the distribution network within tolerable limits. This is already done within some wind power projects, where the power electronic converter is used for dynamic voltage control in the distribution system [31]. In general, DG technologies using either a power electronics converter [114] or a synchronous generator could be used for dynamic voltage control. The approach, however, is rather seldom used—the author is only aware of 3 projects worldwide—due to the following two reasons:

(i) Interconnection rules usually do not allow an active participation in the control of the distribution network. This might change with the new IEEE Standard for Distributed Resources Interconnected with Electric Power Systems, which is currently under discussion. A change of the interconnection rules still leaves open questions: What is the economic value of dynamic voltage control with DG, or in other words: How much must the network operator pay the DG operator for the voltage control service. In most projects where DG current provides dynamic voltage control, the service was requested by the network operator.

(ii) If DG provides active voltage control the remaining voltage control system, for example tap changer or capacitor banks, might have to be coordinated with the DG voltage control system to avoid voltage hunting. Voltage control results in fast change of voltage level in the distribution system due to interaction between different voltage control systems. The coordination between the different voltage

control systems could be done with the help of modern communication systems.

Power Quality

When discussing the impact of DG on power quality, there are typically two major concerns, namely, voltage flicker and harmonics.

Voltage Flicker

As defined in [37], voltage flicker is an impression of unsteadiness of visual sensation induced by a light stimulus whose luminance or spectral distribution fluctuates with time. In distribution networks the most common cause of flicker is a rapid variation of load current. However, not only load variations cause flicker, but also DG can directly or indirectly contribute to voltage flicker. The main causes of flicker are

- (i) Starting of a large DG unit
- (ii) Sudden and large variations of the output of DG
- (iii) Interactions between DG and the voltage controlling equipment of the feeder.

Voltage flicker mitigation method and its effectiveness depend on many factors and can be quite complicated. If the rating of DG is significant and the output of DG is subject to frequent and significant change, then voltage flicker may be felt by some customers. The simplest mitigation method in such a case would be to require the owner of DG to reduce the number of DG starts and/or large variation of the output power. If DG is interfaced with the grid via a converter, then reduction of starting currents is relatively easy to accomplish. In particular, wind farms have been seen as potential cause of voltage flicker due to wind speed variations or power output variation due to passage of the wind turbine blades through the tower shadow. However, the design of modern wind turbines has been changed such that large variations of the output power within a short time period can be effectively avoided (variable speed).

Harmonics

It is widely recognized that the presence of nonlinear components of power systems, e.g., power converters or saturated transformers, manifests in the appearance of harmonics [37]. The presence of harmonics in a power system is undesirable for a number of reasons, some of which are:

- (i) Harmonics increase power loss in both utility and customer equipment
- (ii) Sometimes harmonics may provoke malfunctioning of sensitive load or control equipment [86]
- (iii) Harmonics having significant magnitudes can cause a reduction of lifetime of motors, transformers, capacitor banks, and some other equipment.

Power electronic devices, as used for DG, might cause harmonics. The magnitude and the order of harmonic currents injected by dc/ac converters depend on the technology of the converter and the mode of its operation. For example, a forced-commutated converter with pulse-width-modulation operated in the linear range, will introduce only harmonics in the range of high frequencies, i.e., at and/or around multiples of the carrier frequency [85]. Recent advances in semiconductor technology (e.g. IGBT's) allow the use of higher carrier frequencies; which, for example, allows the generation of quite clean current waveform in compliant with the IEEE 519 standard. IGBT based converter are used for many DG technologies. It can therefore be concluded that modern high power electronics technology can be used to solve the relevant power quality phenomena associated with DG.

Voltage Sags

Theoretically, distributed generation based on power converters can be used to reduce the depth of voltage sags. In this case, the converter must act as a static VAR compensator or dynamic voltage restorer. In principle, power electronic converter can be designed to operate in those modes; however, presently most of distributed generation converters seem to be incapable of performing this task. A basic requirement is that the distributed generation system has sufficient capacity to compensate for the utility voltage reduction and maintain acceptable voltage level for the duration of the voltage sag. As is stated in [37], the improvement of power quality in respect to voltage sags by using distributed generation is “a good function to consider in the future”. In quasi-stationary operation the qualitative impact of distributed generation on voltage magnitude is practically indistinguishable from that of a large [negative] load. Indeed, switching of a large load causes voltage magnitude variations, which is similar to the effect that DG output power variation has. The output power variations of a large load and a distributed generator utilizing renewable energy source e.g. wind or solar energy are subject to daily and seasonal variations. On the other hand, in many respects DG affects power quality of the grid in a very specific way. For example, the owner of a distributed generator—if the DG technology allows—has full control of the output power and voltage

Table 8.2: Fault currents levels of some DG [21].

Type of generator	Fault currents, [%] of the rated current
Inverter	100 – 400
Separately excited SG	First few cycles: 500 – 1000 Permanent: 200 – 400
Induction generator or self excited SG	First few cycles: 500 – 1000 Permanent: nearly 0

magnitude of DG. This is different from the situation with large loads which are often controlled by industrial processes. Furthermore, the installation of new load never improves the quality of electric power, while DG has the ability to reduce the harmonic contamination of the current/voltage wave shapes thus enhancing power quality. Therefore comparing the impact of a distributed generator and a load having comparable ratings, it can be concluded that in general the impact of DG on quality of electric power should be more positive than that of the equivalent load.

Change in Short Circuit Power

The distribution power systems are designed and built to withstand certain thermal and mechanical stresses in both normal and emergency states. The presence of DG changes the designed regimes of operation of the grid, which also results in an increase of fault current levels. Quantitatively the impact on the fault currents depends on the capacity/penetration of DG and the DG technology deployed. Detailed assessment of the impact that DG might have on the fault currents is very challenging as the impact largely depends upon a number of factors, e.g., its operation mode, interface of the DG, system voltage prior to the fault, and some other. Table 8.2 provides a qualitative estimation of fault currents for synchronous and asynchronous generators, as well as inverters. The values given in the table only apply to faults at the terminals of the respective generator. As the impedance of distribution lines is high compared to that of transmission lines, the fault currents will decrease rapidly with distance from the distributed generator.

It should be noted that those DG technologies which do not possess energy storage devices, e.g., storage of kinetic or potential or chemical energy are unable to essentially contribute to short circuit power. A photovoltaic element without a battery is one such typical example.

Protection System

By definition, protective relays and systems are power system components which should “operate the correct circuit breakers so as to disconnect only the faulty equipment from the system as quickly as possible, thus minimizing the trouble and damage caused by faults when they do occur” [125]. There are a number of power system protection devices whose functionality ranges from overcurrent protection to bus-zone protection [17]. The section will focus on overcurrent protection, the most commonly used protection in distribution systems. As mentioned before, the power flow in distribution systems is usually in one direction—from the source to the customers. Correspondingly, the protection schemes of distributions grids are designed for this mode of operation. The presence of DG may alter the topology of the distribution grid and the pattern of the power flow. Depending on the characteristics of DG (its rated power, technology used, mode of operation), the location of DG and network configuration, the impact of DG on the overcurrent protection may vary. To exemplify the statement, consider the distribution grid shown in Fig. 8.1. Normally, the protection of power systems is tuned in such a way that only faulted parts of the system are isolated at a fault. This tuning is termed “protection coordination.” Suppose now that all the DG units is disconnected from the grid and a fault located at B occurs on the system, see Fig. 8.1. The overcurrent protection coordination assures that the protection device P_3 reacts, thereby avoiding much interruption of power delivery to the other customers. Alternatively, suppose that DG is now connected to the grid. Clearly, under some operating conditions the power on the lines may flow either downstream or upstream. This has certain implications on the operation of the protection schemes. Assume again a fault located at B . Then the short circuit current flowing through the protection device P_3 is greater than that of the device P_2 . On the other hand, if a fault located at A is encountered, the fault current of P_2 is greater than the current flowing through device P_3 . This example clearly indicates that DG will certainly impact the protection scheme of the distribution grid. More examples similar to this can be found in [44]. There are at least two solutions to the problem described above. Apparently, the simplest solution is to require all DG units be disconnected when a fault occurs on the grid. This is the current practice for most DG interconnections. If the protection system of DG units are able to detect the fault and rapidly disconnect from the network, DG will not interfere with the normal operation of the protection system. Most interconnection standards therefore require disconnection of DG if a fault occurs. However, this is not always desired, particular when DG penetration is high in a distribution network. Nowadays, more and more distribution networks

are automated and equipped with SCADA systems. The primary objective of these systems is to improve reliability of the grid, but they can also be helpful in dynamic coordination of the system protection relays. In brief, a SCADA system might allow the coordinated control of the protection system, by analyzing the relevant data (system voltages, level of loading, the DG production, etc.) and operating the reclosers/circuit breakers that would isolate the fault without much disturbance to other customers or unnecessary disconnection of DG.

Reliability

The assessment of impacts that DG might have on the grid is complicated by several considerations, including the following ones

- Main application of DG.
- Plans concerning the future development of the grid.
- The technology of DG.

Combination of the aforementioned factors determines the overall impact that DG can have on the system reliability. Let us examine qualitatively these factors. To simplify analysis, let us only consider distributed generators with fully controllable output power. That is, such DGs as photovoltaic arrays or wind turbines are left outside the scope of the analysis. According to [26], there are three main applications of DG, namely, providing back up power, peak load shaving, and net metering. It can be argued that the impact of DG on the overall system reliability depends on the application. For instance, DG installed with the purpose to provide back up power will certainly increase the reliability of power supply to the critical load it is protecting. However, the positive impact on the reliability of the power delivery to other customers will be only marginal. Positive impacts that DG can have on the grid are more expressed when the main aim of the DG is to reduce the peak power demand. The positive impact originates from the fact that electric power is generated and consumed on-site thereby unloading the main feeder, which is likely to increase the overall system reliability due to a reduced rate of failures on the distribution grid.

The impact of net metering on the overall system reliability can be two-fold. On the one hand, net metering may contribute to peak load shaving and thus enhance reliability of power delivery. On the other hand, this application, in principle, causes bidirectional power flows, which under certain circumstances can depress reliability of the grid. In addition, the presence of such distributed generators can

mask the load growth and therefore increase the number of customers which can be affected by power interruption due to a failure of the DG. For instance, if a distributed generator is installed in the middle of a feeder, then at the substation end of the feeder an increase of the load behind the DG may be difficult to recognize. This might lead to an increased number of customers affected by a fault on the feeder or the DG itself. In conclusion it can be stated that major impacts that DG can have on the system reliability is highly dependent on the DG characteristics, grid characteristics as well as the application of DG. The same DG technology utilized for different applications will affect system reliability in different ways, ranging from very positive impact (peak load shaving) to quite negative (load growth masking, changing the load flow pattern). A more detailed treatment of the impact of distributed generation on the power grid and methods useful for quantifying the impact can be found in [26]. It must however be stated that “despite these conflicts, DG installations on utility distribution systems can nearly always be successfully engineered” [37].

8.5 Network Control and Stability Issues

The following sections will briefly discuss what impact a significant penetration of DG might have on control and stability of power systems. Within the discussion about DG and control/stability issue often the question about a critical penetration level of DG emerges. In the author’s opinion, the critical penetration level does not necessarily have to be defined as it will depend on the network design and the technology used, if there is actually any critical penetration level for DG. It is sometimes speculated in the literature on DG that distributed generators will certainly lead to control and stability issues. In what follows an attempt is made to qualitatively show that *in general* such a statement cannot be made, at least for relatively small penetration levels. The discussion in this section echoes the conclusions from the previous chapters in this thesis; however, an attempt is made to extrapolate these conclusions to a general multimachine power system, which—at present—can only be done by performing basic qualitative analysis.

Islanding

A loss-of-main or islanding problem can occur if a circuit breaker in a distribution system opens, which could result in an islanding of a DG unit. If the loss-of-main is not detected by the DG unit, for example due to insufficient fault current, the DG unit will continue to operate. If the DG unit is able to match active and reactive

power of the load in the islanded system precisely, then the islanded system could continue to operate. In this case a safety issue remains, as the network staff might assume that the islanded network is not energized. It is, however, very unrealistic that DG will exactly match the load in the system during the time the circuit breaker opens, hence large frequency or voltage variations will occur when the DG unit tries to supply load. Hence, most interconnection rules require a loss-of-main detection system which automatically disconnects the DG unit in case of a loss-of-main and the unit remains disconnect until the grid is restored. In the UK, G59 recommendations requires that all DG units connected to MV or LV with a rating greater than 150 kVA have a loss-of-main detection system [63]. Apparently, many customers have an interest to operate DG in parallel to the network as long as the network is available, but if a network outage occurs they would like to operate the DG unit as emergency power supply or back-up unit. In this case, the DG unit must disconnect from the main grid and must quickly match the local load demand.

Availability of Relevant Data

When analyzing stability of a power system, both dynamic and transient stability issues should be addressed in order to numerically assure the proper and reliable operation. Be it dynamic or transient stability study, it is extremely important to have models of the system reflecting the main dynamical features of the system with reasonable accuracy. Thus, to obtain reliable results from a study, one ultimately needs the data of the system components. This implies that the owners of DG should make all relevant technical characteristics of DG available. Here, not only the static characteristics of the DG unit are important, but also the characteristics of the main controls such as the governor, voltage regulator, and excitation system of a synchronous generator, etc. should be available.

Dynamic Models of DG Technologies

As the distribution grids are becoming more active their behavior will more resemble that of a transmission network. When the penetration level passes a certain threshold it will no longer be appropriate to model the distribution networks as just static loads characterized by the amount of active and reactive power being consumed. Just as in the case of the transmission grid, it will be necessary to accurately model both the distributed generators and their loads in order to address such issues as stability and control of DG resources. The importance of the modeling of the new DG technologies has already been realized by the researchers and

engineers and resulted in a number of scientific articles reporting the development of dynamic models of fuel cell systems, microturbines, double fed induction machines, and generic loads [38, 41, 72, 78, 94, 115–117, 123, 135]. Depending on the dynamical phenomena of interest, various models can be used in the analysis and simulations; however, it should be noted that presently most of the commercially available power simulation packages do not have detailed models of such DG technologies as a fuel cell or doubly-fed induction machines. Therefore, presently the system analyst has to face the challenge of modeling various components without relying on the availability of well-established models. If for some reason analytical modeling is inaccurate or infeasible, alternative ways of obtaining reliable models should be sought. One such solution is to apply a system identification technique. System identification techniques have proven useful and robust numerical tools for obtaining reliable models of dynamical systems in various fields of modern engineering, e.g., biomedicine, signal processing, aerospace industry and are now gaining more momentum in power system applications. Certain results have already been obtained in identification of linear and nonlinear models of fuel cell stack and an aggregate industrial load [72], [112]. In conclusion it can be stated that the choice of the dynamic model to be used in a particular case strongly depends in the nature of the study. That is, when assessing the dynamic stability of a power system, linear models—possibly obtained with the help of a linear identification method—will suffice. When a linear system is obtained by linearization of a nonlinear model, an explicit assumption is made on the magnitude of deviations of the system's states from an equilibrium point—the deviations should be small for all times. If this assumption is violated, the results from the linearized model may not be reliable. If this is the case, the use of linear tools becomes a choice of questionable value and application of nonlinear techniques should be considered as a viable alternative. When studying transient stability issues in electric power systems, nonlinear models are commonly used [88]. The necessity to model power systems with nonlinear differential equations originates from the following fact: When a power system is subjected to a sudden and severe disturbance, its states (generators shaft angular frequencies, exciter voltages, etc.) may deviate significantly from the pre-fault steady state. Moreover, a new post-fault equilibrium may be different from the pre-fault, which implies that linear models for pre- and post-fault are also different. All these considerations suggest that nonlinear system analysis should be applied to a certain class of power system studies. There are many nonlinear analysis tools that can be used for stability studies in power system applications. One of the most commonly used techniques is the Lyapunov direct method and its modifications presented in Chapter 4 and [43, 64, 95].

Change of Short Circuit Capacity

The installation of new distributed generators on the distribution networks potentially brings a number of benefits; however, it also may cause some side effects. One of those effects is the increased level of short circuit capacity (SCC) of the distribution networks. Although sometimes it is desirable to have a high SCC, e.g., at the point of connection of the inverter of a line commutated HVDC station or in the presence of large loads with rapidly varying demands, in general the increase of the SCC potentially indicates a problem. The problem is two-fold:

- (i) Increased fault currents and
- (ii) Voltage control issues.

Now these topics will be considered in more detail. To facilitate the exposition, assume a DG unit has been installed at a busbar A of an abstract distribution grid. Prior to the installation of DG, busbar A was a pure PQ node; with the distributed generator installed it becomes active and produces a certain amount of power at a constant power factor. Suppose a fault occurred in a neighborhood of busbar A . As Tab. 8.2 suggests, during a fault a distributed generator can inject into the busbar fault currents of a magnitude ten times greater than its rated current. Such currents can cause two types of problems: thermal and mechanical stress to the busbar. It is well known that the mechanical force acting on a busbar during a fault is proportional to the square of the fault current. In addition to the mechanical stress under faulted conditions the busbar will also be exposed to thermal stress, which can also cause damage to the busbar. Another issue to be addressed in connection with the increase of SCC is the voltage control problem. If the voltage of A at steady state is 1 p.u., then after a sudden load level reduction the voltage of A might increase beyond the desirable limits. The presence of shunt capacitors and/or filters installed to compensate for the reactive power or harmonics absorption may further worsen the situation. We would like however to mention that so far only the worst case scenarios have been considered. In reality the situation might actually be less severe. That is, normally low voltage lines and cables do have resistance values of a comparable magnitude with that of the reactance. Thus, the relative impedance [Ω/km] of the distribution lines is greater than that of transmission lines. Therefore, the fault currents will quickly dwindle as the distance between A and the fault increases causing less or no damage to A .

It should be noticed that the overwhelming majority (up to 70–80%) of the faults are one-phase-to ground and are of temporary character, which also reduces

the severity of the impact that the fault currents have on A . Finally, it is worth mentioning that the fault currents heavily depend in the grounding of both the distributed generator and distribution grid. Among the positive sides of an increased SCC is the fact that A becomes a more stiff voltage source thus reducing the magnitude of voltage sags caused by a remote earth fault or switching of large nearby loads.

Inertia Constant

As was already discussed in Section 8.3, presently there are available a number of various DG technologies which might differ significantly from a conventional synchronous generator in many respects. For instance, some distributed generators are interfaced with the grid via a converter, which is uncommon for conventional synchronous generators.

It can be argued that when conducting rotor angle stability studies, the most significant features of new DG units (except those built on SG's) are reduced damping and low inertia constants. In extreme cases, e.g., fuel cell systems, the inertia constant is undefined. To elucidate the latter statement, let us consider a synchronous generator. The swing equation for the generator is shown below:

$$\frac{2H}{\omega_0} \frac{d^2 \delta}{dt^2} = T_m - T_e(\delta, \dot{\delta}),$$

where δ , T_m , and T_e are the rotor angle, mechanical torque of the turbine, and the electrical torque produced by the generator, respectively. The quantity $H = J\omega_{m,base}^2/P_{base}$ is termed the inertia constant and is related to the kinetic energy of the rotating mass of the generator [88]. Clearly, this definition does not apply to systems without rotating masses. Let us now assess implications that reduced inertia constants have on the rotor angle stability of the power system. As an example a wind turbine having light rotor and relatively large installed capacity is analyzed. For this purpose the swing equation can be rewritten in per unit as

$$\frac{2H}{\omega_0} \frac{d^2 \delta}{dt^2} = T_{m,pu} - T_{e,pu}(\delta, \dot{\delta}).$$

Assume now that a solid three-phase short circuit has occurred at the terminals of the wind turbine, i.e., $T_{e,pu} = 0$. Then the critical clearing time can be calculated as follows

$$t_{cr} = \sqrt{\frac{4\delta_{cr}}{\omega_0} \frac{H}{T_{m,pu}}}.$$

Thus, as the ratio $H/T_{m,pu}$ decreases, so does the critical clearing time t_{cr} . Therefore, in order to preserve stability of the wind turbine, the protection system has to isolate the fault faster compared to the case of an equivalent synchronous generator having the same rating. It should however be noted that the low inertia constants of new DG technologies also impact such an important quantity of the power system as frequency. To show this, we postulate that DG units which do not utilize the conversion of mechanical energy into electrical have zero inertia constant, than the ratio

$$\frac{\sum_k H_k}{\sum_j T_{m,pu,j}}$$

decreases as the penetration level increases and a fraction of the newly installed DG consists of “massless” generators such as, for example, fuel cells. This implies that when a contingency occurs on the power system which leads to the loss of some conventional generators, the system frequency will experience a deeper sag that would have been shallower had one chosen synchronous generator-based DG. This is evident from the equation

$$\frac{d^2 \delta}{dt^2} = \frac{\omega_0}{2H} (T_{m,pu} - T_{e,pu}),$$

which indicates that the system frequency will reduce at a greater rate when H is reduced. It can also be stressed that low inertia constants not only represent difficulties under a fault conditions, but also during normal operation the control of output power of a low-inertia generator is more complicated. This phenomenon has been observed in [135], where a step increase of the output power of a microturbine caused significant rotor oscillations for approximately 20 seconds. This type of response can severely affect the ability of microturbines to follow rapid load variations.

Voltage Stability

Voltage stability of an electric power system can be defined in several ways depending on the desirable emphasis: small or large signal stability, possible causes of instability, etc. For now let the following definition be adopted:

A power system at a given operating state and subject to a given disturbance is voltage stable if voltages near loads approach post-disturbance equilibrium values. The disturbed state is within the region of attraction of the stable post-disturbance equilibrium.

In simpler terms, a power system is voltage stable if the voltages of nodes in some proximity of loads (load centers) following a disturbance approach an acceptable post-disturbance steady state values.

Among the most important factors determining voltage stability of a power system are characteristics of the load and voltage control equipment of the network. To emphasize the importance of this fact, voltage stability is sometimes referred to as load stability. Normally, the reactive power component of the load and reactive power losses play the major role in causing voltage stability problems. Due to adverse effects of asynchronous motor and constant energy loads are considered to be especially prone to provoking voltage stability problems [122]. Generally speaking, voltage stability is a dynamic phenomenon, which implies that full-scale modeling of the power system behavior might be needed for rigorous analysis of voltage stability [96, 130]. In some cases involving slow forms of voltage instability, detailed dynamic analysis is not needed; voltage stability can be assessed by adequately modified load flow analysis [96]. For simplicity, in this section the load response is assumed slow, which allows the use of load flow analysis for voltage stability studies. As stated earlier in this section, one of the most important factors affecting voltage stability is the ability of system generation and transmission to match the reactive power consumption due to the reactive load and losses [33, 84, 122]. We thus conjecture that the major impact of DG on voltage stability of the grid will be determined by the power angle of the distributed generator. Let us now consider the DG technologies listed in Section 8.3 from the perspective of their impact on the grid voltage stability, i.e., their ability to generate reactive power.

Synchronous generator

Conventional synchronous generators are capable of both generating and absorbing reactive power. Therefore, the use of DG's utilizing overexcited synchronous generators will allow the production of reactive power on-site. The local generation of reactive power reduces its import from the feeder, thus reducing the associated losses, and improving the voltage profile. As a consequence, the voltage security is also improved.

P - V curves have been traditionally used as a graphical tool for studying voltage stability in electric power systems. Figure 8.3 shows conceptually the impact of a synchronous generator on voltage stability of a hypothetic node. As can be seen in the figure, the installation of a distributed generator of ΔP MW shifts the operation point on the associated P - V curve from point A to point B , which results in a raise

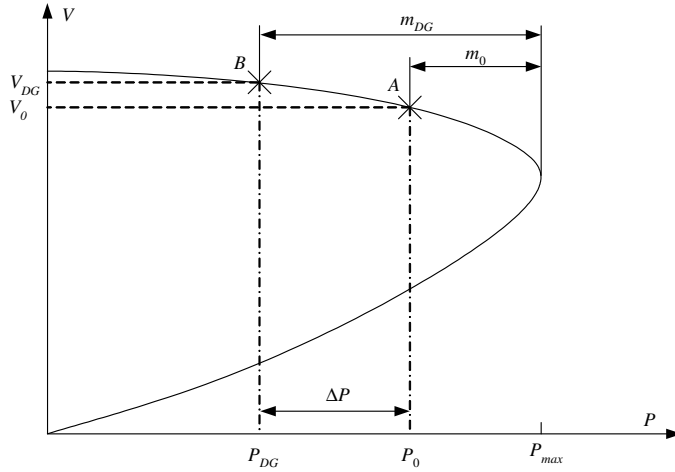


Figure 8.3: P - V curve: Enlargement of voltage stability margin

of the node voltage by the amount $V_{DG} - V_0$ and enhanced voltage security: the stability margin increases from m_0 to m_{DG} . An immediate conclusion to be drawn here is: the installation of a distributed generation will most likely enhance the voltage stability of the grid as long as the DG rating is smaller than twice the local loading level. This conclusion has been confirmed by computer simulations reported in reference [84]. DG interfaced with the grid by self-commutated power electronic converters. The utilization of self-commutated converters allows fast and precise control of the output voltage magnitude and angle. Therefore, reactive power can be either generated or absorbed, depending on the control mode. Since normally the power factor of such a converter is close to unity, no reactive power is injected in the network; however, the overall impact of the distributed generator on the voltage stability is positive. This is due to the improved voltage profiles as well as decreased reactive power losses, as the equation below suggests.

$$Q_{loss} = \frac{(P_{load} - P_{DG})^2 + (Q_{load} - Q_{DG})^2}{V^2} X_{line}.$$

In the expression above P_{load} , Q_{load} , P_{DG} , and Q_{DG} are the active and reactive power of the load and DG, respectively. X_{line} is the aggregate reactance of the line connecting the load to the feeding substation. Note that for simplicity the resistance of the line is neglected. Clearly, as the active power injected by the distributed generator increases, the reactive power loss decreases. Thus, positive

impact on the voltage stability. Case studies presented in reference [110] report a significant improvement of transient stability by a fuel cell power plant interfaced with a power electronics converter.

Asynchronous generators

An asynchronous generator possesses a number of features that make it very suitable for DG. Among these features are: relatively inexpensive prices, insignificant maintenance requirements, in addition these motors are robust. On the other hand, when directly connected to the grid, this type of DG will always consume reactive power thus contributing to the factors increasing the probability of encountering voltage stability problems. The reactive power consumption of asynchronous generators is normally compensated by shunt capacitor banks. This however is only a partial solution to the voltage stability problem, since a voltage reduction will decrease the amount of reactive power generated by the capacitor banks, while increasing the reactive power consumption of the asynchronous generator. Therefore, there is a risk that instead of supporting the grid at an undervoltage situation the asynchronous generator will further depress the system voltage. This might in principle trigger a voltage stability problem. There exist however effective ways to alleviate possible voltage stability problems with asynchronous generators, namely, installation of a static VAr system or using a self-commutated converter to interface the generator with the grid. As the overwhelming majority of newly installed asynchronous generators are equipped with a self-commutated power converter, the detrimental impact of the induction generator on voltage stability of the network is to a great extent eliminated. Moreover, the injection of active power reduces the power losses thus further enhancing voltage stability of the grid.

Line Commutated Converters

It is a well-known fact that conventional line commutated converters always consume reactive power. The amount of the consumed reactive power is can be as high as 30% of the rated power of the converter [the number has to be double-checked]. To compensate for the Q demand, capacitor banks are normally installed on the ac side of the converter. This makes a line commutated converter qualitatively equivalent to a directly connected induction generator. Therefore, under certain circumstances, the presence of such a converter can negatively affect voltage stability. We would like however draw the reader's attention to the following chain of facts: the latest achievements in high power electronics which resulted

in the advent of relatively inexpensive devices possessing excellent technical characteristics. Moreover, often the capacities of DG are quite small, which makes the utilization of advanced power electronics devices economically beneficial. It can therefore be anticipated with certain degree of confidence that in the near future most of the power electronics converters will be self-commutated. In general, it can be concluded that the presence of DG does not adversely affect voltage stability. The utilization of asynchronous generators directly connected to the can potentially cause voltage stability problems; however, the present trends in the manufacturing of asynchronous generators indicate that the fraction of converter interfaced generators gradually grows, reducing the likelihood of encountering voltage stability related problems. The qualitative analysis performed in this section only concern steady state operation of the tandem DG–distribution network.

On the Quantification of Maximum Penetration Levels

Quantification of the maximum allowable amount of DG that can be connected to a distribution network without jeopardizing the operation standards is highly case specific depending upon the specific circumstances related to the operation of both DG and the utility. For instance, one of the key factors is the mode of DG operation, i.e., if the DG output is following the load variations or not. If DG is not following the load variations, increasing DG penetration will usually violate voltage standards, before reaching any other limitation. In some cases, if synchronous generators are placed in meshed low voltage grids, the short circuit level might reach unacceptable levels before voltage standards are violated. Technically, both these issues can be solved by reconfiguration or upgrading of the network.

In distribution networks already reconfigured for DG, thermal limits on some lines or substations can be the limiting factors defining the maximum penetration levels. Some network operators might be willing to except those overloadings, if they occur only for a very short time. Some European network operators actually accept a 20% overloading of their overhead lines, if the overloading is caused by wind power, as it is expected that the high wind speed at the times of the overloading will also cool the overhead lines. If overloading is excepted, the network must be further upgraded or reconfigured. It should be emphasized that, if reconfiguration and upgrading of the distribution network is taking into account, virtually there are only a few technical limitations for the penetration ratio of DG.

With increasing DG penetration ratios, the network will be reconfiguring and upgrading, thereby becoming more flexible and may be evolving from a LV to a MV grid system. Hence, the integration of DG into distribution systems becomes

an economic issue rather than a technical one. There are a few real-world existing wind-diesel systems in operation which support this statement. Such system, for example on Rathlin Island (Northern Island), Froya Island (Norway), or Denham (Australia) achieve a wind power penetration ratio of up to 100% for short periods of times and annual average wind penetrations of 70% to 94%, [39,49]. The wind-diesel system in the Australian city of Esperance, for example, supplies power to around 12000 of its inhabitants. It consists of eight diesel generators with a combined capacity of 14 MW and two wind farms with a combined capacity of 2.4 MW. It is reported that the system is capable of adequately responding to all power fluctuations, including wind power fluctuation and load fluctuations. At nights with low system loads and high wind speeds, the wind farms provide up to 75% of the total system load without problems. In average the wind farms supplies around 14% of the system demand, [102].

*“In all human affairs there are efforts, and there are results,
and the strength of the effort is the measure of the result.”*

— J. Allen [16]

Chapter 9

Closure

This chapter recapitulates the main results obtained in the framework of this project by providing general conclusions and discussions on the key findings, which is followed by suggestions for possible extensions of the work reported in the dissertation.

9.1 Conclusions

The main focus of this project has been placed upon the development of analytical tools for stability analysis of power systems with large amounts of distributed generation. The results obtained can be roughly categorized into four main groups, namely, (i) transient stability analysis, (ii) voltage collapse analysis of power systems with intermittent generation and/or stochastic loads, (iii) identification of aggregate power system loads, and (iv) design of robust control for the enhancement of load following capabilities of solid oxide fuel cell-driven power plants.

Along these lines, the main conclusions obtained in this project can be summarized as follows.

Transient Stability

- Numerous attempts were made in order to construct a Lyapunov or Lyapunov energy-like function for a single asynchronous generator, which, however, did not lead to the discovery of a suitable Lyapunov function. In particular, the Krasovskii method, the Energy Metric algorithm, and the First Integral of

Motion failed in synthesizing an energy function for the single asynchronous generator model [with damping neglected].

- The difficulties associated with the construction of a Lyapunov (or energy) function for a single generator strongly suggest that the construction of a practical Lyapunov function for a multimachine power system consisting of both synchronous and asynchronous generators might be a very challenging task. The Converse Lyapunov theorems combined with the empirical existence of a stable equilibrium in such power systems imply that there always exists a Lyapunov function for the system, e.g., a quadratic Lyapunov function. However, it is very likely that the use of quadratic Lyapunov functions is impractical due to the excessive conservatism of the estimates of the region of attraction. At present it is not clear if a suitable practical Lyapunov or energy function can be found for a multimachine power system.
- It was demonstrated in this thesis that the use of Extended Invariance Principle can yield a family of extended Lyapunov functions that could be used in the transient stability analysis. In addition, has been demonstrated in the thesis that there exists an extended Lyapunov function for the three-machine power system.
- Numerical time-domain simulations of both single asynchronous machine and the three-machine power systems confirmed that the estimated attraction regions are reasonable accurate. For instance, for the three-machine power system the conservatism amounted to approximately 3.6%.
- It was observed in the literature that for power systems without asynchronous generators the attraction region estimates obtained with the help of extended Lyapunov functions are more conservative than the estimates which conventional energy functions give. Therefore, it is quite likely that for multimachine power systems the extended Lyapunov functions might yield attraction region estimates that are somewhat conservative. However, at present the only alternative is to use the extended Lyapunov functions for analytical stability studies of such power systems, since to date no pure Lyapunov or energy function has been found for a power system with asynchronous generators.

Voltage Stability

- The intrinsic intermittent behavior of wind farms has stimulated research in the area of voltage stability analysis of power system with large amounts of wind power.
- It was demonstrated in this dissertation that the problems of calculating the critical loading and the maximal loadability in a power system can be treated in a stochastic framework, i.e., certain system parameters could be treated as bounded stochastic parameters.
- It is known that the problems of calculating the critical loading and the maximal loadability can be reduced to certain optimization problems. It has been proposed in this thesis that these optimization problems can be reformulated such that the parameters become interval-valued. Then the methods of interval arithmetic could be applied to solve these optimization problems. Thus, performing *one* optimization, it is possible to determine the set of *all* values that the critical loading or maximal loadability assume for any combinations of the uncertain parameters.
- To exemplify the application of the proposed methodology, a simple three-bus power system was used. For this sample power system the results obtained have been found accurate and nonconservative.

Identification of Aggregate Power System Loads

- Two power system load identification techniques are proposed in this thesis. The load models are based on well established equations describing the nonlinear recovery mechanisms of load. The models are then reformulated in the framework of stochastic system identification theory.
- A linear and nonlinear output error estimators are introduced and analyzed, and generic equations applicable to identification of aggregate models of power system loads are developed and studied in detail.
- The asymptotic behavior of the estimates is studied by means of numerical experiments with artificially created data, demonstrating that the estimates are asymptotically unbiased for the nonlinear load model and their variance attains the Cramér-Rao lower bound.

- To avoid numerical problems associated with possible multiple minima of the objective function, a global minimization technique was utilized.
- The load identification techniques were applied in order to identify the load of a paper mill. Field measurements taken and linear and nonlinear load models were accurately identified.

Robust Controller Design

- The load following capabilities of a solid oxide fuel cell-driven power plant were explored by means of numerical experiments. It was found that auxiliary control could improve the load following functionality of the SOFC plant.
- To enhance these load following capabilities, a robust two-degree-of-freedom \mathcal{H}_∞ controller was designed.
- Nonlinear dynamic simulations were used in order to verify the performance of the compensated SOFC power plant. It appeared that the robust controller was capable of improving the set point tracking of the plant and significantly enhanced rejection of disturbances acting on the plant.

General Discussion on the Impact of DG on the Utility

The DG technologies were qualitatively analyzed and their impact on the power system was discussed. Here, such questions as the impact on the voltage control, inertia constants, power quality, fault current levels, protection system, reliability, and stability were studied.

Based on the discussion, it can be concluded that the impact of DG depends on the penetration level of DG in the distribution network as well as on the type of DG technology. If DG is properly sized, sited and selected in terms of technology it can clearly provide benefits to control, operation and stability of the power system.

9.2 Suggestions for Future Work

Transient Stability

In the future work the following issues should be addressed

- Using the extended Lyapunov function for the three-machine power system considered in this thesis, it would be interesting to study analytically the impact that asynchronous generators have on the dynamic performance of the power system. From such a study more insights could be gained about the role of asynchronous generators in providing additional damping.
- Generalization of the results obtained in this chapter to a multi-machine power system.
- Estimation of the conservatism of the estimates of the domain of attraction provided by the EIP for multimachine power systems.

Voltage Stability

- Application of the methodology described in this dissertation to larger power systems.
- Rigorous evaluation of the numerical properties of the interval optimization.
- Analysis of the conservatism of the enclosures
- Convergence analysis of the proposed method for voltage collapse analysis of large-scale power systems.

*“Pure mathematics is, in its way,
the poetry of logical ideas.”*
— A. Einstein

Appendix A

Interval Arithmetics

One of the most natural and convenient ways to analyze sets of numbers is to use interval arithmetic. The key concept of interval arithmetics is that of an interval. An interval $[x]$ is unambiguously defined as a closed connected set of reals [52], i.e.,

$$[x] = \{x \in \mathbb{R} \mid \underline{x} \leq x \leq \bar{x}\} \in \mathbb{IR}. \quad (\text{A.1})$$

In the equation above, \underline{x} and \bar{x} stand for the lower and upper bound of the interval $[x]$, respectively. In this Appendix, we enclose all interval variables in square brackets to distinguish them from the real numbers. Many of the main operations from real analysis can be readily extended to interval arithmetic. For instance, for two intervals $[x] = [\underline{x}, \bar{x}]$ and $[y] = [\underline{y}, \bar{y}]$ the operations of summation, subtraction, and multiplication are defined as

$$[x] + [y] = [\underline{x} + \underline{y}, \bar{x} + \bar{y}] \quad (\text{A.2})$$

$$[x] - [y] = [\underline{x} - \bar{y}, \bar{x} - \underline{y}] \quad (\text{A.3})$$

$$[x] \cdot [y] = [\min\{\underline{x}\underline{y}, \underline{x}\bar{y}, \bar{x}\underline{y}, \bar{x}\bar{y}\}, \max\{\underline{x}\underline{y}, \underline{x}\bar{y}, \bar{x}\underline{y}, \bar{x}\bar{y}\}] \quad (\text{A.4})$$

Division of two intervals is defined in a slightly different way

$$[x]/[y] = [x] \cdot [1/\bar{y}, 1/\underline{y}], \text{ if } 0 \notin [y].$$

In addition to the basic arithmetic operations, several new operators are introduced, e.g., the width and midpoint of an interval:

$$w([x]) = \bar{x} - \underline{x}$$

$$\check{x} = \text{mid}([x]) = \frac{\underline{x} + \bar{x}}{2}.$$

It is worthwhile noticing that $w([x])$ can be viewed as a norm in the space \mathbb{IR} ; however, it is only a seminorm, since $w(\xi) = 0, \forall \xi \in \mathbb{R}$. As can be easily verified by direct inspection of (A.2)–(A.4), $[x] - [x] \neq 0, \forall [x] : w([x]) \neq 0$.

The concepts of interval vectors and operations on them are trivially extended from the real analysis, i.e., an interval vector $\mathbf{x} \in \mathbb{IR}^n$ is defined as a Cartesian product of intervals $[x_i]$

$$\mathbf{x} = [x_1] \times [x_2] \times \cdots \times [x_n], \quad (\text{A.5})$$

$$\xi \mathbf{x} = (\xi [x_1]) \times (\xi [x_2]) \times \cdots \times (\xi [x_n]), \xi \in \mathbb{R}, \quad (\text{A.6})$$

$$\mathbf{x}'[\mathbf{x}] = \sum_{k=1}^n [x_k] \cdot [y_k], \quad (\text{A.7})$$

Interval matrix operations are defined similarly to the operations on real matrices. Finally, an interval-valued function f is defined as follows

$$f([x]) = \{f(\xi) \mid \xi \in [x] \cap \text{dom}(f)\}, \quad (\text{A.8})$$

where ‘ $\text{dom}(f)$ ’ designates the domain of f .

Using the interval operations introduced in this section, the properties of the sets Ω_L and $\bar{\Omega}_l$ can be readily studied.

Appendix B

Some Mathematical Facts

B.1 Linear Algebra

Consider the matrix $H \in \mathbb{R}^{n \times n}$. Suppose that H is positive definite, i.e., $H \succ 0$. Then the following statements are equivalent

1. $x'Hx > 0, \forall x$.
2. If λ_i is an eigenvalue of H , then $\lambda_i > 0, \forall i$.
3. All leading minors M_k of H are positive definite (Sylvester's criterion).

If matrix H is negative definite, i.e., $H \prec 0$, the opposite to facts 1 – 3 holds. For positive semidefinite $H \succcurlyeq 0$, the strict inequalities in facts 1 – 3 are relaxed.

Assume that H has n distinct eigenvalues $\{\lambda_i\}_1^n$. Then there exists a nonsingular matrix $T : T^{-1}HT = \Lambda$, where $\Lambda = \text{diag}(\lambda_1, \lambda_2, \dots, \lambda_n)$.

Suppose that H is symmetric, i.e., $H = H'$. Then, $\lambda_i \in \mathbb{R}, \forall i$. Let us order the real eigenvalues of H such that $\lambda_1 > \lambda_2 > \dots > \lambda_n$. Then, for all x , the following inequalities hold

$$\lambda_n \|x\|_2^2 \leq x'Hx \tag{B.1}$$

$$x'Hx \leq \lambda_1 \|x\|_2^2. \tag{B.2}$$

The trace operator of a matrix is defined as the sum of the diagonal elements of the matrix, i.e.,

$$\text{Trace } H = \sum_{k=1}^n h_{kk}.$$

B.2 Calculus

Differentiation of quadratic forms

Consider the quadratic form $q = 1/2x'Qx$. Differentiation of q with respect to the argument is done as is shown below.

$$\begin{aligned}\frac{\partial q}{\partial x} &= \frac{1}{2} \frac{\partial (x'Qx)}{\partial x} \\ &= \frac{1}{2} \left[\frac{\partial x'}{\partial x} Qx + (x' \otimes I_n) \frac{\partial Qx}{\partial x} \right] \\ &= \frac{1}{2} (Q + Q')x.\end{aligned}\tag{B.3}$$

In the special case $Q = Q'$, the derivative $\partial q/\partial x$ simplifies to Qx .

Line integral independent of path

Consider the vector-valued function $f \in C^1$ in some domain D . Then, the line integral

$$\int_{\Gamma} f(x) dx$$

is path independent iff:

- $f = \nabla F$, where F is some function, or
- $\text{curl} f = 0$, assuming that D is simply connected.

Taylor series expansion

Consider the vector-valued function $f \in C^n$ in some domain $D \in \mathbb{R}^m$. Then, in D , f can be approximated by a Taylor series expanded around an x_0 as follows.

$$f(x_0 + \delta) \approx \sum_{k=1}^n \frac{1}{k!} (\delta' \nabla)^k f|_{x_0},\tag{B.4}$$

where $(\delta' \nabla)^k$ denotes an operator that acts on $f(x)$ k times. ∇f is often referred to as the Jacobian of f , while $\nabla^2 f$ is known as the Hessian of f . If it is known that (B.4) exists and that $\|\delta\|$ is small, then $f(x_0 + \delta)$ can be satisfactorily approximated by the sum $f(x_0) + \delta' \nabla f|_{x_0}$. This procedure of truncating the higher order terms is commonly termed linearization.

Appendix C

Linearized Model of SOFC

Linearizing the nonlinear fuel cell model (3.20)–(3.22) and using equation (3.19), the following state-space model of the solid oxide fuel cell is obtained

$$A = \begin{bmatrix} -1.336 & 6.459 \cdot 10^3 & -379.934 & 9.69 \cdot 10^3 & 0 \\ 0 & 0 & 0 & 0 & 0.2 \\ 0 & 0 & -0.013 & 0 & 0 \\ 0 & 0 & 0 & -3 \cdot 10^{-4} & 0.175 \\ 0 & 0 & 0 & 0 & -0.2 \end{bmatrix}$$

$$B = \begin{bmatrix} 18.87 & 37.4 & 299.6 \\ 0 & 0 & 0 \\ 0 & 0 & 0 \\ 0 & 0 & 0 \\ 0 & 0 & 0 \end{bmatrix}$$

$$C = [3.9 \cdot 10^{-3} \quad 21.56 \quad -1.268 \quad 32.35 \quad 0]$$

$$D = 0$$

The numerical values of the system parameters can be found in Table C.1 [135]. The rated voltage of the fuel cell is equal to 333.8 V under rated power output. In this model it is assumed that the fuel cell inverter was operated at a unity power factor.

Table C.1: Parameters in SOFC plant model

Parameter	Representation	Value
P_{rate}	Rated power	100 kW
P_{ref}	Active power reference	100 kW
T	Absolute temperature	1273 K
F	Faraday's constant	96487 C/mol
R	Universal gas constant	8314 J/(kmol K)
E_0	Ideal standard potential	1.18 V
N_0	Number of cells in the stack	384
K_r	Constant, $K_r = N_0/4F$	0.996×10^{-6} kmol/(s A)
U_{max}	Maximum fuel utilization	0.9
U_{min}	Minimum fuel utilization	0.8
U_{opt}	Optimal fuel utilization	0.85
K_{H_2}	Valve molar constant for hydrogen	8.43×10^{-4} kmol/(s atm)
K_{H_2O}	Valve molar constant for water	2.81×10^{-4} kmol/(s atm)
K_{O_2}	Valve molar constant for oxygen	2.52×10^{-4} kmol/(s atm)
τ_{H_2}	Response time for hydrogen	26.1 s
τ_{H_2O}	Response time for water	78.3 s
τ_{O_2}	Response time for oxygen	2.91 s
r	Ohmic losses	0.126 Ω
T_e	Electrical response time	0.8 s
T_f	Fuel processor response time	5 s
$r_{H O}$	Ratio of hydrogen to oxygen	1.145
$\cos \phi$	Power factor	1.0

Bibliography

- [1] The European Wind Energy Association, press release. Available online at <http://www.ewea.org/>.
- [2] Distributed utility valuation project – monograph. Eprri report tr-102807, final report, Electric Power Research Institute, Palo Alto, USA, August 1993.
- [3] Load representation for dynamic performance analysis (of power systems). *IEEE Transactions on Power Systems*, 8(8):472–482, May 1993.
- [4] Bibliography on load models for power flow and dynamic performance simulation. *IEEE Transactions on Power Systems*, 10(1):523–538, February 1995.
- [5] *Analysis and Control of Power System Oscillations*. CIGRE, Technical Report 38.01.07, December 1996.
- [6] Impact of embedded generation on distribution networks. *Institution of Electrical Engineers (IEE)*. Digest No: 1996/191, London, UK, 1996.
- [7] Colloquium on system implications of embedded generation and its protection and control. *Institution of Electrical Engineers (IEE)*. Digest No: 1998/227, London, UK, February 1998.
- [8] Impact of increasing contribution of dispersed generation on the power system. Final Report. CIGRE Study Committee 37 (WG 37-23), CIGRE, Paris, September 1998.
- [9] *Fuel Cell Handbook*. EG&G Services Parsons, Inc. Science Applications International Corporation, 5th edition, 2000.

- [10] WIP. Wind Power for the 21st Century - The Challenge of High Wind Power Penetration for the New Energy Markets. *Conference Proceedings, Kassel, Germany*, September 2000. Published by WIP-Munich/ Germany.
- [11] CIRED. Technical Theme 4: Dispersed Generation, Management and Utilization of Electricity. *Proceedings of 16th International conference on Electricity Distribution. Amsterdam, Netherlands, IEE Conference Publication No: 482, Part 1: Contributions*, June 2001.
- [12] *Financing hydrogen technology in a turbulent market*, June 2001.
- [13] T. Ackermann, G. Andersson, and L. Söder. Distributed generation: a definition. *Electric Power Systems Research*, (57):195–204, 2001.
- [14] V. Akhmatov and H. Knudsen. An aggregate model of a grid-connected, large-scale, offshore wind farm for power stability investigations importance of windmill mechanical system. *International Journal of Electrical Power & Energy Systems*, 24(9):709–717, November 2002.
- [15] V. Akhmatov, H. Knudsen, and A. H. Nielsen. Advanced simulation of windmills in the electric power supply. *International Journal of Electrical Power & Energy Systems*, 22(6):421–434, August 2000.
- [16] James Allen. *As You Thinketh*. Putnam Publishing Group, 1959.
- [17] P. M. Anderson. *Power System Protection*. IEEE Press Power Engineering Series, 1999.
- [18] G. Andersson. *Power System Dynamics and Stability. An introduction*. Department of Electrical Engineering, Royal Institute of Technology, 1997.
- [19] N. Balabanian and T. A. Bickart. *Electrical Network Theory*. John Wiley & Sons, 1969.
- [20] Gary J. Balas, John C. Doyle, Keith Glover, Andy Packard, and Roy Smith. “ μ -Analysis and Synthesis Toolbox. User’s Guide”. 1998.
- [21] P. Barker and R. De Mello. Determining the Impact of Distributed Generation on Power Systems: Part 1–Radial Distribution Systems. *IEEE Power Engineering Society Summer Meeting*, 3(1645–1656), 2000.
- [22] L. Blomen and M. Mugerwa. *Fuel Cell Systems*. Plenum Press, 1993.

- [23] I. Boldea and S.A. Nasar. *Electric machine dynamics*. Macmillan, cop., New York, 1986.
- [24] A. M. Borbely. *Distributed Generation: The Power Paradigm for the New Millennium*. CRC Press, 2001.
- [25] N. G. Bretas and L. F. C. Alberto. Lyapunov Functions for Power Systems with Transfer Conductances: Extension of the Invariance Principle. *IEEE Transactions on Power Systems*, 18(2):769–777, 2003.
- [26] R. Brown and L. Freeman. Analyzing the reliability impact of distributed generation. *IEEE PES Power Summer Meeting*, 2:1013–1018, July 2001.
- [27] M. Burth, G. C. Verghese, and M. Velez-Reyes. Subset selection for improved parameter estimation in on-line identification of a synchronous generator. *IEEE Transactions on Power Systems*, 14:218–225, February 1999.
- [28] C. Cañizares. Applications of Optimization to Voltage Collapse Analysis. *IEEE/PES Summer Meeting, San Diego. Panel Session: "Optimization in Voltage Collapse Analysis"*, July 1998.
- [29] C. A. Cañizares, A. Berizzi, and P. Marannino. FACTS Controllers to Maximize Available Transfer Capability. *Proceedings of the Bulk Power Systems Dynamics and Control IV Seminar, IREP/NTUA, Santorini, Greece*, pages 633–641, August 1998.
- [30] C. A. Cañizares and Z. T. Faur. Analysis of SVC and TCSC Controllers in Voltage Collapse. *IEEE Transactions on Power Systems*, 14, 1999.
- [31] J. F. Christensen, A. Grueland Sorensen, N. Hatziaargyriou, and M. Donnelly. Methods and Models for Evaluating the Impact of Decentralized Generation. *CIGRE, Paper presented on behalf of Study Committee 38*, 1998.
- [32] S. Conti, S. Raiti, G. Tina, and U. Vagliasindi. Study of the Impact of PV Generation on Voltage Profile in LV Distribution Networks. *Proceedings IEEE Porto PowerTech2001*, September 2001.
- [33] T. Van Cutsem and C. Vournas. *Voltage Stability of Electric Power Systems*. Kluwer Academic Publishers, 1998.
- [34] J. C. Das and J. Casey. Effects of excitation controls on operation of synchronous motors. *Industrial & Commercial Power Systems Technical Conference*, 1999.

- [35] L. G. Dias and M.E. El-Hawary. Nonlinear parameter estimation experiments for static load modelling in electric power systems. *IEE Proceedings on Generation, Transmission and Distribution*, 136(2):68–77, March 1989.
- [36] J. C. Doyle, K. Glover, P. P. Khargonekar, and B. A. Francis. State-space solutions to standard \mathcal{H}_2 and \mathcal{H}_∞ control problems. *IEEE Transactions on Automatic Control*, 34(8):831–847, August 1989.
- [37] R. Dugan and T. McDermott. Operating Conflicts for Distributed Generation on Distribution Systems. *Rural Electric Power Conference*, pages A3/1 – A3/6, 2001.
- [38] R. Neifer E. Welfonder and M. Spanner. Development and Experimental Identification of Dynamic Models For Wind Turbines. *Control Engineering Practice*, 5(1):63–73, January 1997.
- [39] P. Lundsager et. al. Isolated Systems with Wind Power Main Report. *Risø National Laboratory, Risø, Denmark*, June 2001. Available for download at: <http://www.risoe.dk/rispubl/VEA/veapdf/tris-r-1256.pdf>.
- [40] W. Favoreel, B. De Moor, and P. Van Overschee. Model-free subspace-based LQG-design. *Proceedings of the American Control Conference, San Diego, California*, pages 3372–3376, June 1999.
- [41] Andrés Feijóo, José Cidrás, and Camilo Carrillo. A Third Order Model for The Doubly-Fed Induction Machine. *Electric Power Systems Research*, 56(2):121, November 2000.
- [42] A. Garulli, L. Giarrè, and Giovanni Zappa. Identification of approximated models in a worst-case setting. *IEEE Transactions on Automatic Control*, 47:2046–2050, December 2002.
- [43] M. Ghandari. *Control Lyapunov Functions: A Control Strategy for Damping of Power Oscillations in Large Power Systems*. PhD thesis, Royal Institute of Technology, November 2000.
- [44] A. Girgis and S. Brahma. Effect of distributed generation on protective device coordination in distribution system. *LESCOPE '01 Conference on Large Engineering Systems*, pages 115–119, 2001.
- [45] G. H. Golub and C. F. van Loan. *Matrix Computations*. The Johns Hopkins University Press, London, 3rd edition, 1996.

- [46] M. Grubb and R. Vigotti. Renewable energy strategies for europe - volume ii. *Electricity Systems and Primary Electricity Sources. The Royal Institute of International Affairs, London, UK, 1995.*
- [47] E. Handschin. *Real time control of electric power systems.* Proceedings of the symposium on real-time control of electric power systems, Elsevier Publishing Company, 1971.
- [48] E. Hansen. *Topic in Interval Analysis.* Oxford University Press, 1969.
- [49] L. H. Hansen and P. Lundsager. Review of Relevant Studies of Isolated Systems. *Risø National Laboratory, Risø, Denmark, December 2000.* Available for download at: <http://www.risoe.dk/rispubl/VEA/veapdf/ris-r-1109.pdf>.
- [50] J. W. Helton and O. Merino. *Classical Control Using \mathcal{H}_∞ Methods Theory. Optimization and Design.* Society for Industrial and Applied Mathematics, 1998.
- [51] D. S. Henderson. Synchronous or induction generators? – the choice for small scale generation. *In Proceedings: Opportunities and Advances in International Power Generation, March 1996.*
- [52] T. Hickey, Q. Ju, and M. H. Van Emden. Interval Arithmetics: From Principles to Implementation. *Journal of the ACM*, 48(5):1038–1068, September 2001.
- [53] D. Hill. Nonlinear Dynamic Load Models with Recovery for Voltage Stability Studies. *IEEE Transactions on Power Systems*, 8(1):166–176, February 1993.
- [54] D. J. Hill and I. M. Y. Mareels. Stability Theory for Differential/Algebraic Systems with Applications to Power Systems. *IEEE Transactions on Circuits and Systems*, pages 1416–1423, November 1990.
- [55] J. H. Hirschenhofer. Fuel Cell Status: 1996. *IEEE AES Magazine*, March 1997.
- [56] E. Hirst and B. Kirkby. Creating competitive markets for ancillary services. Technical report, Oak Ridge National Laboratory, Oak Ridge, TN, 1997.
- [57] I. A. Hiskens. Nonlinear dynamic model evaluation from disturbance measurements. *IEEE Transactions on Power Systems*, 16:702–710, November 2001.

- [58] I. A. Hiskens and Y. V. Makarov. Calculation of power system critical loading conditions. *Proc. Electrical Engineering Congress, Sydney, Australia*, pages 185–189, November 1994.
- [59] L. Ingber. Adaptive simulated annealing (ASA): lessons learned. *Control and Cybernetics*, 25(1):33–54, 1996.
- [60] A. Ishigame and T. Taniguchi. Transient stability analysis for power system using lyapunov function with load characteristics. *IEEE Power Engineering Society General Meeting*, 2:13–17, July 2003.
- [61] L. Jaulin and E. Walter. Guaranteed nonlinear parameter estimation from bounded-error data via interval analysis. *Math. Comput. Simul.*, 35:123–137, 1993.
- [62] N. Jenkins. Embedded generation - tutorial. *Power Engineering Journal*, pages 145–150, June 1995.
- [63] Nick Jenkins, Ron Allan, Peter Crossley, Daniel Kirschen, and Goran Strbac. *Embedded Generation*. Institute Of Electrical Engineers (IEE), London, UK, 2000.
- [64] N. Kakimoto, Y. Ohsawa, and M. Hayashi. Transient Stability Analysis of Multimachine Power System with Flux decays via Lyapunov's Direct Method. *IEEE Transactions on Power Apparatus and Systems*, PAS-99(5):1819–1828, Sept/Oct 1980.
- [65] R. Kalman. Discovery and invention: The newtonian revolution in systems technology. *Journal of Guidance and Control*, 26(6):833–837, October 2003.
- [66] D. Karlsson and D. Hill. Modelling and identification of nonlinear dynamic loads in power systems. *IEEE Transactions on Power Systems*, 9(1):157–166, February 1994.
- [67] Y. Kataoka. A Probabilistic Nodal Loading Model and Worst Case Solutions for Electric Power System Voltage Stability Assessment. *IEEE Transactions on Power Systems*, 18, 2003.
- [68] H. Khalil. *Nonlinear Systems*. Prentice-Hall, Englewood Cliffs NJ, 1996.
- [69] E. W. Kimbark. *Power System Stability*. IEEE Press, 1995.

- [70] S. Kirkpatrick, C. D. Gelatt, and M. P. Vecchi. Optimization by simulated annealing. *Science, Number 4598, 13 May 1983*, 220, 4598:671–680, 1983.
- [71] M. Klein, G. J. Rogers, and P. Kundur. A fundamental study of inter-area oscillations in power systems. *Transactions on Power Systems*, 6(3):914 – 921, August 1991.
- [72] V. Knyazkin, C. Cañizares, and L. Söder. On the Parameter Estimation and Modeling of Aggregate Power System Loads. *IEEE Transactions on Power Systems*, 19(2):1023–1031, May 2004.
- [73] P. Krause. *Analysis of Electric Machinery*. Mc Graw-Hill Inc., 1986.
- [74] P. Kundur. *Power System Stability and Control*. EPRI power system engineering series. McGraw-Hill, Inc., 1994.
- [75] P. Kundur, J. Paserba, V. Ajjarapu, G. Andersson, A. Bose, C. Canizares, N. Hatziargyriou, D. Hill, A. Stankovic, C. Taylor, T. Van Cutsem, and V. Vittal. Definition and Classification of Power System Stability IEEE/CIGRE Joint Task Force on Stability Terms and Definitions. *Transactions on Power Systems: Accepted for future publication*.
- [76] H. Kwakernaak. Robust Control and \mathcal{H}_∞ -Optimization—Tutorial Paper. *Automatica*, 29(2):255–273, 1993.
- [77] Å. Larsson. *Guidelines for Grid Connection of Wind Turbines*. Dept. of Electrical Power Engineering at Chalmers University of Technology, Göteborg, Sweden.
- [78] R. Lasseter. Dynamic models for micro-turbines and fuel cells. *IEEE PES Summer Meeting*, 2:761–766, 2001.
- [79] L. Ljung. *System Identification – Theory for the User*. Prentice Hall, Englewood Cliffs, N.J., 1987.
- [80] L. Ljung. *System Identification Toolbox. User’s Guide*. The MathWorks, Inc., 1997.
- [81] Y. Makarov, V. Maslennikov, and D. Hill. Revealing loads having the biggest influence on power system small disturbance stability. *IEEE Transactions on Power Systems*, 11(4):2018–2023, November 1996.

- [82] Y. V. Makarov and I. A. Hiskens. A continuation method approach to finding the closest saddle node bifurcation point. *Proceedings of the NSF/ECC Workshop on Bulk Power System Voltage Phenomena III, Davos, Switzerland*, August 1994.
- [83] N. Metropolis, A. W. Rosenbluth, M. N. Rosenbluth, A. A. Teller, and E. Teller. Equations of state calculations by fast computing machines. *Journal Chemical Physics*, 21:1087–1091, June 1953.
- [84] J.V. Milanovic and T.M. David. Stability of distribution networks with embedded generators and induction motors. *IEEE PES Winter Meeting*, 2:1023–1028, 2002.
- [85] N. Mohan, T. Underland, and W. Robbins. *Power Electronics: Converters, Applications and Design*. J. Wiley & Sons, 1989.
- [86] E. Mollerstedt and B. Bernhardsson. Out of control because of harmonics-an analysis of the harmonic response of an inverter locomotive. *IEEE Control Systems Magazine*, 20(4):70–81, August 2000.
- [87] I. J. Nagrath and D. P. Kothari. *Modern Power System Analysis*. Tata McGraw-Hill Company Limited, New Delhi, 1985.
- [88] Yao nan Yu. *Electric Power System Dynamics*. Academic Press, New York, 1983.
- [89] O. Nelles. *Nonlinear system identification: from classical approaches to neural networks and fuzzy models*. Berlin, Springer, 2001.
- [90] J. A. Oliver. Generation Characteristics Task Force, Study Committees 11, 37, 38, and 39. *Electra*, (185):15–33, August 1999.
- [91] AIEE Subcommittee on Interconnections and Stability Factors. First Report of Power System Stability. *AIEE Transactions*, pages 51–80, 1926.
- [92] R. H. J. M. Otten and L. P. P. P van Ginneken. *The Annealing Algorithm*. Kluwer Academic Publishers, 1989.
- [93] P. Van Overschee and B. De Moor. Subspace algorithms for the stochastic identification problem. *Proceedings of the 30th Conference on Decision and Control, Brighton, England*, pages 1321–1326, Dec. 1991.

- [94] J. Padulles, G. W. Ault, and J. R. McDonald. An integrated SOFC plant dynamic model for power systems simulation. *J. Power Sources*, 86:496–500, 2000.
- [95] M. Pai. *Energy Function Analysis for Power System Stability*. Kluwer Academic Publishers, 1989.
- [96] M. K. Pal. Voltage stability: Analysis needs, modelling requirement, and modelling accuracy. *IEE Proceedings-C*, 140(4), July 1993.
- [97] Unnati Patel. DG Power Quality, Protection and Reliability Case Studies Report. Program: Reliable, Low Cost Distributed Generator/Utility System Interconnect. *GE Corporate Research and Development, Niskayuna, NY, USA*, 2001. Available at: http://www.eren.doe.gov/distributedpower/PDFs/GE_DGCaseStudies.pdf.
- [98] J. K. Pedersen, K. O. Helgelsen-Pedersen, N. Kjlstad Poulsen, V. Akhmatov, and A. Hejde Nielsen. Contribution to a dynamic wind turbine model validation from a wind farm islanding experiment. *Electric Power Systems Research*, 64(1):41–51, January 2003.
- [99] N. S. Rau. The state of energy storage in electric utility systems and its effect on renewable energy sources. Technical report, National Renewable Energy Laboratory, Golden, USA, August 1994.
- [100] H. M. Rodrigues, L. F. C. Alberto, and N. G. Bretas. On the Invariance Principle. Generalizations and Applications to Synchronism. *IEEE Transactions on Circuits and Systems*, 47(5):730–739, May 2000.
- [101] G. Rogers. *Power system oscillations*. The Kluwer international series in engineering and computer science. Kluwer Academic Publishers, 2000.
- [102] M. Rosser. 70 % Penetration of Wind Energy into a Rural Grid - 2.4 MW of Wind Capacity Interconnected with a 14 MW Diesel Power Station. *Proceedings Wind Energy Workshop 1997, Asia Pacific Wind Energy Centre, Centre for Electrical Power Engineering, Monash University, Calyton, Australia*, 1997.
- [103] N. Rouche, P. Habets, and M. Laloy. *Stability Theory by Liapunov's Direct Method*. Springer-Verlag, 1977.

- [104] W. Rudin. *Principles of Mathematical Analysis*. McGraw-Hill, 19.
- [105] S. M. Rump. *Developemnts in Reliable Computing*, chapter INTLAB-INTerval LABoratory, pages 77–104. Kluwer Academic Publishers, 1999.
- [106] Z. Saad-Saoud and N. Jenkins. Simple wind farm dynamic model. *IEE Proc.-Gener. Transm. Distrib.*, 142(5):545–548, September 1995.
- [107] P. W. Sauer and M. A. Pai. *Power System Dynamics and Stability*. Prentice Hall, New Jersey, 1998.
- [108] D. Schultz and J. Melsa. *State functions and linear control systems*. Series in Electronic Systems. Mc-Graw-Hill Book Company, 1967.
- [109] R. P. Schultz. Impacts of new technology and generation and storage processes on power system stability and operability. In *Proceedings of DOE/ ORNL Conference “Research needs for the Effective Integration of New Technologies into the Electric Utility”*, pages 193–219, 1983.
- [110] K. Sedghisigarchi and A. Feliachi. Control of grid-connected fuel cell power plant for transient stability enhancement. *IEEE PES Winter Meeting*, 1:383–388, January 2002.
- [111] K.C. Sharman. Maximum likelihood parameter estimation by simulated annealing. *International Conference on Acoustics, Speech, and Signal Processing*, pages 2741 –2744, April 1988.
- [112] A. Simoglou, P. Argyropoulos, E. B. Martin, K. Scott, A. J. Morris, and W. M. Taama. Dynamic Modelling of the Voltage Response of Direct Methanol Fuel Cells And Stacks Part I: Model Development And Validation. *Chemical Engineering Science*, 56(23):6761–6772, December 2001.
- [113] J. Sjöberg, Q. Zhang, L. Ljung, A. Beneveniste, B. Delyon, P.-Y. Glorennec, H. Hjalmarsson, and A. Juditsky. Nonlinear Black-box Modeling in System Identification: a Unified Overview. *Automatica*, 31(12):1691–1724, 1995.
- [114] J.G. Slootweg, S.W.H de Haan, H. Polinder, and W. L. Kling. Voltage control methods with grid connected wind turbines: A tutorial review. *Wind Engineering*, 25(6):353–365, 2001.
- [115] J.G. Slootweg, H. Polinder, and W.L. Kling. Dynamic modelling of a wind turbine with direct drive synchronous generator and back to back voltage

source converter and its controls. *Proceedings of the European Wind Energy Conference, Copenhagen*, July 2001.

- [116] J.G. Slootweg, H. Polinder, and W.L. Kling. Dynamic modelling of a wind turbine with doubly fed induction generator. *IEEE PES Summer Meeting*, July 2001.
- [117] J.G. Slootweg, H. Polinder, and W.L. Kling. Initialization of wind turbine models in power system dynamics simulations. *2001 IEEE Porto Power Tech Conference*, September 2001.
- [118] T. Söderström and P. Stoica. *System Identification*. Prentice Hall, Englewood Cliffs, N.J., 1989.
- [119] Yong-Hua Song and Malcolm R. Irving. Optimisation techniques for electrical power systems Part 2 Heuristic optimisation methods. *IEE Power Engineering Journal*, pages 151–60, June 2001.
- [120] P. Sørensen, A.D. Hansen, L. Janosi, J. Bech, and B. Bak-Jensen. Simulation of interaction between wind farm and power system. *Risø National Laboratory, Riso, Denmark*, December 2001. Available at <http://www.risoe.dk/rispubl/VEA/veapdf/ris-r-1281.pdf>.
- [121] C.P. Steinmetz. Power Control and Stability of Electric Generating Stations. *AIEE Transactions, Part II*, XXXIX:1215–1287, July 1920.
- [122] C. W. Taylor. *Power System Voltage Stability*. McGraw-Hill, Inc., 1994.
- [123] H. Knudsen V. Akhmatov. Modelling of windmill induction generators in dynamic simulation programs. *IEEE Power Tech 1999 Conference, Budapest*, 1999.
- [124] Richard J. Vaccaro. *Digital control: a state-space approach*. McGraw-Hill series in electrical and computer engineering. New York: McGraw-Hill, 1995.
- [125] A. R. van C. Warrington. *Protective relays. Their theory and practice*. Chapman & Hall LTD, 1971.
- [126] S. E. Veyo. Solid Oxide Fuel Cell Distributed Power Generation. *3^d Annual Distributed Resources Conference*.

- [127] M. Vidyasagar. *Nonlinear Systems Analysis*. Electrical Engineering, Prentice-Hall, 1978.
- [128] T. L. Vincent and W. J. Grantham. *Nonlinear and Optimal Control Systems*. John Wiley & Sons, Jun 1997.
- [129] R. E. Vinograd. *The inadequacy of the method of characteristic exponents for the study of nonlinear differential equations*. Mat. Sbornik, 41 (83), 1957. In Russian.
- [130] K.T. Vu, Chen-Ching Liu, C. W. Taylor, and K. M. Jimma. Voltage Instability: Mechanisms and Control Strategies. *Proceedings of the IEEE*, 83(11):1442 – 1455, November 1995.
- [131] E. T. Wall and M. L. Moe. An Energy Metric Algorithm for the Generation of Liapunov Functions. *IEEE Transactions on Automatic Control*, (Correspondence), AC-13:121–122, 1968.
- [132] W. Xu, E. Vaahedi, Y. Mansour, and J. Tamby. Voltage Stability Load Parameter Determination from Field Tests on B. C. Hydro’s System. *IEEE Transactions on Power Systems*, 12:1290–1297, August 1997.
- [133] G. Zames. Feedback optimal sensitivity: model preference transformation, multiplicative seminorms and approximate inverses. *IEEE Trans. on Automatic Control*, 26:301–320, 1981.
- [134] K. Zhou, J. G. Doyle, and K. Glover. *Robust and Optimal Control*. Prentice Hall, Upper Saddle River, 1996.
- [135] Y. Zhu and K. Tomsovic. Development of models for analyzing the load-following performance of microturbines and fuel cells. *Electric Power Systems Research*, 62:1–11, 2002.